THE ROLE OF HYPOXIA IN METABOLISM AND NEPHRON DEVELOPMENT

by

Kasey Ryann Cargill

Bachelors of Science, University of New Haven, 2015

Submitted to the Graduate Faculty of

The School of Medicine in partial fulfillment

of the requirements for the degree of

Doctor of Philosophy

University of Pittsburgh

2019

UNIVERSITY OF PITTSBURGH

School of Medicine

This dissertation was presented

by

Kasey Ryann Cargill

It was defended on

July 12, 2019

and approved by

Eric Goetzman, Associate Professor, Department of Pediatrics

Jacqueline Ho, Assistant Professor, Department of Pediatrics

Sruti Shiva, Associate Professor, Department of Pharmacology

Michael Tsang, Associate Professor, Department of Developmental Biology

Dissertation Director: Sunder Sims-Lucas, Assistant Professor, Department of Pediatrics

THE ROLE OF HYPOXIA IN METABOLISM AND NEPHRON DEVELOPMENT

Kasey Ryann Cargill, Ph.D.

University of Pittsburgh, 2019

Self-renewing cell populations, such as stem and cancer cells, are highly metabolically active and proliferate by up regulating glycolytic metabolism. Nephron progenitors—which give rise to nephrons—are particularly metabolically active and similarly rely on the glycolysis pathway to drive proliferation. Conversely, as nephron progenitors mature they switch to mitochondrial oxidative phosphorylation coinciding with loss of stemness and rapid differentiation. The mechanism driving this metabolic switch and subsequent differentiation is currently unknown. Oxygenation is an important developmental process tightly regulated by several oxygen-dependent molecules. Although the kidney develops in a relatively hypoxic environment, as the renal vasculature matures, oxygen tension increases. The major hypoxia-responsive pathway expressed in the developing kidney allows for the recruitment of the ubiquitin ligase von Hippel Lindau (VHL) to mark the transcription factor hypoxia-inducible factor 1α (HIF-1α) for proteasomal degradation, a process that we hypothesize leads to normal nephron progenitor differentiation. Prolonged hypoxic insult however, interrupts this pathway such that HIF-1α remains stabilized and activates transcription of genes involved in cellular processes including angiogenesis, cell cycle regulation, and metabolism. This investigation reveals a previously unknown mechanism controlling the balance between nephron progenitor

self-renewal and differentiation. Collectively, this study found that hypoxia and the VHL/HIF pathway play a critical role in this process by mediating the metabolic switch that is required for nephron progenitor differentiation.

TABLE OF CONTENTS

LIST OF TABLES

LIST OF FIGURES

ACKNOWLEDGEMENTS

I would like to start by thanking my advisor, Dr. Sunder Sims-Lucas for allowing me to join his laboratory as his first graduate student. As someone with minimal research experience, I greatly appreciate the opportunity he gave to me as we navigated this process together. I appreciate all that I have learned and for the opportunity to think independently and drive my projects to completion. Secondly, I'd like to thank my thesis committee chair, Dr. Michael Tsang as well as my committee members Dr. Jacqueline Ho, Dr. Eric Goetzman, and Dr. Sruti Shiva for their guidance on the project outlined herein. Their expertise was critical to the development and execution of my success. To the past and present members of the Sims-Lucas lab I want to thank you all for your help throughout the past four years. Specifically, I'd like to thank Elina Mukherjee and Dr. Takuto Chiba—you were both instrumental in my work and I could not have completed everything without you.

I'd also like to thank my past mentors at the University of New Haven, in particular Dr. Brooke Kammrath for her support and encouragement and to my professors in the Department of Biological Sciences. Thank you for showing me a passion for science and for teaching me the skills necessary to succeed in my graduate education. I hope to continue my career as a life long learner and mentor future scientists in the same manner.

Lastly, I could not have made it this far without support from my friends and family. I'd like to extend my sincerest dedication to the memory of my dear friend Collin Kroll who

believed in me even when I didn't believe in myself. Our friendship never failed to motivate me to reach my highest potential. I would also like to extend a special thank you to my wife Christina for your continued encouragement, sacrifice, and patience throughout this journey.

Once again, thank you to everyone for your guidance, love, and support and for giving me the strength to achieve my degree.

1.0 INTRODUCTION

A portion of this section was adapted from the author's version of a review paper. The definitive version of this work was published in *Pediatric Nephrology*.

"Metabolic Requirements of the Nephron"

DOI: 10.1007/s00467-018-4157-2

Kasey Cargill[1,2] and Sunder Sims-Lucas[1,2*]

[1]Department of Pediatrics, Division of Nephrology, UPMC Children's Hospital of Pittsburgh, Pittsburgh, PA, USA.

[2]University of Pittsburgh School of Medicine, Pittsburgh, PA, USA.

1.1 KIDNEY DEVELOPMENT

1.1.1 Transient kidney structures

Mammalian organogenesis arises from three basic germ cell layers known as the ectoderm (spinal cord and nervous system), mesoderm (bones, kidney, and blood), and endoderm (gut and gastrointestinal tract) [1]. The developing metanephric kidney is derived from the intermediate mesoderm, which also gives rise to the reproductive system and urinary tract. The kidney initially progresses through two transient structures early in development, known as the pronephros and mesonephros (Figure 1) [2]. Both the pronephros and mesonephros form and, in mammals, subsequently deteriorate prior to the formation of the metanephric kidney [1].

The pronephros is the first primitive kidney structure in mammals including mice and humans. It is largely non-functional and includes a few tubular structures that empty into primary ducts [2, 3]. In humans, the pronephros completely disappears by the 4th week of gestation. The mesonephros arises soon after pronephros degeneration and remains from the 4th to the 8th weeks of gestation in humans. The mesonephros is comprised of more complex tubular structures that serve as the primary excretory organ during these weeks and gradually deteriorates. Some parts of the mesonephros tubules and duct system remain and become incorporated into primitive gonads [3]. As the kidney passes through these intermediate structures, it migrates downwards from the heart region to fuse with the urogenital sinus. Soon after the development and migration of the mesonephros, the metanephros forms by the 5th week of human gestation (embryonic day 10.5 [E10.5] in mice). This kidney structure is permanent and becomes a fully functional organ.

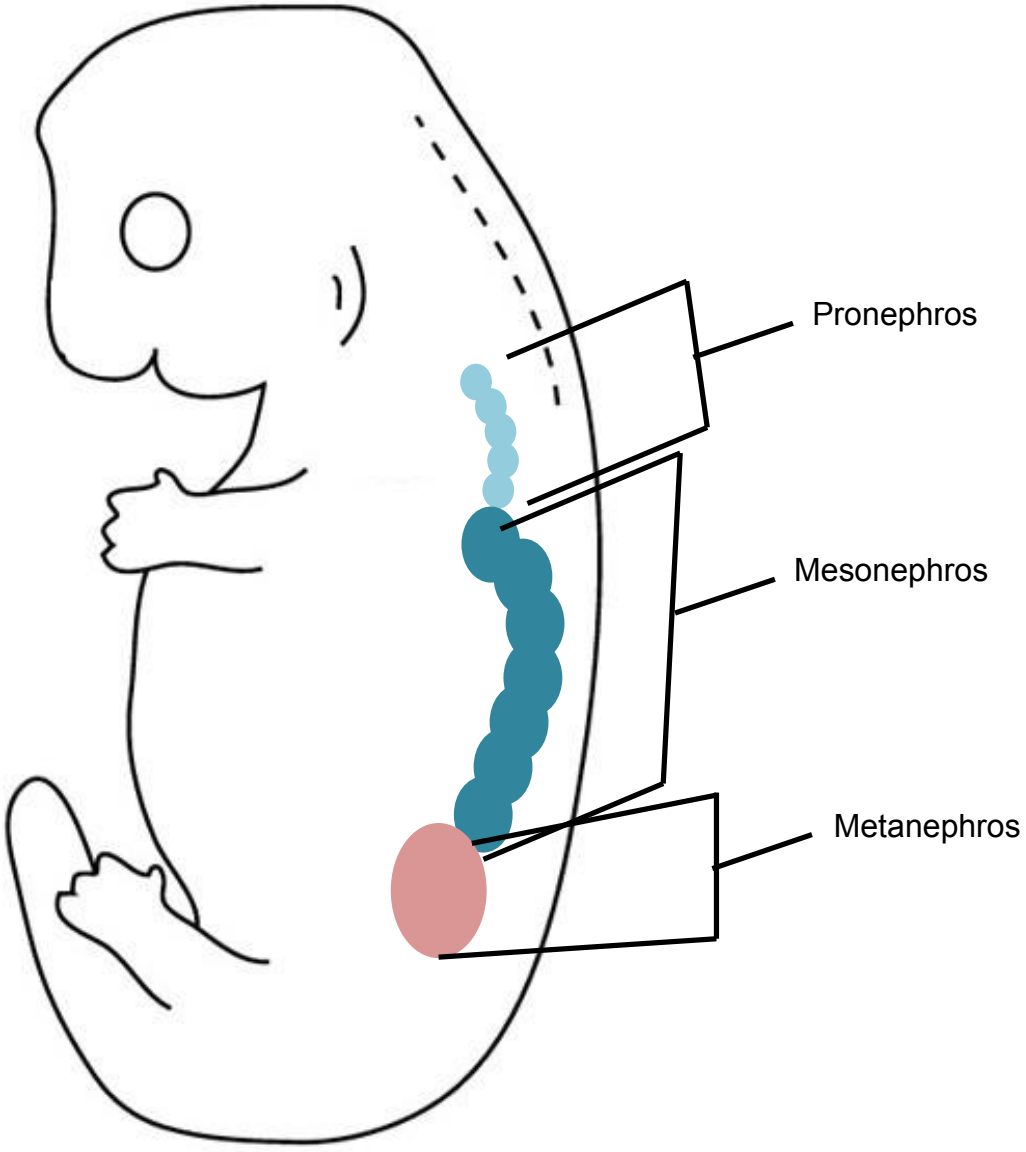

Figure 1: Early kidney organogenesis

Stages of early kidney development: pronephros (light blue), mesonephros (dark blue), metanephros (pink).

1.1.2 Ureteric epithelium and metanephric mesenchyme

The metanephros is comprised of complex tubular networks, extensive collecting duct branching, and nephron abundance. Functional kidney development involves complex signaling processes

between two tissue types: the metanephric mesenchyme (MM) and the ureteric epithelium (UE) (Figures 2-3). Reciprocal signaling between these two structures prompts elongation and branching of the UE, which ultimately forms the collecting duct system [4]. Simultaneously, the MM undergoes division into the renal stroma and nephron progenitors [5]. The stroma gives rise to the interstitial and connective tissues, pericytes, mesangium of the glomerulus (cluster of capillaries around the end of the kidney tubule), and some endothelium in adult kidneys as well as some of the renal blood vessels to facilitate oxygen delivery in the developing kidney. The stroma is also thought to play a major role in the fibrotic response after kidney injury. The self-renewing nephron progenitors condense around the UE branches to give rise to nephrons, the functional units of the kidney [2, 4]. Nephrogenesis (period of nephron formation) involves strict and sequential genetic expression dictating nephron progenitor differentiation into mature cells. This process begins with the formation of pre-tubular aggregates, which develop into renal vesicles and eventually form the mature nephron (Figure 2) [6, 7]. Once the nephron progenitors have matured into renal vesicles, they undergo a mesenchyme to epithelial transition (MET), which will lead to the formation of glomeruli and tubular epithelial cells including the proximal and distal tubules [2, 8]. Total nephron number is determined during development and no new nephrons form once nephrogenesis has concluded, which occurs around gestation week 36 in humans (post natal day 3 [P3] in mice) [9]. Any perturbation to nephron formation causing decreased nephron endowment increases an individual's susceptibility to renal diseases [9-11]. Therefore, a greater understanding of these developmental processes will provide insight into the underlying mechanisms leading to serious renal disease [12-14].

1.1.3 Nephron progenitors and nephron-derived structures

Nephron progenitors are a population of self-renewing cells that differentiate into the functional unit of the kidney called the nephrons. Structurally, nephrons are composed of glomeruli, proximal tubules, the loop of Henle, and distal tubules, which drain into UE-derived collecting ducts (Figure 2) [7]. The epithelialized glomerular and tubular segments are all derived from nephron progenitors. Filtrate first enters and passes through the glomerulus, a structure surrounded by highly specialized epithelial cells called podocytes. Together, the podocytes, glomerular basement membrane, and glomerular endothelial cells make up the glomerular filter and restrict large proteins and molecules from entering into the nephron [2]. Once small molecules such as water, salts, and sugars pass through the glomerular filter, the filtrate (urine) encounters the proximal tubule region. Proximal tubules are responsible for reabsorbing metabolic solutes from the urine filtrate [2]. The urine then flows into the loop of Henle where water and sodium chloride recovery occurs [15]. Next, the urine flows through the distal tubules, which are responsible for magnesium, calcium, and potassium reabsorption as well as water absorption [2]. From the distal tubules the urine flows into the collecting ducts—responsible for water reabsorption—before moving into the urinary tract system.

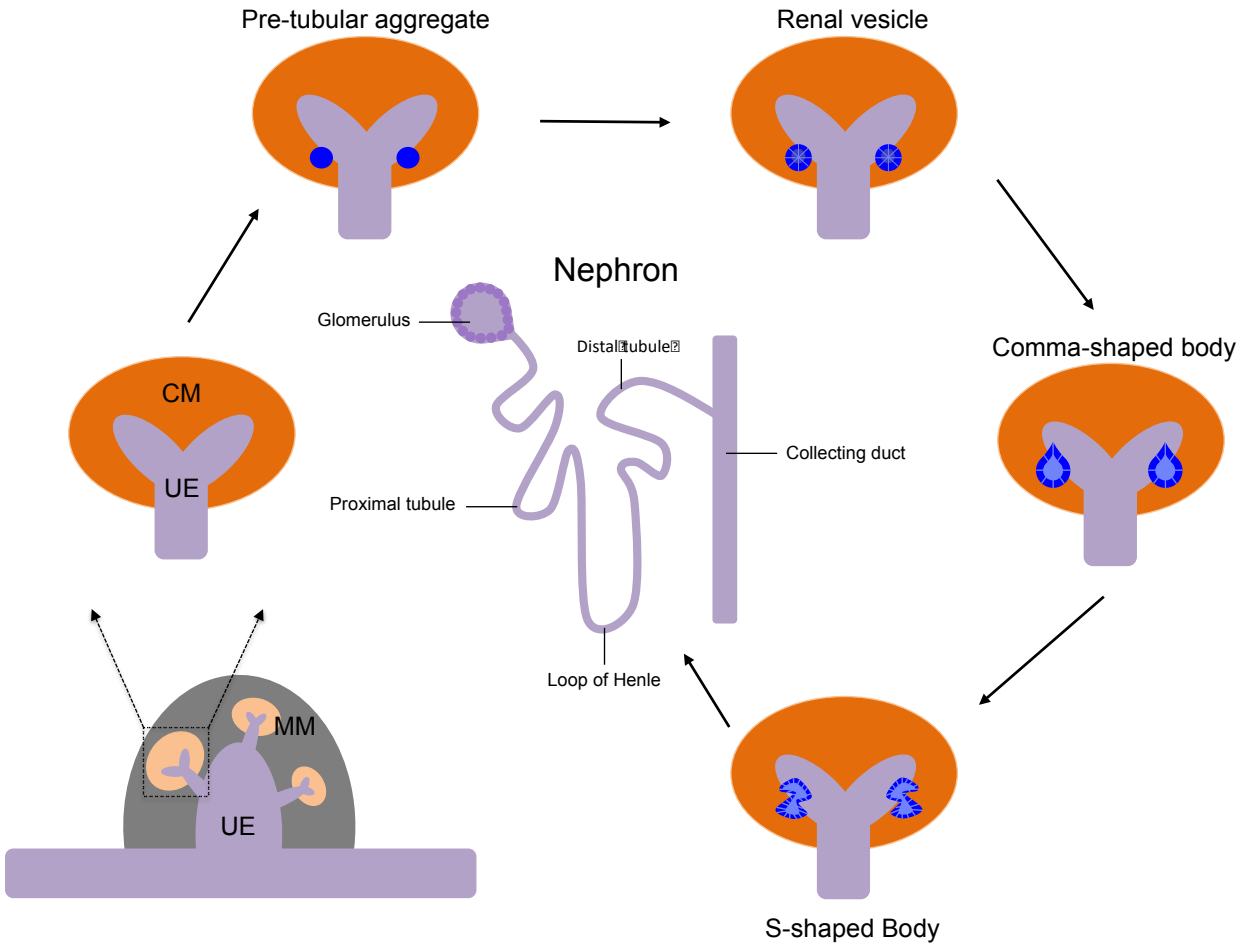

Figure 2: Basic kidney development
During nephrogenesis, nephron progenitors condense around the ureteric bud tips (purple) to form the cap mesenchyme (orange). Once differentiation cues are received by the nephron progenitors, they will mature into sequential structures 1) pre-tubular aggregate 2) renal vesicle 3) comma-shaped body 4) S-shaped body 5) mature nephron.

1.1.4 Kidney function and clinical significance

The primary function of the kidney is to eliminate waste, filter blood, and maintain physiological processes including pH and electrolyte homeostasis, blood pressure, and nutrient reabsorption [6, 7, 16]. These functions are predominantly accomplished by the nephron. As a whole, the nephron is responsible for filtration and reabsorption through specialized cells and ion transporters. Since the nephron is the major structure involved in kidney function, robust nephron number is critical

for kidney function. In fact, humans have approximately 200,000 – 2,500,000 nephrons per kidney endowed at birth (~10,000 – 15,000 per mouse kidney) [17, 18]. Although this is a large range of nephron number, falling below this threshold greatly decreases kidney function and increases an individual's susceptibility to diseases such as hypertension and chronic kidney disease (CKD), which have a prevalence of 29% and 14%, respectively, in the United States [9, 10, 19-22]. Moreover, congenital abnormalities of the kidney and urinary tract (CAKUT) constitute approximately 25% of abnormalities identified prenatally and affect 1 in 500 pediatric patients (4.2 cases per 10,000 births) [23]. It has also been revealed that approximately 50% of pediatric patients with end stage renal disease (ESRD) have disease due to a CAKUT [24]. Although CAKUT includes a broad range of renal abnormalities, failure of normal nephron development has been identified as one major cause of renal malformation [24, 25].

1.2 GENETIC EXPRESSION DICTATING KIDNEY DEVELOPMENT

This section will describe a limited number of molecules involved in kidney development essential for understanding the entirety of this work. In the metanephric kidney, the MM secretes the signaling molecule glial-derived growth factor (GDNF) and fibroblast growth factor 10 (FGF10) to induce bifurcation and branching of the UE. Branching of the UE forms ureteric bud tips (UB), which the MM condenses around to form cap mesenchyme (CM). Cells derived from the UE lineage express markers such as paired box gene 2 (PAX2) marking the UBs [26]. The nephron progenitors reside in the CM region and are marked by expression of sine oculis homeobox homolog 2 (SIX2) and Cbp/P300-interacting transactivator 1 (CITED1; Figure 3) [6, 7]. The transcription factors SIX2 and WT1 play major roles in the maintenance of the

proliferating progenitor population and in early pre-tubular aggregation, respectively [7]. SIX2 is expressed in both self-renewing nephron progenitors and those poised for differentiation [7, 27, 28], while WT1 is expressed in late-stage progenitors and during early pre-tubular aggregates [6, 7]. The transcriptional co-activator CITED1 does not have a specific role and is expressed only in self-renewing nephron progenitors. Further, maintenance of SIX2+ self-renewing nephron progenitors is balanced by canonical wingless-type MMTB integration site family member 9B (WNT9B) signaling from the UE, therefore as CITED1, SIX2, and WT1 becomes down regulated, WNT9B is expressed and plays a role in inducing differentiation [29].

As the nephron progenitors exit the nephron progenitor pool, CITED1 and SIX2 become down regulated while markers such as lymphoid enhancer binding factor 1 (LEF1), wingless-type MMTV integration site family member 4 (WNT4), and lim homeobox protein 1 (LHX1) are up regulated (Figure 3) [2, 30]. These latter markers are expressed in pre-tubular aggregates and renal vesicles. As nephron progenitors mature and the expression of differentiation markers increases, the cells are committed to undergo differentiation via a mesenchymal to epithelia transition (MET) [11, 31]. Together, these regulators play important roles in the self-renewal, and differentiation of nephron progenitors and aid in the formation of robust nephron numbers.

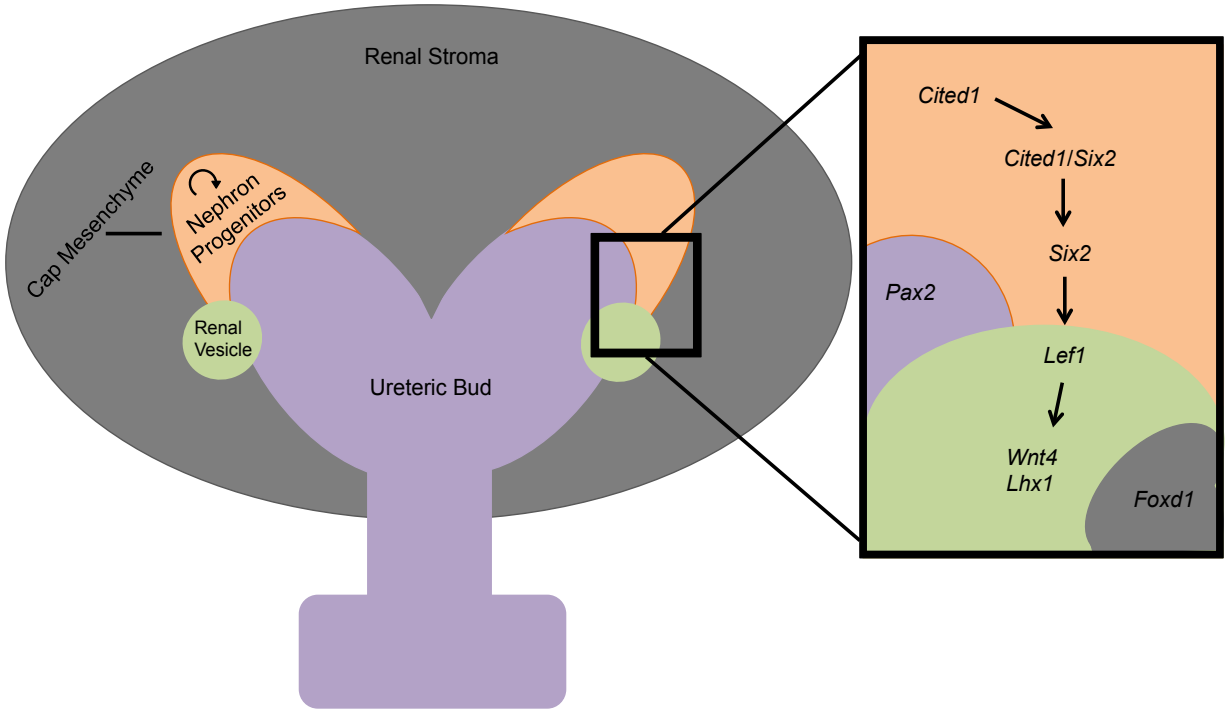

Figure 3: Genetic expression of nephron formation
During nephrogenesis, nephron progenitors condense around the ureteric bud tips (purple) to form the cap mesenchyme (orange). The distinct developmental stages are dictated by the expression of molecules such as Cited1 (self-renewing), Six2 (self-renewing/poised for differentiation), Lef1 (early differentiation), Wnt4 (differentiation), and Lhx1 (differentiation) to name a few.

1.3 METABOLIC PROCESSES

1.3.1 Glycolysis

Cellular metabolism relies mainly on two forms of energy production: glycolysis and mitochondrial respiration. Glycolysis is the preferred mechanism for ATP energy production in developing stem and progenitors cells [32], such as nephron progenitors [17] (Table 1). Glycolytic metabolism can occur under anaerobic (without oxygen) or aerobic (with oxygen) conditions. Glycolysis is the catabolism of glucose to generate ATP and the reducing equivalent NADH. Glucose enters cells through specialized glucose transporter proteins where it then

undergoes a series of enzymatic reactions in the cytosol (Figure 4). The end product of this pathway is pyruvate. Furthermore, two pyruvate molecules are generated from every one glucose molecule [33]. From here, the presence or absence of oxygen dictates the fate of pyruvate.

During aerobic glycolysis, pyruvate is shunted into the mitochondria allowing for more energy production [33, 34]. Once pyruvate enters the mitochondria, it is oxidized into acetyl-coenzyme A (acetyl-coA) and used in the tricarboxylic acid cycle (TCA cycle) [35] as described in section 1.3.2. Anaerobic glycolysis, however, is the primary mechanism for ATP production in cells lacking oxygen availability [36]. Anaerobic glycolysis is characterized by the reduction of pyruvate to lactate (Figure 4), which is then transported out of the cell to be utilized as a metabolic intermediate by adjacent cells [36]. Although this reduction of pyruvate to lactate primarily occurs in the absence of oxygen, it can occur under oxygenated conditions through the Warburg effect [37], a phenomenon that leads to increased production of lactate through glycolysis in rapidly proliferating cells, first observed by Dr. Otto Warburg in the 1950s [38].

Table 1: Metabolic pathways utilized by the nephron

Table 1: Metabolic Pathways Utilized by the Nephron	
Structure	*Predominant Predicted Metabolisms*
Young nephron progenitor	– Glycolysis – Pentose phosphate pathway
Old nephron progenitor	– Oxidative phosphorylation – Pentose phosphate pathway
Glomerulus	– Glycolysis – Oxidative phosphorylation
Proximal tubule	– Gluconeogenesis – Fatty acid Oxidation – Oxidative Phosphorylation
Loop of Henle	– Glycolysis – Fatty acid Oxidation – Oxidative Phosphorylation
Distal tubule	– Glycolysis – Fatty Acid Oxidation – Oxidative phosphorylation
Collecting ducts	– Gluconeogenesis – Glycolysis

1.3.2 Pentose phosphate pathway

It is essential to note that parallel to glycolysis, highly proliferative cells like nephron progenitors require synthesis of biomolecules such as nucleotides in addition to ATP and NADH (Table 1). Nucleotide precursors are generated by the pentose phosphate pathway (PPP; Figure 4), which provides ribose-5-phosphate, sugars (pentose), and NADPH [39]. Importantly, the first step of glycolysis generates glucose-6-phosphate. Glucose-6-phosphate can proceed through glycolysis or it can be shuttled into the PPP [39]. The PPP consists of an oxidative phase characterized by the oxidation of NADPH from $NADP^+$, and a non-oxidative phase resulting in pentose sugars and ribose-5-phosphate [39]. A previous investigation involving nephron progenitors has shown that PPP dysregulation may have some affect on renal development [28]. Moreover in a brief study of diabetic kidney development, Steer *et al* determined that there is a correlation between renal growth and the PPP [40, 41], however mechanisms of PPP utilization in the nephron and nephron progenitors have not been further studied. It is apparent that the PPP has not been readily interrogated in nephrons and nephron progenitors and future work in this lesser studied pathway would provide valuable insight into metabolic intermediate requirements in these cells.

1.3.3 Gluconeogenesis: "reverse glycolysis"

Interestingly, the kidney is unique in that it is the only organ other than the liver to perform gluconeogenesis or reverse glycolysis [42, 43]. Gluconeogenesis is a metabolic pathway utilized to maintain glucose homeostasis [44, 45]. In fact, the kidney has recently been shown to contribute to up to 20% of all glucose production [44]. Gluconeogenesis is a pathway that generated glucose from non-carbohydrate molecules such as glutamine (Figure 4) [46]. The

pathway is considered “reverse glycolysis” because many of the intermediate conversions during glycolysis are done in the opposite direction by the same enzymes utilized during glycolysis [47]. The exceptions to this include enzymes that catalyze the rate-limiting steps of glycolysis (hexokinase, phosphofructokinase, and pyruvate kinase), which are not bi-directional [47]. Therefore gluconeogenesis differs from glycolysis at those conversion points. The resulting glucose can then be metabolized to help maintain blood glucose levels [48].

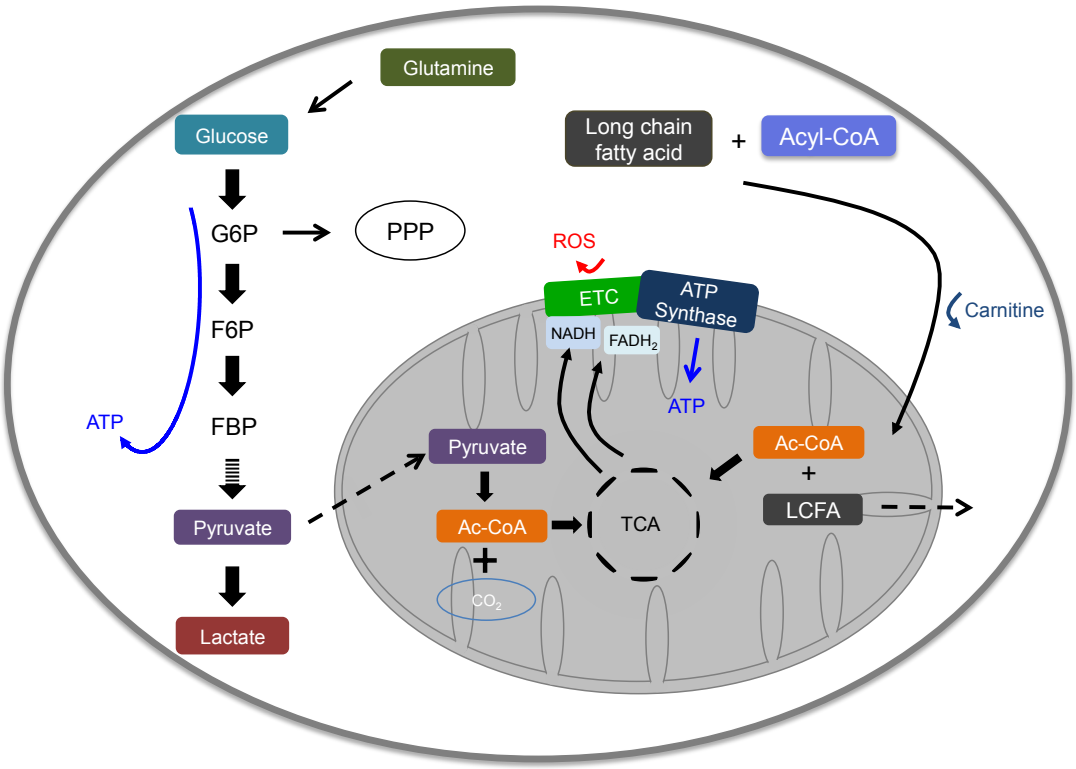

Figure 4: Overview of metabolic processes
Glucose molecules (blue) enter the cell and are ultimately converted into pyruvate (purple). An alternative fate for glucose-6-phosphate (G6P) is that it can be shuttled into the pentose phosphate pathway (PPP) where it is used for nucleotide, NADP, sugar, and amino acid synthesis. After glycolysis, pyruvate can either undergo conversion to lactate (red) or be transported into mitochondria and utilized in the first step of the TCA cycle through conversion into acetyl-coenzyme A (Ac-CoA; orange). Alternatively fatty acid oxidation occurs when an acyl-coenzyme A (acyl-coA; light purple) and a long chain fatty acid (LCFA; dark grey) molecule are transported into mitochondria with the transporter carnitine. Once inside the mitochondria, the fatty acid-acyl-coA molecule is cleaved into an ac-coA and a shorter LCFA. The ac-coA is shuttled into the TCA cycle while the LCFA is exported from the mitochondria to undergo another round of oxidation. Reactive oxygen species (ROS) are generated from the electron transport chain (ETC; green). Gluconeogenesis (reverse glycolysis) can also occur and in the kidney typically involves the conversion of glutamine (green) to glucose (blue).

1.3.4 Fatty acid oxidation

β-oxidation is a metabolic process that involves the catabolism of fatty acids and is named such due to the oxidation of the β -carbon to a carbonyl carbon in a fatty acid molecule. This type of metabolism is an oxygen-dependent process that occurs primarily in the mitochondria, however this can also occur to a lesser extent in peroxisomes [49]. Since the proximal tubules are the second most abundant sources of mitochondria (second to the heart), fatty acid oxidation and mitochondrial respiration play a large role in proximal tubule function (Table 1) [50]. During this metabolic process, fatty acids that are transported into the cell are conjugated to acyl-coenzyme A (acyl-coA) for activation (Figure 4) [51]. The conjugated fatty-acyl-coA molecule is then transported into the mitochondria via the co-transporter carnitine (Figure 4) [52]. In the mitochondria, the fatty acyl-coA is next cleaved into a shorter chain fatty acyl-coA and an acetyl-coA [52]. The acetyl-coA enters into the tricarboxylic acid (TCA) cycle while the fatty acyl-coA continues through β-oxidation until only acetyl-coA molecules remain, which are incorporated into the TCA cycle [51]. This process generates a large range of ATP (anywhere from 30-200 ATP) depending on the size of the fatty acid [51].

1.3.5 Mitochondrial respiration

Mitochondrial respiration includes various biochemical pathways including the TCA cycle, oxidative phosphorylation, and fatty acid oxidation [53]. The major function of mitochondria is to generate ATP for cellular metabolism, which is required for renal cell function and injury recovery. One way the mitochondria generates energy and metabolic intermediates is through the TCA cycle [54]. In this pathway, pyruvate or fatty acyl-coA molecules enter into the

mitochondrial matrix to undergo conversion into acetyl-coA and a series of chemical reactions that produce 3 NADH, 1 $FADH_2$, 2 CO_2, and 1 ATP (Figure 4) [55]. Although the TCA cycle itself does not directly produce large quantities of ATP, the products NADH and $FADH_2$ are known as electron carriers and are utilized in the electron transport chain during the next step of mitochondrial respiration called oxidative phosphorylation [55, 56].

Oxidative phosphorylation is utilized by a majority of the nephron segments [42, 57, 58] including nephron progenitors exiting the progenitor niche [17] (Table 1). During the metabolic process of oxidative phosphorylation, electrons are passed through five protein complexes, collectively called the electron transport chain (ETC), to create a proton gradient (Figure 4) [56]. To begin this "chain," the electron carriers NADH and $FADH_2$ shuttle electrons acquired through the TCA cycle and donate the electrons to one of the first two complexes of the ETC. NADH and $FADH_2$ are then reduced and can be recycled back through the TCA cycle [55]. NADH donates its electrons to NADH dehydrogenase (Complex I) while $FADH_2$ donates to succinate dehydrogenase (Complex II) [59]. Both Complex I and Complex II donate their electrons onto ubiquinone [60]. All electrons are then shuttled to cytochrome c reductase (Complex III) [61] before flowing through to cytochrome c oxidase (Complex IV) and being donated to the final electron acceptor, oxygen, to form H_2O. Throughout the flow of electrons, protons are passing through complexes I, III, and IV into the intermembrane space to build a proton gradient [55]. By a process called chemiosmosis, the protons flow back through a protein complex called ATP synthase (Complex V) [62]. As the name suggests, ATP synthase uses the energy stored in the proton gradient to drive the synthesis of ATP [54]. Oxidative phosphorylation and ATP synthase generates a majority of the energy used by cells [55]. Combining aerobic glycolysis (net gain 2 ATP per glucose), the TCA cycle (net gain 4 ATP per glucose), and oxidative phosphorylation

together generate a net of approximately 32-38 ATP per glucose molecule [56]. This high output of energy allows nephrons, particularly proximal tubule structures, to perform complex functions such as ion transport and water reabsorption.

1.3.6 Reactive oxygen species

Although mitochondria are considered the "power house of the cell," they also produce toxic metabolic byproducts known as reactive oxygen species (ROS) [63]. ROS are generated primarily by the electron transport chain as electrons leak back through the inner mitochondrial membrane (Figure 4) [64]. Leakage of electrons leads to the formation of superoxide and hydrogen peroxide ROS molecules (Figure 4) [65]. Higher ROS production can result in oxidative damage and tissue pathologies. Conversely, ROS can act as second messengers in critical signaling pathways and may even be a necessary molecule for basic biological processes [66]. Although there is new evidence that ROS can play a positive role in a cell (such as driving cellular proliferation, function, and viability) [66], too many ROS can be damaging and lead to cell death. Given that mitochondria generate the majority of cellular aerobic energy and ROS, they are common sources of dysregulation and disease, such as in hypertension, diabetes mellitus, and acute and chronic kidney diseases [65, 67, 68].

1.3.7 Nephron progenitor metabolism

Nephron progenitors are highly metabolically active, and rely on high rates of glycolysis to support energy and nucleotide demands during periods of proliferation and self-renewal [69]. In mice, nephron progenitors show age-dependent metabolic switching. Nephron progenitors at

embryonic day 13.5 (E13.5) exhibit higher rates of glycolysis and overall ATP production compared to postnatal day 0 (P0) progenitors [17]. E13.5 nephron progenitors utilize mostly glycolysis and low levels of oxidative phosphorylation, while the opposite is true for P0 nephron progenitors (Table 1) [17]. The mechanisms controlling these different metabolic profiles of nephron progenitors are unknown.

One possibility is in the inherent nature of nephron progenitor development, which occurs in a relatively hypoxic environment and promotes hypoxia-inducible factor (HIF) expression. HIFs regulate several genes including those implicated in glycolysis, mitochondrial metabolism, cell proliferation/apoptosis, and cell cycle [70]. HIFs are stabilized during hypoxia, however when oxygen is present, they are hydroxylated by prolyl-4-hydroxylase domain (PHD) dioxygenases [71] and subsequently degraded by the ubiquitin ligase von Hippel-Lindau (VHL). PHD oxygen sensors have also been shown to be essential during nephrogenesis and inactivation of both PHD2 and PHD3 in Foxd1+ stromal cells results in reduced glomerular number, nephron dysfunction, and kidney malformation [71]. Although HIFs heavily influence metabolism during periods of hypoxia, inhibition of glycolysis can induce premature nephron progenitor differentiation [17], which suggests that additional mechanisms, such as PHDs, may contribute to the interplay between metabolism and cell fate through mitochondrial regulation.

In addition to HIF-mediated cellular hypoxia response, tumor protein 53 (p53) is expressed in nephron progenitors and has been implicated in their cell cycle regulation and metabolism [72]. P53 inactivation leads to the promotion of carbohydrate and lipid metabolism as well as autophagy and ROS through the up-regulation of the mammalian target of rapamycin (mTOR) and AMP-activated protein kinase (AMPK) pathways [73]. Although p53 is most notably studied in cancer and other disease models, it is also a crucial protein for regulating self-

renewal and the metabolic demands of nephron progenitors in the developing kidney. A recent study showed that mice with a conditional deletion of p53 specifically in the nephron progenitors (under the control of Six2:cre) exhibited renal abnormalities including altered self-renewal and nephron deficit as well as dysregulated energy metabolism [11]. P53-depleted nephron progenitors exhibited suppression of glucose metabolism pathways, which suggests a cell-type specific role for p53 [11]. Together, these studies suggest that p53 is more than a tumor suppressor protein and also plays a large role in regulating metabolism in nephron progenitors.

1.3.8 Nephron metabolism

The second characterized renal structure that is highly metabolically active is the proximal tubules. Proximal tubules are a derivative of nephron progenitors and involved in fluid reabsorption driven by sodium transport. Proximal tubular function requires ATP, which is why they are the second most abundant sources of mitochondria (with the most abundant source of mitochondria being the heart) [50]. Proximal tubules almost exclusively rely on oxidative phosphorylation metabolism primarily driven by β-oxidation of fatty acids [74]. Moreover, proximal tubules are not known to rely on glycolysis for ATP generation, although the reason behind this is not currently understood [50]. One potential reason is that glycolytic metabolism is a process reserved for self-renewing and proliferating cell populations. Although the proximal tubules are a terminally differentiated structure, they have some capacity to undergo repair when damaged such as after ischemic acute kidney injury (AKI). After AKI, the surviving proximal tubule epithelial cells initiate a dedifferentiation process to proliferate and replace sloughed and damaged cells [74, 75]. The dedifferentiation process, where cells become progenitor-like, is characterized by decreased fatty acid oxidation and increased glycolysis and lactate secretion

[74]. As the epithelium redifferentiates, the metabolic profile of the tubules returns to primarily mitochondrial respiration, however if the metabolic profile is not restored, renal pathologies emerge [67, 68, 74]. Other structures that comprise the nephron have not been well metabolically characterized. However, some studies predominantly done in the 1980s investigated enzyme abundance and function in isolated segments of the nephron. These studies found that each segment has a unique metabolic profile, which likely corresponds to its function. Based on these investigations, the specific metabolic pathways of each segment can be hypothesized. A summary of the predicted metabolic pathways utilized along the nephron is shown in Table 1. Although the proteins expressed and their function is known, future investigations into kidney metabolism should include experimentation to definitively determine the types of metabolisms used along the nephron.

1.3.9 Metabolism of a diseased kidney

Wilms Tumor

Wilms tumor is the most commonly encountered renal tumor in children accounting for 95% of all pediatric renal cancers and affecting approximately 650 new patients each year [76]. Two tumor-suppressing genes are frequently associated with the development of Wilms tumor: *Wilms Tumor 1* and *2* (*WT1/WT2).* These genes are expressed in nephron progenitors and pre-tubular aggregates and expression is required for kidney development [77]. However, other genetic and epigenetic mutations have also been identified [78]. These tumors are thought to result from persistent nephron progenitor cells that remain capable of proliferation and differentiation [78].

Similar to many other cancers, Wilms tumor exhibits metabolic alterations and the Warburg effect [78]. A hallmark of Wilms tumor is that it can affect three types of tissue:

epithelial, stromal, and blastemal [78]. Interestingly, the mitochondrial energy requirement of these three tissue types differs in patients with triphasic Wilms tumor [78]. Wilms tumor stromal tissue exhibits severe loss of mitochondria quantity and oxidative phosphorylation capacity [79], while the epithelial and blastemal tissues retain normal mitochondrial density [79]. Moreover, in addition to mitochondrial suppression, several other metabolic proteins are decreased such as those involved in long-chain fatty acid metabolism and amino acid metabolism [80]. Although these metabolic differences are known, only limited investigation has been done into the mechanisms leading to mitochondrial suppression.

Approximately 6% of Wilms tumor patients have p53 mutations leading to the repression of HIF-1α [78]. In *p53* knockout cell lines, pharmacological reactivation of p53 leads to suppression of aerobic glycolysis (the Warburg effect) [81]. HIF-1α is primarily localized in the nucleus in Wilms tumor tissue [82] suggesting that it contributes to the metabolic dysregulation phenotype. Like most cancers, Wilms tumor has a heavy reliance on glycolysis, thus pharmacological and molecular targeting of this metabolic pathway may prove successful as a novel therapeutic strategy.

Renal Cell Carcinoma

VHL, the major regulator of HIFs, is a tumor suppressor protein, which is a protein that, when mutated, causes tumorigenesis and cancer development, particularly in the kidney [83]. Loss of VHL plays a prominent role in the pathogenesis of clear cell renal cell carcinoma (ccRCC), and up to 70% of all ccRCC cases are attributed to *VHL* gene defects [84]. Although ccRCC is relatively rare in pediatric patients, it still accounts for up to 2% of pediatric renal cancers and is associated with poor prognosis and ineffective treatment options. Similar to other cancer types,

ccRCC is highly invasive and characterized by metabolic reprogramming towards glycolysis resulting in increased cellular proliferation and evasion of apoptosis to aid in rapid tumor growth [38]. In *in vitro VHL-/VHL+* model systems, forced VHL expression leads to decreased glycolysis and glycolytic activity while TCA enzymes and ETC protein expressions were increased [83]. Moreover, VHL-deficient ccRCC cell lines exhibit HIF-dependent decreases in mitochondrial content associated with peroxisome proliferator-activated receptor gamma coactivator 1α (PGC-1α; mitochondrial biogenesis regulator) suppression [85]. PGC-1α is essential for mitochondrial function in proximal tubules and its expression leads to decreased tumor growth in ccRCC-derived cell lines [85]. Mice with a nephron progenitor-specific *VHL* deletions did not develop ccRCC or exhibit any tumor growth [86]. However, mice with nephron progenitor-specific *VHL-BAP1* (a deubiquitinating enzyme that acts as a tumor suppressor) deletions, double knockout was sufficient for mice to spontaneously develop a ccRCC phenotype [86]. This suggests that the ccRCC phenotype may not present solely from loss of VHL and may instead be derived from an accumulation of mutations in multiple tumor suppressor genes. Further, research investigating this would shed light on the pathogenicity of these mutations and may lead to new therapeutics to treat this aggressive disease. Moreover, current cancer treatments have shifted towards targeting the metabolic reprogramming phenotype using inhibitors of glycolysis outlined in the following review [87]. These same therapeutics should be further investigated for use in invasive cancers such as ccRCC.

Acute Kidney Injury

Acute kidney injury (AKI) is classified as a sudden loss in kidney function resulting in waste buildup and electrolyte imbalance [88]. Although it is a common clinical disorder, it often results

in high morbidity and mortality with no effective treatment plan [88]. A recent worldwide study into the prevalence of AKI in pediatric patients ages 3 months to 25 years found that the overall incidence of AKI in critically ill children was approximately 27% [89]. AKI typically targets the proximal tubules and since they have high mitochondrial abundance, it is unsurprising that a hallmark of AKI is tubular ATP depletion [88].

Since mitochondria are implicated in AKI manifestation and current treatments are lacking, the mitochondria are promising targets for drug discovery in treating AKI. One such target in the mitochondria is the metabolically linked sirtuin protein deacylase family. Sirtuins are important regulators of pathways involved in cellular proliferation, cell survival, metabolism, apoptosis, and DNA repair [90]. There are seven mammalian sirtuin proteins (SIRT1-SIRT7) [91] with SIRT1 and SIRT3 being the most well characterized in the kidney. Of the seven SIRT proteins, only SIRT3, SIRT4, and SIRT5 localize to the mitochondria. Although SIRT1 does not localize to the mitochondria, it has significant influence on metabolism by mediating mitochondrial activity through proteins such as PGC-1α [91]. PGC-1α knockout mice subjected to AKI fail to regain normal renal function showing that PGC-1α expression is required for renal protection against AKI [92]. This is likely because PGC-1α regulates NAD^+, which is consumed by SIRT proteins. Mouse models of AKI have shown that SIRT1 and SIRT2 exhibit renal protective effects in cisplatin-induced AKI. Moreover, these sirtuins prevent against renal fibrogenesis and in addition to SIRT3 have been associated with kidney longevity [93]. Further, SIRT1 and SIRT3 are currently being investigated as therapeutic targets for AKI and kidney disease as they both have important roles mediating antioxidant and anti-inflammatory effects in the kidney [94]. These ongoing studies are critical for the development of new strategies for the treatment of kidney diseases.

Another repercussion of AKI in the proximal tubules is metabolic reprogramming after injury. The proximal tubules are terminally differentiated structures, however they have the capacity to undergo repair when damaged. After AKI, the surviving proximal tubule epithelial cells initiate a dedifferentiation process to proliferate and replace sloughed and damaged cells [74]. The dedifferentiation process where cells become progenitor-like is characterized by decreased FAO and increased glycolysis and lactate secretion [74]. As the epithelium redifferentiates, the metabolic profile of the tubules returns to primarily mitochondrial respiration, however if the metabolic profile is not restored, renal pathologies emerge [67, 68, 74]. Understanding the metabolic changes associated with injury and repair will greatly benefit the field and provide novel molecular targets for AKI treatment.

Polycystic Kidney Disease

Polycystic kidney disease (PKD) is the fourth leading cause of renal failure (accounts for up to 10% of end stage renal disease cases worldwide). PKD is characterized by development of fluid-filled cysts in the kidney, most commonly in tubular regions of the nephron [95]. Although PKD symptoms typically present around 35 years of age, symptoms can begin as early as within a few months after birth [96]. The most common forms of the disease are caused by mutations in the genes *polycystin 1* and *2* (*PKD1*/*PKD2)* [95]. Recent studies in PKD etiology suggest that metabolism may be critical for disease development and progression [95, 97]. Rowe *et al* found that mouse embryonic fibroblasts (MEFs) isolated from kidney-specific *Pkd1* knockout mice exhibited decreased glucose levels and increased lactate [97]. Furthermore, when these cells were glucose deprived, ATP levels decreased, while mitochondrial inhibition had little effect [97]. Therefore, it was concluded that glucose metabolism is necessary in cells lacking *Pkd1,* a

phenotype reminiscent of the Warburg effect. Although Rowe *et al* found that mitochondrial inhibition did not alter ATP levels, another recent study found that in mouse models of autosomal dominant PKD (ADPKD) and in human ADPKD-derived cells, mitochondrial density and biogenesis were significantly decreased [98]. Further, this study showed that mitochondrial dysfunction and PGC-1α down regulation likely contribute to pathogenic cyst formation [98]. This highly proliferative, cancer-like phenotype with mitochondrial abnormalities should lead PKD research towards treatments such as glycolysis inhibition. In fact, Rowe *et al* generated and treated two PKD mouse models with the glycolysis inhibitor 2-deoxyglucose (2DG) and found a decrease in disease progression [97], suggesting that glucose metabolism plays a large role in disease development. Further, another recent study utilizing the serine-threonine kinase *Lkb1* deficient mouse model found that the kidneys of these mice required glutamine for ureteric bud branching and proliferation [99]. This is important because glutamine can be used as a fuel source in the TCA and as the carbon backbone for gluconeogenesis. In line with the collective findings of these studies on PKD, metabolic reprogramming and altered metabolite utilization is a commonality between normal kidney development, cancer, and renal diseases and thus the potential of metabolic pathways as therapeutic targets must be interrogated.

Chronic Kidney Disease

Chronic kidney disease (CKD) is simply defined as any condition that leads to abnormalities in kidney function or structure over a period of time greater than 3 months [100]. CKD is a common disease affecting more than 10% of adults in the United States [21], however because current detection methods are lacking, patients are typically unaware of their CKD until it reaches a later stage [101]. Unfortunately, this delay in disease treatment can lead to poor patient

prognosis because there is not a known cure. CKD is uncommon in children, however when pediatric cases arise, they are at significantly higher risk for health complications and experience increased susceptibility to disease later in life [102]. This necessitates research into enhanced CKD diagnostics, mechanistic understanding, and treatment options.

More recently, links between metabolic dysfunction, mitochondrial abnormalities, and CKD progression has been investigated. Although these types of studies are increasing in popularity, the mechanisms contributing to mitochondrial regulation and kidney function are still relatively unknown. It is now widely accepted that mitochondrial dysfunction plays a role in CKD [103-105], however whether is it a driver of pathology or a secondary effect as a consequence of the disease has not been completely elucidated. A recent genomic screen studying genetic dysregulation in patients with CKD found that out of the 44 most dysregulated genes, 11 of those genes were involved in oxidative phosphorylation [104]. Further investigation revealed these patients exhibited increased ETC protein expression but these proteins had overall decreased activity and high levels of oxidative damage [104]. This led the researchers to conclude that ROS is likely a major driver of the disease pathology [104]. Further in a recent review by the same group, the authors highlight the involvement of ROS in disease progression and interrogate the potential therapeutic benefits of molecules with antioxidant properties in targeting the mitochondria and treating CKD [105]. In addition to ROS, a few other pathways have been recently investigated for their role in mediating mitochondrial dysfunction in CKD. It is well established that the primary function of the kidney is reabsorption, which is done through ATP-dependent molecules [103]. In CKD patients and animal models the nuclear receptor called the estrogen related receptor gamma (ERRγ) has been found to be an important regulator of mitochondrial oxidative phosphorylation and FAO [103]. ERRγ regulates hundreds of genes

involved in these metabolic pathways and is decreased in CKD [103]. Therefore, ERRγ may be a novel receptor targeted for CKD prevention in the future. Lastly, one pathological symptom of severe CKD is fibrosis. Other molecules that regulate mitochondrial function and biogenesis are PPARα and PGC-1α (described in more detail above). These molecules are both highly expressed in renal tubular cells due to the dense mitochondrial load [106]. Developmental pathways, such as Notch, have been linked to the generation of fibrosis as it is highly activated in CKD [106]. As such, PPARα and PGC-1α expression is decreased in CKD models as well as in cisplatin-induced AKI [106, 107]. Han *et al* found that forced expression of PGC-1α protected mice against Notch-induced kidney fibrosis and could even reverse the mitochondrial defects associated with Notch overexpression [106]. Studies such as these are recognizing the importance of mitochondria in renal disease and are proposing new mechanisms that will better help the field combat and cure CKD. Although there is increased interest in the role of metabolism in renal diseases, there are still many gaps in our knowledge and understanding of the complex mechanisms contributing to disease. However, studies such as those described have presented new, novel targets for drug discovery and potential therapeutics such as antioxidants, Notch pathways, and ERRγ expression.

1.4 HYPOXIA AND THE DEVELOPING KIDNEY

1.4.1 Hypoxia and kidney development

It has been previously shown that hypoxia plays a large role in kidney development [205]. In fact, the kidney initially develops in a relatively hypoxia environment ranging from

approximately 5-8% O_2 *in utero* [10]. Rymer *et al* (2014) investigated renal vasculature development and blood flow and revealed that perfusion of the vasculature likely drives nephron progenitor differentiation suggesting that an influx of oxygen is required in order for nephron progenitors to receive differentiation cues [205]. This work found that at E15.5 in mice, perfusion of the vessels did not cross into the nephrogenic zone where the nephron progenitors reside, however the mature nephrons were extensively perfused allowed blood to pass into the glomeruli for filtration [205]. It is also thought that this phenomena leads to normal development and is essential for establishing nephron number. Mechanistically, this process if facilitated by the VHL/HIF pathway (the major oxygen-sensing pathway expressed in the developing kidney) described below.

1.4.2 Hypoxia-inducible factors

Hypoxia inducible factors (HIFs) are a family of transcription factors highly expressed during hypoxia in the kidney [108-110]. Moreover, approximately 2% of all human genes are indirectly or directly regulated by HIFs [83]. Three HIF-α and two HIF-β isoforms are currently known and are constituted by a basis helix-loop-helix-PAS structure: HIF-1α, HIF-2α, HIF-3α, and HIF-1β and HIF-2β [110]. Expression of HIF-α molecules is strictly regulated by the E3 ubiquitin ligase von Hippel Lindau (VHL) such that VHL targets HIFs for proteasomal degradation when oxygen is abundant (Figure 5) [111, 112]. Prior to VHL-mediated degradation, HIF-α proteins are hydroxylated by prolyl hydroxylase domain (PHD) proteins [110, 113]. These PHD proteins require oxygen, Fe^{2+}, and 2-oxoglutarate for activation [110]. Constitutively expressed HIF-β molecules, however, are not oxygen-dependent and are therefore not regulated by PHDs and VHL. HIF-1α is the most well characterized developmental isoform and has been heavily

implicated in mediating cellular processes during both physiological and pathological hypoxia [108, 114, 115].

Kidney formation is highly dependent on oxygen concentration, and during early fetal development the kidneys are initially exposed to a physiologically hypoxic gradient [116, 117]. This process of gradual oxygenation likely drives proliferation and then differentiation of the nephron progenitor population [108], but the exact mechanism is poorly understood. Most notably, HIF-1α is highly expressed when the developing kidney is exposed to physiological hypoxia [108, 117-119]. However, as the vasculature of the developing kidney matures, oxygen levels increase, facilitating HIF-1α degradation via VHL [117]. Metabolically, HIF expression during hypoxia aids in significant increases in anaerobic glycolysis by targeting glucose transporters and glycolysis genes [38, 70, 120]. Simultaneously, HIF-1α acts as a genetic repressor of enzymes involved in the mitochondrial oxidation of pyruvate, a key step in mitochondrial respiration [70, 120, 121]. Up-regulation of glycolysis by HIF-1α allows stem cells to rapidly proliferate and self-renew. However, as the vasculature matures, VHL down regulates HIF-1α [122] and the cells switch to rely on mitochondrial respiration. Since HIFs have been linked to metabolism and nephron progenitors have unique metabolic characteristics and high HIF-1α expression [123], it is likely that these proteins facilitate the metabolic profile of nephron progenitors during nephrogenesis. HIFs have also been implicated in numerous other cellular processes including angiogenesis, vascularization, cell cycle regulation, proliferation, and apoptosis [124-129]. Early investigations into HIF-1α attempted to use global knockout mouse models, which proved to be embryonic lethal [130], therefore conditional deletions are most commonly generated for analysis.

1.4.3 Von Hippel Lindau

VHL, the major regulator of HIFs, is also considered a tumor suppressor protein, which is a protein that, when mutated, causes tumorigenesis and cancer development. VHL inactivation in humans leads to a phenotype known as autosomal dominant Von Hippel Lindau (VHL) Disease and is largely characterized by invasive tumor growth particularly in the kidney [83]. *VHL* gene mutations also play a predominant role in the pathogenesis of clear cell renal cell carcinoma (ccRCC), and are often also associated with VHL Disease. In fact, up to 70% of all ccRCC cases are attributed to *VHL* gene defects [84].

Although HIF-1α is considered the major target of VHL, HIF-2α is more highly expressed and implicated in ccRCC [131]. In this case, HIF-2α acts as a metabolic regulator leading to increased glycolysis, decreased gluconeogenesis, and increased lactate fermentation in the tumor microenvironment (the Warburg effect) [38, 132]. This metabolic reprogramming allows for increased cellular proliferation and evasion of apoptosis [38]. In *in vitro VHL* knockdown and knockout model systems, forced VHL expression lead to decreased glycolysis and glycolytic activity while TCA enzymes and ETC protein expressions were increased [83]. Moreover, VHL-deficient ccRCC cell lines exhibit HIF-dependent decreases in mitochondrial content associated with PGC-1α suppression. PGC-1α is a PPARγ co-activator, which is a family of transcription factors regulated to coordinate mitochondrial biogenesis [85]. Further, PGC-1α is essential for mitochondrial function in proximal tubules and PGC-1α expression decreases tumor growth in ccRCC-derived cell lines [85]. Moving into a mouse model, Iyer *et al* generated a global VHL knockout mouse, which resulted in embryonic lethality prior to kidney development [108, 133, 134]. Wang *et al* generated mice with a conditional deletion of *VHL* specifically in the nephron progenitors under a Six2creGFP and found that they did not develop ccRCC or exhibit

any tumor growth [86]. However, if VHL is knocked out in conjunction with a nephron progenitor-specific BAP1 (tumor suppression protein) deletion, the double knockout was sufficient for mice to spontaneously develop kidney tumors and renal cell carcinoma [86]. These VHL-BAP1 double knockout mice also exhibited HIF-1 and HIF-2-dependent metabolism gene up regulation [86].

These *in vitro* and *in vivo* studies demonstrate the importance of VHL in regulating metabolism, although conclusive mechanisms are currently not well known. Although, VHL has not been previously characterized as a driver of metabolic processes during kidney development, recent investigations in zebrafish demonstrate the importance of VHL in pronephros formation, blood vessel formation, and renal function [135, 136].

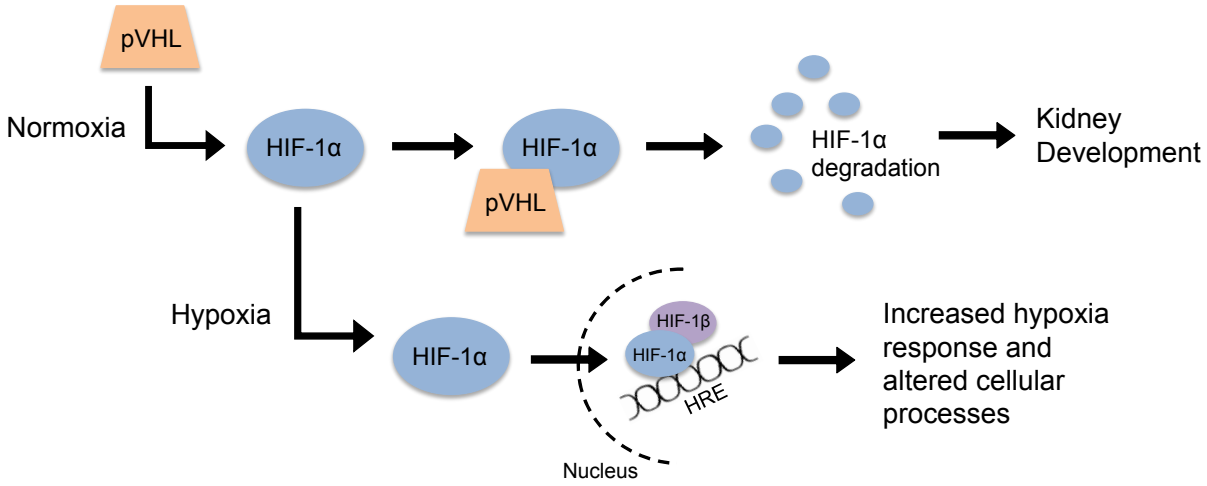

Figure 5: The VHL/HIF pathway
During normoxia, pVHL is recruited to nephron progenitors to ubiquitinate HIF-1α for proteasomal degradation. However, during hypoxia, HIF-1α binds to its β-subunit in the nucleus to initiate transcription of hypoxia response elements (HREs) resulting in abnormal nephron differentiation.

1.4.4 Causes of pathological prenatal hypoxia

As previously discussed, the kidneys develop in a relatively hypoxic environment ranging anywhere between 1 and 9% O_2 [116, 117]. This range constitutes normal physiology hypoxia, while O_2 < 1% is classified as pathological hypoxia [113, 137, 138]. Exposure to pathological hypoxia during embryogenesis has been shown to negatively impact fetal growth and development [113]. Moreover, pathological hypoxia during development can increase disease susceptibility and lead to adverse health conditions later in life [139]. Fetal hypoxia can be caused by a number of insults including: maternal smoking, environmental pollutants, placental insufficiency, and fetal anemia to name a few. Placental insufficiency is one of the most common (affecting 3-5% of pregnancies) causes of intrauterine hypoxia [139] and, depending on the severity, causes defects in metabolic, endocrine, and hematological systems. Specifically in the kidney, fetal exposure to pathological hypoxia has been linked to decreased nephron number [10, 18, 22]. Since the nephron is responsible for a majority of kidney functions, perturbations to nephron endowment significantly increase susceptibility to diseases such as CKD and ESRD.

1.4.5 Introduction to the experimental chapters

The following experimental chapters are aimed at detailing the relationship between hypoxia, metabolism, and kidney development. This work will focus on 1) an *in vitro* characterization of hypoxia adaptation and metabolic reprogramming 2) the effect of prenatal hypoxia exposure on the developing kidney and long-term disease susceptibility 3) the role of VHL in mediating metabolic switching and nephron progenitor fate and 4) the role of VHL in mitochondrial function and metabolism.

2.0 THE EFFECT OF HYPOXIA ON RENAL CELL METABOLISM

This chapter is an ongoing study and more experimentation is required before it can be considered for publication.

"Pathological Hypoxia Reveals Metabolic Reprogramming in Human Embryonic Kidney Cells"

Kasey Cargill[1,2], Elizabeth Crinzi[1], and Sunder Sims-Lucas[1,2] *

[1]Division of Nephrology, Department of Pediatrics, UPMC Children's Hospital of Pittsburgh, Pittsburgh, PA, USA.

[2]University of Pittsburgh School of Medicine, Pittsburgh, PA, USA.

2.1 CHAPTER SUMMARY

Placental insufficiency, characterized by fetal nutrient and oxygen deprivation, is a leading cause of Intrauterine Growth Restriction (IUGR), a condition that affects 12% of deliveries and causes 75% of perinatal deaths in the United States. For patients diagnosed with IUGR, the developing fetus exhibits a preferential redirection of oxygen and blood flow away from the kidney, leading to organ underdevelopment and increased risk for disease later in life. Although the kidneys initially develop in a hypoxic environment, as its vasculature matures, renal blood flow increases to facilitate oxygen delivery. Oxygenation is a process that is closely regulated by transcription factors called hypoxia-inducible factors (HIFs), which are highly expressed during hypoxia. HIFs help cells adapt to periods of hypoxia by regulating cellular processes such as glucose metabolism, mitochondrial respiration, cell division, and apoptosis. Our hypothesis for this investigation is that pathological hypoxia results in metabolic reprogramming towards anaerobic glycolysis over mitochondrial respiration. To test this hypothesis, Human Embryonic Kidney cells (HEK293) were cultured in either normoxia (~20% O_2) or hypoxia (1% O_2) for 24 or 48 hours. We evaluated cell viability, cell proliferation, gene expression, and ROS production. There were no significant differences in cell viability between normoxic and hypoxic cells. Cells exposed to hypoxia exhibited decreased cellular proliferation after 24 hours, however recovered by 48 hours of exposure. Our data also revealed metabolic gene expression differences at both 24 and 48 hours and a decrease in ROS after 48 hours of hypoxia. Together, our data suggests that renal embryonic cells exposed to hypoxia exhibit a delay in adaptation to hypoxia that occurs after 24 hours and the cells experience metabolic reprogramming towards glycolysis to aid in hypoxia adaptation, promote cell survival, and repress harmful ROS.

2.2 INTRODUCTION

Hypoxia is a pathological condition defined as a reduction or lack of oxygen availability [117]. In aerobic organisms, such as mammals, oxygen is necessary to facilitate several molecular and biological processes including cellular energy production. When oxygen is not available, cells undergo complex reprogramming to adapt to the hypoxic insult. Placental insufficiency, a disease characterized by fetal oxygen deprivation, is a leading cause of Intrauterine Growth Restriction (IUGR) [140, 141], a condition that affects up to 7% of all pregnancies and leads to 75% of perinatal deaths [142, 143]. In patients suffering from placental insufficiency and IUGR, the developing fetus exhibits a preferential redirection of oxygen and blood flow away from the kidney in favor of the brain and heart [139], leading to organ underdevelopment and increased disease susceptibility in pediatric patients as well as later in life. Although the kidney develops in a relatively hypoxia environment, as the vasculature matures to increase blood flow, oxygen levels increase [118]. This process is characterized by the expression of hypoxia-inducible factors (HIFs), which are highly expressed during developmental and pathological hypoxia [117]. HIFs are transcription factors that aid in cellular adaptation and response to low oxygen conditions [109, 117]. The primary purpose of HIFs is to facilitate cellular processes that increase oxygen flow, but also allow cells to adapt and evade cell death [109].

In previous stem cell hypoxia studies, it was shown that HIFs have several gene targets involved in glycolysis metabolism [120, 121, 144]. It was also shown that HIF-1α specifically has a dual role of promoting glycolysis while actively inhibiting oxidative phosphorylation [115, 121, 145-148]. Anaerobic glycolysis is the primary type of metabolism performed during periods of low oxygen. Cells can quickly utilize glucose to generate ATP energy and electron carriers to support cellular functions such as self-renewal and proliferation [32]. Stem, progenitor, immune,

and cancer cells are most widely associated with using HIFs and glycolysis to rapidly expand their populations [32, 69, 149-152]. Moreover, stem and progenitor cells originate during development when sufficient oxygen is unavailable, therefore HIFs are expressed to maintain metabolism and keep cells from undergoing apoptosis. However, once stem and progenitor cells receive signals to undergo differentiation, many switch their metabolisms to the more efficient oxidative phosphorylation [17]. We believe this switch in metabolism is due to increased oxygen availability.

This study investigated the influence of hypoxia on cellular processes in renal cells. Human Embryonic Kidney cells (HEK293) were cultured in normoxia or hypoxia for 24 or 48 hours prior to analysis. Previous research suggests that exposure to hypoxia prevents HIF degradation and there increases the expression of HIFs. We found that hypoxia exposure did not alter cell viability at either time point investigated. Although viability was not unchanged, cellular proliferation was significantly decreased at 24 hours but not at 48 hours, which suggests that cells do not fully adapt to hypoxia until approximately 48 hours. Gene expression alterations were first observed at 24 hours such that cells cultured in hypoxia were using both glycolysis and mitochondrial respiration, however by 48 hours were predominantly using glycolysis. Lastly, we measured ROS as a determinant of cellular health and found that at 24 hours cells had slightly increased, non-significant ROS production, however by 48 hours ROS was significantly decreased. Together, this study shows that HEK-293T cells exhibit a delay in adaptation to hypoxia that occurs between 24 and 48 hours that involves metabolic reprogramming towards glycolysis.

2.3 METHODS AND MATERIALS

2.3.1 Cell culture techniques

HEK-293 (human embryonic kidney cell line) cells were cultured in T75 flasks in Dulbecco's Modified Eagle Medium (DMEM) supplemented with high glucose, sodium pyruvate, GlutaMAX™, and phenol red (Thermo Fisher Scientific). Media was also treated with 10% Fetal Bovine Serum (FBS) and 1% penicillin/streptomycin antibiotic. Culture conditions were set at 5% CO_2 and in either normoxia (21% ambient oxygen) or hypoxia (1% oxygen) for 24 or 48 hours. Hypoxic conditions were obtained using a hypoxia chamber (Rangos Research Center Esni Laboratory). Cells were passaged at ~80% confluency. Experiments were done in at least triplicate in 6-well culture plates.

2.3.2 Real time quantitative polymerase chain reaction (PCR)

Cells were harvested after the appropriate culture time and conditions. RNA was isolated using a miRNeasy RNA isolation Kit (Qiagen). RNA was quantified using a Nanodrop 2000c (Thermo Fisher Scientific). The Superscript First Strand cDNA kit (Invitrogen, CA) was used for cDNA synthesis of 500ng of RNA. The cDNA from these samples was analyzed using a C1000 Thermal Cycler (Bio-Rad, Hercules, CA) to determine the levels of mRNA in the tissues. The following genes were analyzed using this method: *GAPDH*, *LDHA*, *SIRT3*, *TOMM20*, *IDH1*, *KI67*, *NOX4*, and *CASP3*. All gene expression was normalized to *18S*. Primer sequences are listed in Appendix B.

2.3.3 Lactate production determination

Lactate in the supernatants was measured using a Lactate Plus meter (Nova Biomedical) and Lactate Plus lactate test strips (Nova Biomedical).

2.3.4 Trypan blue cell viability assay

Cells were harvested and 1 x 10_6 cells were stained using 0.4% trypan blue solution (Thermo Fisher Scientific). Both viable and non-viable cells were counted on a hemocytometer in duplicate and averaged. The total number of viable cells was divided by the total number of both viable and non-viable cells and multiplied by 100 to obtain percent viability for each sample.

2.3.5 Flow cytometry for reactive oxygen species

Cells were harvested and 1 x 10_6 cells were stained for 15 minutes at 37°C using 5μM MitoSOX™ Red Mitochondrial Superoxide Indicator (Thermo Fisher Scientific; Appendix E) per manufacturer's guidelines. Cells were analyzed on a BD LSRFORTESSA cell analyzer (BD Biosciences) through the Flow Cytometry Core at the Rangos Research Center located at the UPMC Children's Hospital of Pittsburgh. Mean fluorescent intensity was determined using FlowJo software (v10.1).

2.3.6 Cellular proliferation

1 x 10_6 cells were stained for 15 minutes at 37°C using 1mM Violet Proliferation Dye (VDP450; BD Biosciences; Appendix E) per manufacturer's guidelines. Cells were then plated in 6-well plates and cultured for 24 or 48 hours in either normoxia or hypoxia. Cells were harvested and analyzed on a BD LSRFORTESSA cell analyzer (BD Biosciences) through the Flow Cytometry Core at the Rangos Research Center located at the UPMC Children's Hospital of Pittsburgh. Data was analyzed using FlowJo software (v10.1).

2.3.7 Statistical analysis

Minimums of 3 biological replicates were used for each experiment in at least technical duplicate. When comparing two sample groups, statistical significance was determined using a two-tailed Student's t test ($\alpha = 0.05$). Significance was defined as *P<0.05, **P<0.01, and ***P<0.001. Where appropriate, data is presented as mean ± standard error of the mean. Data was analyzed using Microsoft Excel and figures were generated using GraphPad Prism 7.

2.4 RESULTS

2.4.1 Hypoxia exposure does not alter cell viability

To begin our investigation into the significance of hypoxia on renal cell metabolism, HEK293 cells were cultured in normoxia (~21% O_2) or hypoxia (~1% O_2) for 24 and 48 hours. Previous studies have indicated that although hypoxic environments may alter cell viability in certain cell types, hypoxia typically does not significantly affect cellular viability in renal cells [153, 154]. This is particularly true regarding the hypoxic environment surrounding tumorigenic renal cells. In fact, renal cancer cells utilize hypoxia to undergo rapid growth and expansion [154]. In HEK293 cells exposed to hypoxia, there were no significant differences in cell viability at either 24 hours or 48 hours (Figure 6A) Additionally, we did not reveal any significant differences in *CASP3* gene expression after 48 hours of hypoxia (Figure 6B). This suggests that hypoxia does not alter cellular viability in HEK293 cells.

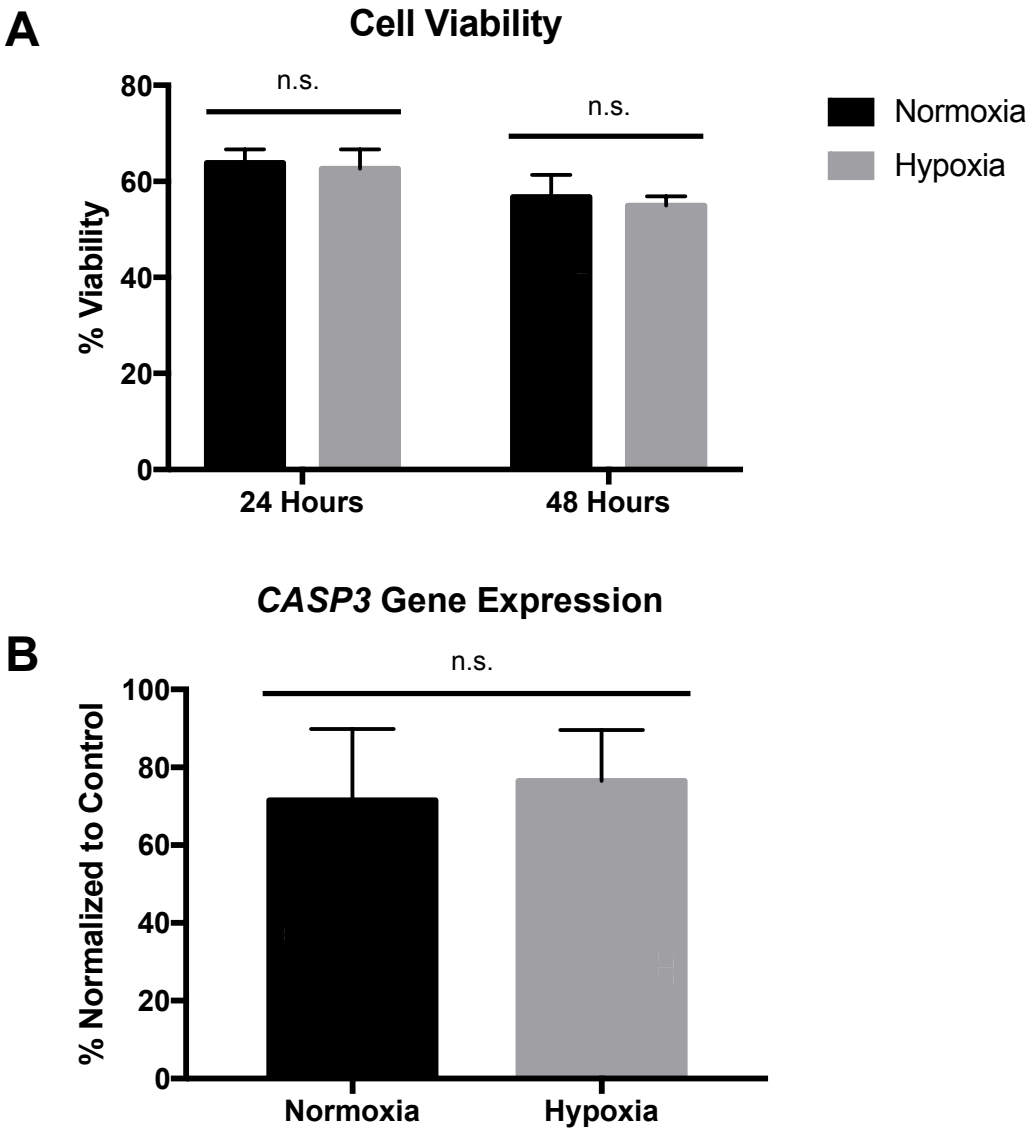

Figure 6: Cell viability is not affected by chronic hypoxia
(A) There were no changes in cell viability after both 24 and 48 hours of 1% O_2 exposure as indicated by manual counting of cells dyed by trypan blue. Error bars indicated as SEM. 24 hour: P=0.82; N=3. 48 hour: P=0.76; N=4. **(B)** *CASP3* (cell death) gene expression was not significantly different between 48-hour normoxia and hypoxia exposure. P=0.83; N=3. Error bars indicated as SEM.

2.4.2 HEK293 cells exhibit a decrease in proliferation prior to hypoxia adaptation

Next, we evaluated the effect of hypoxia on cellular proliferation. RCC cells propagate quickly in hypoxia, therefore we hypothesized that HEK293 cells exposed to hypoxia would exhibit similarly increased proliferation. Cells were stained with proliferation dye and cultured for 24 or 48 hours prior to analysis using flow cytometry. After 24 hours, HEK293 cells exhibited significantly reduced rates of proliferation (average rates are 91% and 82%, respectively) in cells cultured in hypoxia. However, after 48 hours in hypoxia, there were no significant differences between cells in the two culture conditions (Figure 7A-C). Proliferation was further evaluated using *KI67* gene expression, which showed similar trends (Figure 7D). This suggests that adaptation to hypoxia occurs between 24 and 48 hours after initial exposure. Although a reduction in the proliferative rate was not initially anticipated, a period of growth arrest is not entirely unexpected as these cells were acclimated to normoxia, and transitioned abruptly into severe hypoxia. After this initial delay in proliferation, the cells then rapidly begin dividing after adaptation, which is shown by the increase in proliferation that becomes comparable to the normoxia control cells after 48 hours.

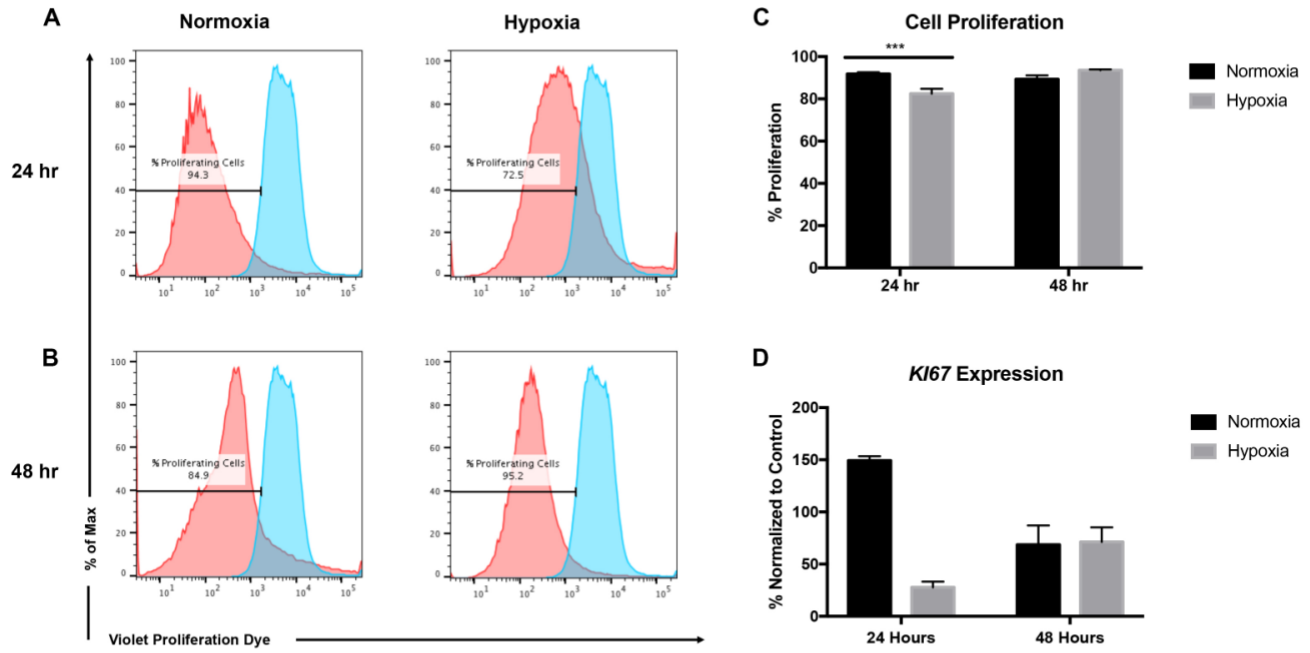

Figure 7: Cells exposed to hypoxia exhibit adaptation delay
(A-C) Cellular proliferation was significantly decreased 24-hours after hypoxia exposure, however proliferation was unaffected by 48 hours as measured by flow cytometry (representative sample shown; averages equal 91% and 82%, respectively). 24 hour: P<0.005; N=6. 48 hour: P=0.18; N=5. Error bars indicated as SEM. **(D)** *KI67* (proliferation marker) gene expression exhibited similar trends to the proliferation data with decreased expression at 24 hours and recovery/adaptation after 48 hours; N=2; significance not determined. Error bars indicated as SEM.

2.4.3 Metabolic gene expression is altered after chronic hypoxia exposure

Several studies have previously indicated that hypoxia promotes anaerobic glycolysis [17, 36, 38, 74, 115, 146, 149, 155-159]. To begin our investigation into the role of hypoxia in mediating metabolic processes, we analyzed gene expression of known glycolysis and mitochondrial metabolic genes. In relation to glycolysis, we saw a significant increase in *LDHA* expression at both 24 and 48 hours and a trending increase in *GAPDH* expression at both time points (Figure 8A). In contrast, we observed comparable expression of *SIRT3*, *TOMM20*, and *IDH1* expression at 24 hours and decreased expression in all three mitochondrial genes by 48 hours of hypoxia (Figure 8B). This indicates that the HEK293 cells likely undergo metabolic reprogramming

towards anaerobic glycolysis between 24 and 48 hours after initial exposure, which is consistent with a delay in adaptation to hypoxia. Moreover, lactate secretion in the media supernatants show significantly increased lactate levels after both 24 and 48 hours of hypoxia exposure (Figure 8C). This suggests that hypoxia leads to an increase in glycolysis in HEK293 cells.

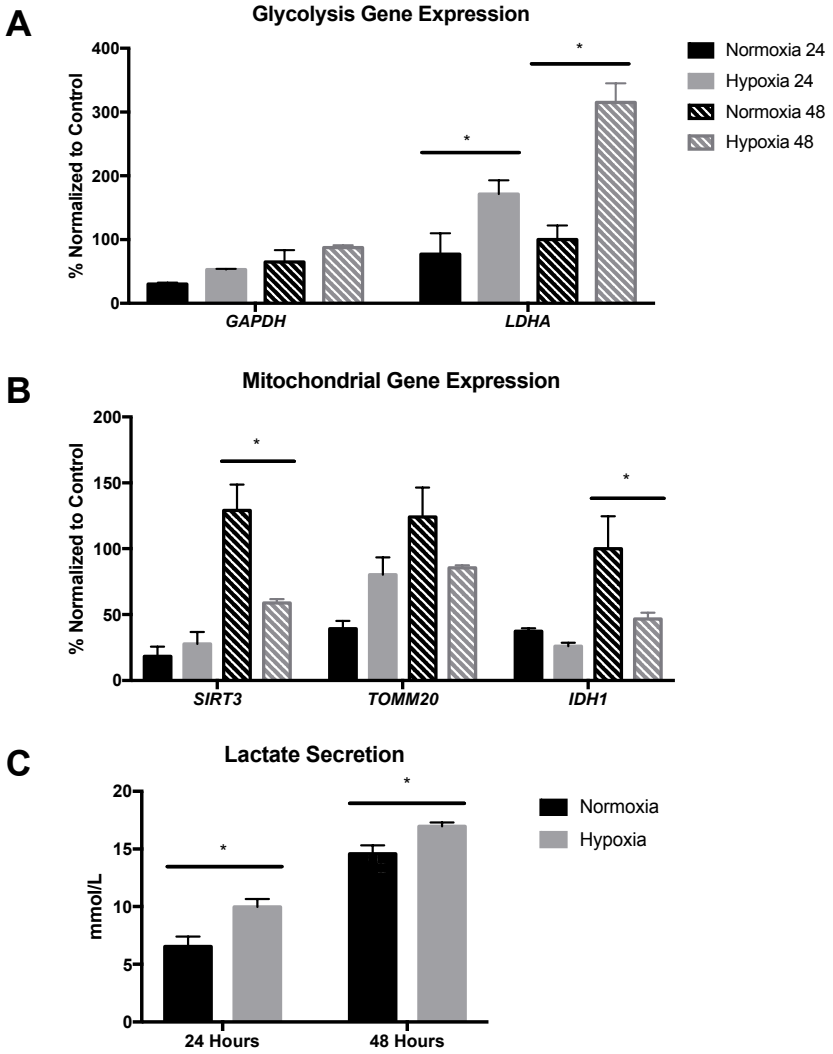

Figure 8: Glycolysis is increased after hypoxia exposure
(A) Glycolysis genes GAPDH and LDHA are significantly increased after 48-hours of hypoxia exposure. 24 hour: P<0.05; N=3. 48 hour: P=0.05; N=3. **(B)** Mitochondrial genes SIRT3, Tomm20, and IDH1 are decreased after 48-hours of hypoxia exposure. 48 hour: P=0.05; N=3. **(C)** Lactate in the media was significantly increased at both 24 and 48 hours after hypoxia exposure. P<0.05. Error bars indicated as SEM.

2.4.4 Hypoxic cells generate less ROS

Lastly, we evaluated mitochondrial function by determining ROS levels. Flow cytometry staining with MitoSox revealed similar levels of ROS after 24 hours of hypoxia (Figure 9A). By 48 hours of hypoxia exposure, the cells showed significantly reduced levels of ROS (Figure 9A). Decreased ROS would be indicative of a decreased reliance on mitochondrial metabolism, and suggests that these cells are in fact utilizing glycolysis. We also believe this further suggests that cells exhibit adaptation to hypoxia between 24 and 48 hours of exposure. Additionally, we evaluated *NOX4* (ROS-producing oxygen sensor) gene expression, which corresponded to the flow cytometry data with reduced ROS by 48 hours (Figure 9B).

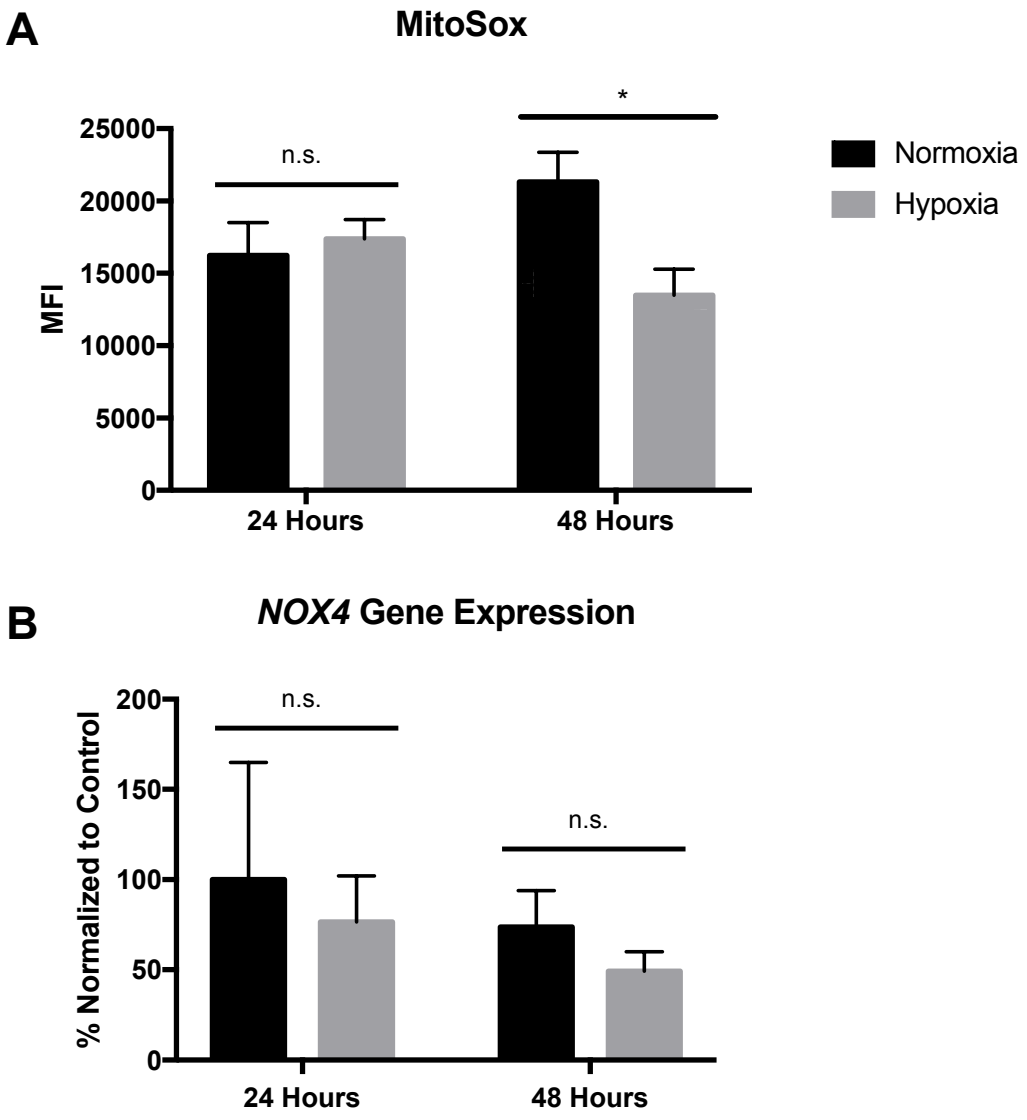

Figure 9: ROS is decreased during hypoxia exposure
(A) ROS is decreased after 48 hours of hypoxia exposure. 24 hours: P=0.69; N=3. 48 hour: P=0.04; N=3. Error bars indicated as SEM. **(B)** *NOX4* (ROS marker) gene expression is trending down in cells exposed to hypoxia. 24 hours: P=0.98; N=3. 48 hour: P=0.15; N=3. Error bars indicated as SEM.

2.5 DISCUSSION

Placental insufficiency and IUGR affect up to 7% of all pregnancies in the United States [142, 143]. Both of these conditions lead to fetal hypoxia, or lack of necessary oxygen supply [117]. Pathological fetal hypoxia often leads to preferential redirection of oxygenated blood towards organs such as the heart and brain over less vital organs [139]. This redirection of blood often leads to kidney underdevelopment and increases susceptibility to kidney disease, diabetes, and hypertension. Molecularly, cellular response to hypoxia is mediated by hypoxia-inducible factor (HIFs) transcription factors in order to facilitate an influx of oxygen and maintain cellular processes [117]. HIFs are highly expressed during hypoxia and regulate genes containing hypoxia response elements (HREs) [11, 115, 150]. Many HREs encode proteins involved in metabolism, primarily glycolysis, to help sustain energy production in the absence of oxygen [144]. Additionally, some HREs are responsible for the down-regulation of oxygen-dependent mitochondrial respiration [121]. Therefore, there is a clear link between oxygen availability and metabolic regulation.

Previous studies have shown that kidney "stem" cells, known as nephron progenitors, utilize different types of metabolism at different points in development [17]. Specifically, self-renewing, proliferative nephron progenitors rely more heavily on glycolysis than mitochondrial respiration, while nephron progenitors undergoing terminal differentiation utilize oxidative phosphorylation to a greater extent [17]. We believe that these differences in metabolism stem from the availability of oxygen at certain time points during development. Utilizing HEK293 cells cultured in normoxia and hypoxia, we found that oxygen availability leads to alterations in metabolic gene expression, proliferation, and ROS. Although alterations were revealed, sufficient adaptation was not apparent until after 24 hours of exposure. This indicates that

adaptation to hypoxia is a complex mechanism that does not occur instantaneously. Indeed, adaptation appeared to be sufficient by 48 hours, shown by a decrease in ROS, increase in glycolysis gene expression, and similar levels of proliferation between hypoxia and normoxia cultured cells. This study raises awareness regarding the interconnectivity between cell growth, metabolism, and hypoxia, particularly in development and cancer progression fields. Further discussion on the future directions and research limitations of this work are described in Chapter 6.1.

3.0 PRENATAL HYPOXIA INCREASES SUSCEPTILIBILTY TO ACUTE KIDNEY INJURY

This is an adaptation of the author's version of the work. The definitive version is being prepared for publication.

"Prenatal Hypoxia Increases Susceptibility to Kidney Injury"

Kasey Cargill[1,2*], Takuto Chiba[1,3*], Anjana Murali[1,2*], Elina Mukherjee[1], Elizabeth Crinzi[1], and Sunder Sims-Lucas[1,2,3]

[1]Division of Nephrology, Department of Pediatrics, UPMC Children's Hospital of Pittsburgh, Pittsburgh, PA, USA.

[2]University of Pittsburgh School of Medicine, Pittsburgh, PA, USA.

[3]Vascular Medicine Institute, University of Pittsburgh, Pittsburgh, Pennsylvania, USA

3.1 CHAPTER SUMMARY

Prenatal hypoxia is a gestational stressor that can result in developmental abnormalities or physiological reprogramming, and often decreases cellular capacity against secondary stress. When a developing fetus is exposed to hypoxia, blood flow is preferentially redirected to vital organs including the brain and heart over other organs including the kidney. Hypoxia-induced injury can lead to structural malformations in the kidney; however, even in the absence of structural lesions, hypoxia can physiologically reprogram the kidney leading to decreased function or increased susceptibility to injury. Our investigation in mice reveals that while prenatal hypoxia does not affect normal development of the kidneys, it primes the kidneys to have an increased susceptibility to kidney injury later in life. We found that our model does not develop structural abnormalities when prenatally exposed to modest 12% O_2 as evident by normal histological characterization and gene expression analysis. Further, adult renal structure and function is comparable to mice exposed to ambient oxygen throughout nephrogenesis. However, after treatment with cisplatin, the offspring of mice housed in hypoxia exhibit significantly reduced renal function and proximal tubule damage following injury. We conclude that exposure to prenatal hypoxia *in utero* physiologically reprograms the kidneys leading to increased susceptibility to injury later in life.

3.2 INTRODUCTION

Intrauterine hypoxia leading to prenatal hypoxia of the fetus is a common gestational stressor that can lead to a range of developmental abnormalities [160]. When prenatal hypoxia occurs, the developing fetus exhibits a preferential redirection of blood flow, including oxygen and nutrient supply, to the brain and heart over organs such as the kidney [139, 161]. Previous studies in mouse and rat models of prenatal hypoxia often utilize a chambered hypoxia device, where pregnant dams are housed at 12% O_2 [162, 163]. These studies show that exposure to mild hypoxia *in utero* can impair pre- and post-natal development [164] and can induce epigenetic modifications [165]. Although both structural and non-structural abnormalities can arise from prenatal exposure to hypoxia, the long-term effect of this stressor in the kidneys is still largely unknown.

The kidneys are the filtration units of the body and the nephron is the functional unit of the kidney responsible for blood filtration, removal of toxic wastes, and regulation of several important physiological functions [6, 7, 16]. Kidney development in the mouse takes place from embryonic day 10.5 (E10.5) through postnatal day 3 (P3) corresponding to approximate gestational weeks 5 through 35 in humans [166]. During this time, a population of self-renewing cells called nephron progenitors rapidly proliferate then undergo differentiation to give rise to the glomerular and renal tubular epithelia of the mature nephron [167]. This process of nephron development occurs under physiological hypoxia (~1-9% O_2) [162], and although temporary changes in oxygen tension are normal, chronic hypoxia can be detrimental [168]. Maternal chronic prenatal hypoxia of less than 10% oxygen has been shown to lead to physical and structural abnormalities [139, 160, 169, 170]. In one study, pregnant dams with a CD1 background housed in 12% O_2 from E14.5 to P1 found that female offspring were unaffected,

however male offspring exhibited decreased body weight, decreased kidney weight, and alterations in tubular development and in the corticomedullary ratio [171]. Although structural abnormalities can arise due to hypoxia exposure, we hypothesize that even in the absence of structural malformations, the kidneys are more susceptible to disease later in life. This increased susceptibility may be a result of physiological reprogramming, a phenomena that decreases cellular functionality of the kidneys to be more susceptible to injury later in life.

One such injury that affects both pediatric and adult patient populations is acute kidney injury (AKI). AKI is an abrupt loss of kidney function characterized by significant decreases in glomerular filtration as well as increases in serum creatinine and blood urea nitrogen (BUN) levels, which lead to high morbidity and mortality rates [172, 173]. It is also a risk factor for progression to chronic kidney disease (CKD) and eventually end-stage renal disease (ESRD) [174]. It is known that AKI is multifactorial and caused by distinct insults including ischemia, nephrotoxins, and sepsis [175]. Cisplatin is a widely used cytotoxic chemotherapeutic agent and is a known nephrotoxin that causes acute and chronic injury in the kidneys [176, 177]. A major complication of cisplatin treatment is AKI, which occurs in up to 30% of patients [176]. Cisplatin targets both nuclear and mitochondrial DNA and for this reason primarily affects the highly metabolically active proximal tubules [177, 178]. While multiple conditions such as aging and CKD also predispose to AKI [179, 180], there is little known about the effect of prenatal hypoxia on susceptibility to AKI.

Herein, we generated a mouse model of prenatal hypoxia and uncovered a sub-pathological role for hypoxia as a mediator of susceptibility to kidney injury. Our study reveals that mice exposed to prenatal hypoxia during nephrogenesis exhibit exacerbated cisplatin-induced AKI in adulthood. Our study highlights the importance of strict regulation of

oxygenation in the developing kidney and suggests prenatal hypoxia may physiologically reprogram the nephrons, leaving them more susceptible to injury.

3.3 METHODS AND MATERIALS

3.3.1 Prenatal hypoxia in mice

C57BL/6 wild type time-mated females (gestation age E10.5; Charles River) were placed in a hypoxia chamber. The chamber was equipped with a purge airlock system, CO_2 and O_2 control indicators, and humidity and gas monitoring control systems designed for live animal experiments. Exposure to 12% hypoxia was initiated on embryonic day 10.5 (E10.5), which coincides with the induction of nephrogenesis. Hypoxia exposure was terminated on postnatal day 3 (P3), which coincides with the conclusion of nephrogenesis. Control mice with normoxia treatment were housed in ambient conditions at 21% O_2. For embryonic renal assessments, pregnant dams were sacrificed on E16 by CO_2 inhalation followed by cervical dislocation. For post-natal renal assessment, hypoxia-exposed pups were transferred to ambient O_2 on P3 and sacrificed at 7 weeks of age by CO_2 inhalation followed by cervical dislocation. Kidney tissue was immediately collected and stored for analysis. The University of Pittsburgh Institutional Animal Care and Use Committee approved all experiments (Approval No. 16088935).

3.3.2 Cisplatin-induced AKI in mice

For the secondary stressor model, another cohort of time-mated female C57BL/6 wild type mice gestation age E10.5 were used following the same normoxia and hypoxia conditions from E10.5 through P3. The mice exposed with hypoxia or normoxia were maintained in regular vivarium with 21% O_2 ambient conditions until 7 weeks of age. At 7 weeks of age, the mice were treated with cisplatin (APP NDC 63323-103-64, 20mg/kg bw, ip; Appendix F) in normal saline or with normal saline vehicle control. The mice were sacrificed 72 hours after cisplatin treatment by cervical dislocation after isoflurane anesthesia. Blood and kidney tissue were immediately collected and stored for analysis. The University of Pittsburgh Institutional Animal Care and Use Committee approved all experiments (Approval No. 16088935).

3.3.3 Tissue collection and histological assessment

Tissue was collected at E16.5 and 7 weeks and immediately flash frozen in liquid nitrogen or fixed in 4% paraformaldehyde (PFA). Fixed tissue was processed and embedded in paraffin. Embedded tissue was sectioned at 4 μm thickness and stained with hematoxylin and eosin (H&E) for histological examination. Renal tubular pathology was semiquantitvely scored in a blind fashion on corticomedullary fields (40x magnification). Samples were imaged using a Leica DM 2500 microscope (Leica) and LAS X software (Leica). Histological scoring was performed in a blinded fashion at 40x magnification on corticomedullary regions of the tissue sections from N=4 animals. Eight sections were evaluated for injury per sample. Glomerular quantification was performed blinded using a low power field. Manual counting was done on the corticomedullary regions of the tissue sections from N=4 animals. Corpuscle and glomerular

quantification was done using ImageJ Software using at least N=4 animals. Lengths were measured in triplicate and averaged per glomeruli or corpuscle. The glomerular-to-corpuscle ratio was done by dividing the average glomerular length per glomeruli by the average corpuscle length per corresponding corpuscle.

3.3.4 Serum analysis

7 week old pups were subjected to cardiac punctures prior to sacrifice for the collection of blood. Blood was subsequently centrifuged for 10 minutes at 10,000rpm to collect serum. Serum was analyzed for blood urea nitrogen and creatinine at the Kansas State Veterinary Diagnostic Laboratory.

3.3.5 Immunofluorescent staining

Immunofluorescent staining was performed on paraffin embedded samples as described above. Sections were deparafinized and rehydrated according to the following: 100% xylene for 5 min, 100% ethanol for 5 minutes, 70% ethanol for 5 minutes, 50% ethanol for 5 minutes. Each step was done in duplicate. Antigen retrieval was done using citrate buffer buffered to pH=6. Slides were put into a pressure cooker and microwaved for approximately 17 minutes. Samples were probed using primary antibodies or lectins (1:100; Appendix D): neural cell adhesion molecule (Ncam; Sigma-Aldrich), sine oculis homeobox homolog 2 (Six2; Proteintech), phosphor-histone H3 (Phh3; Cell Marque), endomucin (Santa Cruz Biotechnology), Wilm's tumor 1 (WT1; Santa Cruz Biotechnology), Lotus tetragonolobus (LTL; Vector Laboratories), Organic anion transporter 1 (OAT1; Alpha Diagnostic International), Dolichos biflorus agglutinin (DBA;

Vector Laboratories), Kidney injury molecule 1 (Kim1; R&D Systems), and Terminal deoxynucleotidyl transferase dUTP nick-end labeling kit (TUNEL; EDM Millipore) all co-stained with DAPI (Thermo Fisher Scientific). Samples were imaged using a Leica microscope (Leica Microsystems) and LAS X software (Leica Microsystems).

3.3.6 Real time quantitative polymerase chain reaction (PCR)

RNA was extracted from the flash frozen kidney tissue at E16.5, E18.5 and 7 weeks using the miRNAeasy Mini Kit (Qiagen). Synthesis of cDNA was done as preciously described in 2.3.2. The following genes were analyzed using this method: *Cited1, Lhx1, Pax2,* and *Wnt4*. Gene expression was normalized to *Rn18s*. Primer sequences are listed in Appendix B.

3.3.7 Statistical analysis

Minimums of 3 biological replicates were used for each experiment in at least technical duplicate. When comparing two sample groups, statistical significance was determined using a two-tailed Student's t test ($\alpha = 0.05$). Significance was defined as *P<0.05, **P<0.01, and ***P<0.001. Where appropriate, data is presented as mean ± standard error of the mean. Data was analyzed using Microsoft Excel and figures were generated using GraphPad Prism 7.

3.4 RESULTS

3.4.1 Prenatal hypoxia does not alter embryonic kidney development

To investigate the effect of hypoxia during kidney development, time-mated C57B/6 female mice were placed into hypoxia chambers with 12% oxygen beginning on embryonic day 10.5 (E10.5) and maintained in hypoxia until the conclusion of nephrogenesis on postnatal day 3 (P3) (Figure 10A). Pregnant control females were housed in ambient oxygen (normoxia) for the duration of their pregnancy. Litter sizes between dams housed in normoxia and hypoxia were similar (P=0.67) with a mean litter size of 4 pups. Hypoxia exposed E16.5 kidneys appeared to undergo normal developmental processes and histological examination did not reveal any significant abnormalities (Figure 10B-E). A cohort of the pups exposed to prenatal hypoxia were transferred to normoxia at P3 and at 7 weeks of age those mice also did not exhibit any significant alterations in renal histology (Figure 10F-I).

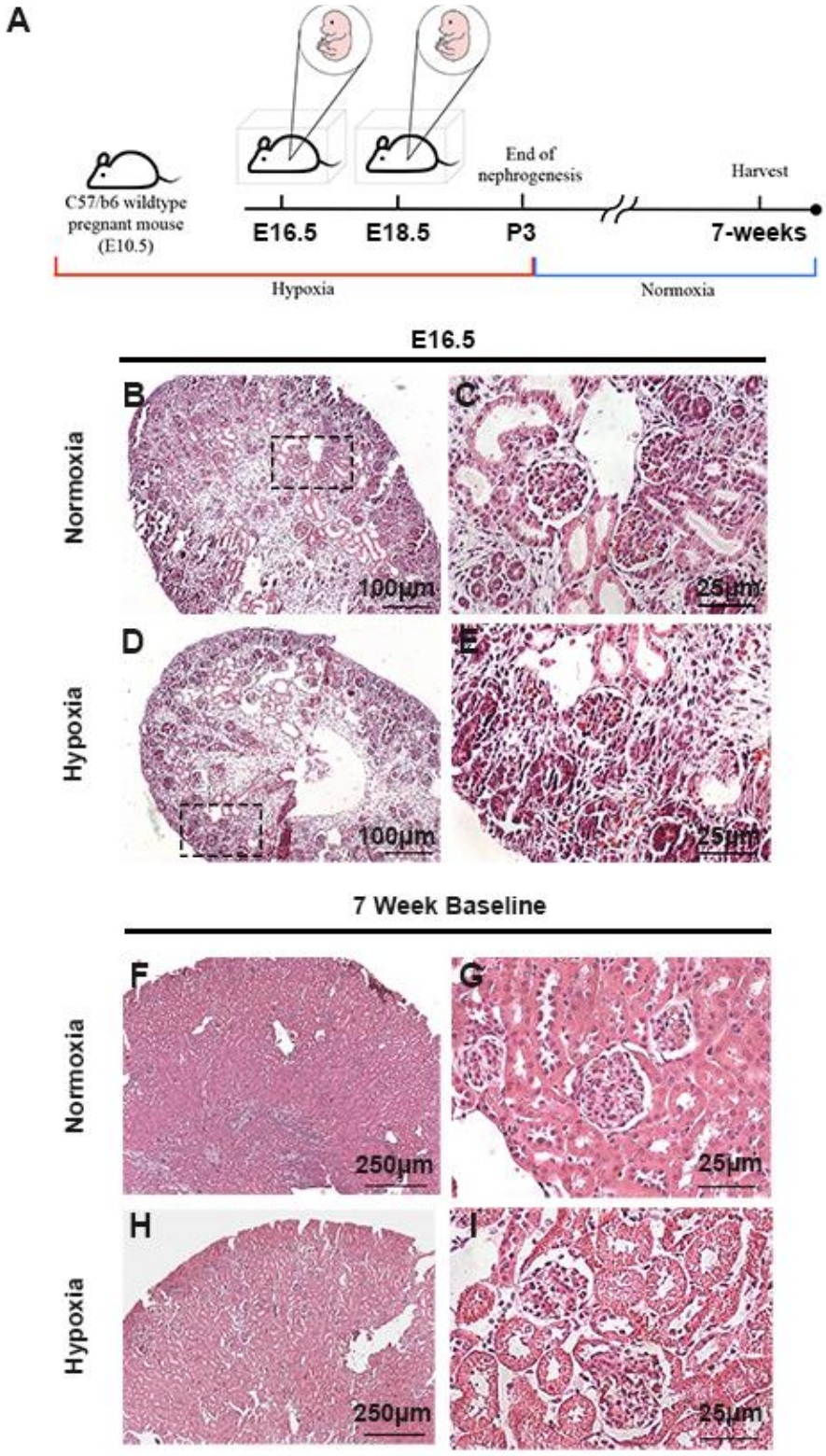

Figure 10: Prenatal hypoxia exposure does not alter histological structure of the kidneys
(**A**) Schematic illustration for the mouse model of prenatal exposure to hypoxia during kidney development. (**B-E**) H&E staining from E16.5 prenatal hypoxia exposed kidneys exhibit normal development. (**F-I**) H&E staining from 7-week mice shows no significant structural abnormalities.

To further investigate whether any developmental defects were present, we performed immunofluorescent staining on E16.5 kidneys to evaluate kidney development using markers for nephron progenitor self-renewal (Sine oculis homeobox homolog 2; Six2) and developing structures (Neural cell adhesion molecule; Ncam). Neither Six2 nor Ncam immunostaining revealed any structural malformations or alterations in nephron number. Proliferation of the nephron progenitors was evaluated by immunostaining against phospho-histone H3 (pHH3), which appeared to be occurring at comparable rates in both normoxia and hypoxia-exposed kidneys. Apoptosis analysis through TUNEL immunostaining showed that cell death was confined to the renal stroma [181] and appeared comparable between normoxia and hypoxia exposed kidneys (Figure 11A-F). Additionally, mRNA levels of nephron progenitors (*Cited1* and *Pax2*) and nephron differentiation (*Wnt4* and *Lhx1*) were not altered between the two cohorts (Figure 11G). Likewise, we performed immunostaining to observe proximal tubule development and ureteric branching, neither of which revealed any abnormalities (Figure 11H-O). Together, this suggests that prenatal exposure to 12% oxygen in the C57B/6 background strain does not lead to alterations in structural kidney development by mid-nephrogenesis.

We next evaluated the progression of renal development at E18.5. Similarly, we immunostained again Six2, Ncam, Phh3, and TUNEL and did not observe any abnormalities at this later stage of nephrogenesis (Figure 12A-F). Gene expression of *Cited1*, *Pax2*, *Wnt4*, and *Lhx1* also remained unchanged between the two groups (Figure 12G). Lastly, we quantified the kidney length and body length of E18.5 animals and did not reveal any differences in the size of the kidneys or bodies of offspring exposed to hypoxia (Figure 12H-I). The kidney-to-body length ratios also remained consistent (Figure 12J). Therefore, there are no structural differences in early, mid, or late kidney development in mice exposed to pre-natal hypoxia.

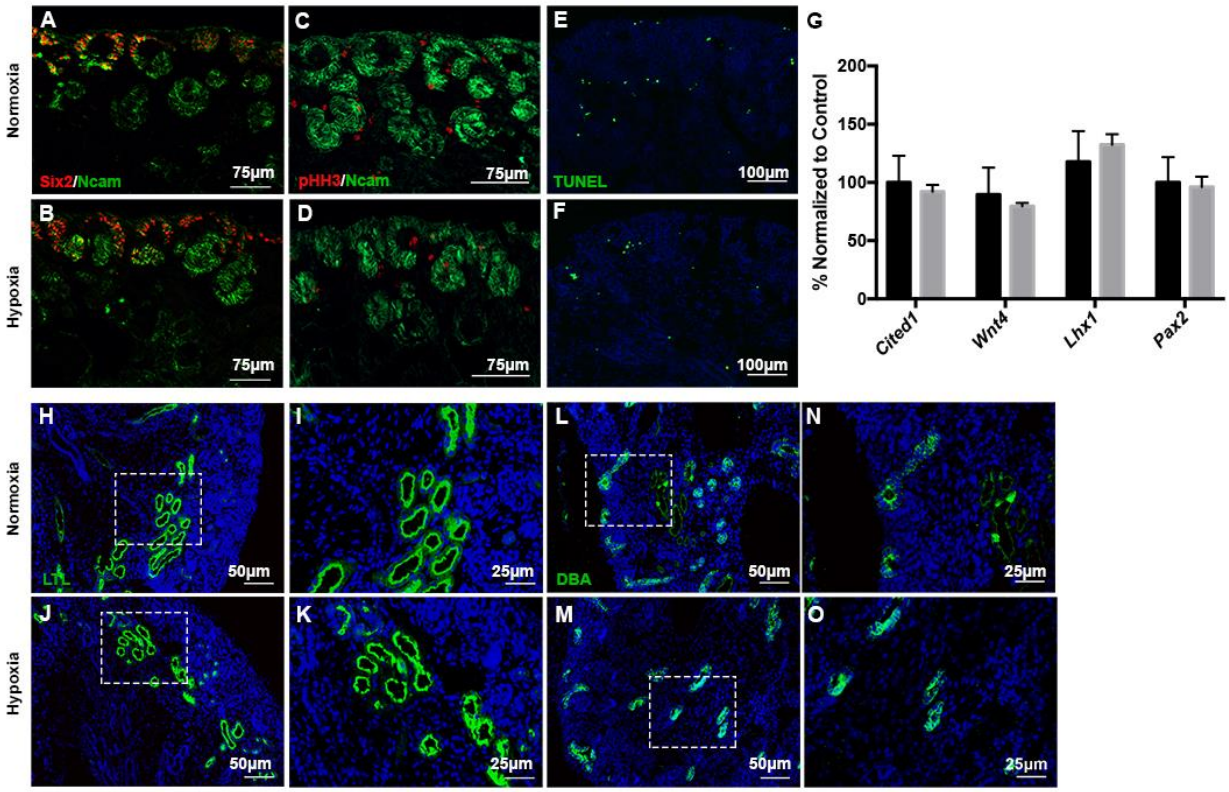

Figure 11: Prenatal hypoxia exposure does not alter development of the kidneys at E16.5
(**A-B**) Immunofluorescent staining with antibodies against Six2 (red) and Ncam (green) show no differences in nephron progenitor differentiation when exposed to prenatal normoxia (top) versus hypoxia (bottom) at E16.5. (**C-D**) Immunofluorescent staining with antibodies against pHH3 (red) and Ncam (green) reveal no differences in cell proliferation in cells exposed to normoxia (top) and hypoxia (bottom). (**E-F**) TUNEL (green) staining exhibits similar apoptosis levels in hypoxic (top) and normoxic cells (bottom). (**G**) RT-qPCR analysis of genes associated with nephron progenitors (*Cited1, Pax2*) and differentiation (*Wnt4* and *Lhx1*) have similar levels of mRNA expression between prenatal normoxia- (black) and hypoxia- (grey) exposed kidneys. N=4. Error bars indicated as SEM. (**H-K**) Immunofluorescent staining with LTL at E16.5 shows no differences in proximal tubule formation between normoxic (top) and hypoxic (bottom) kidneys. (**L-O**) Immunofluorescent staining against DBA at E16.5 exhibits no developmental phenotype during ureteric bud branching and differentiation.

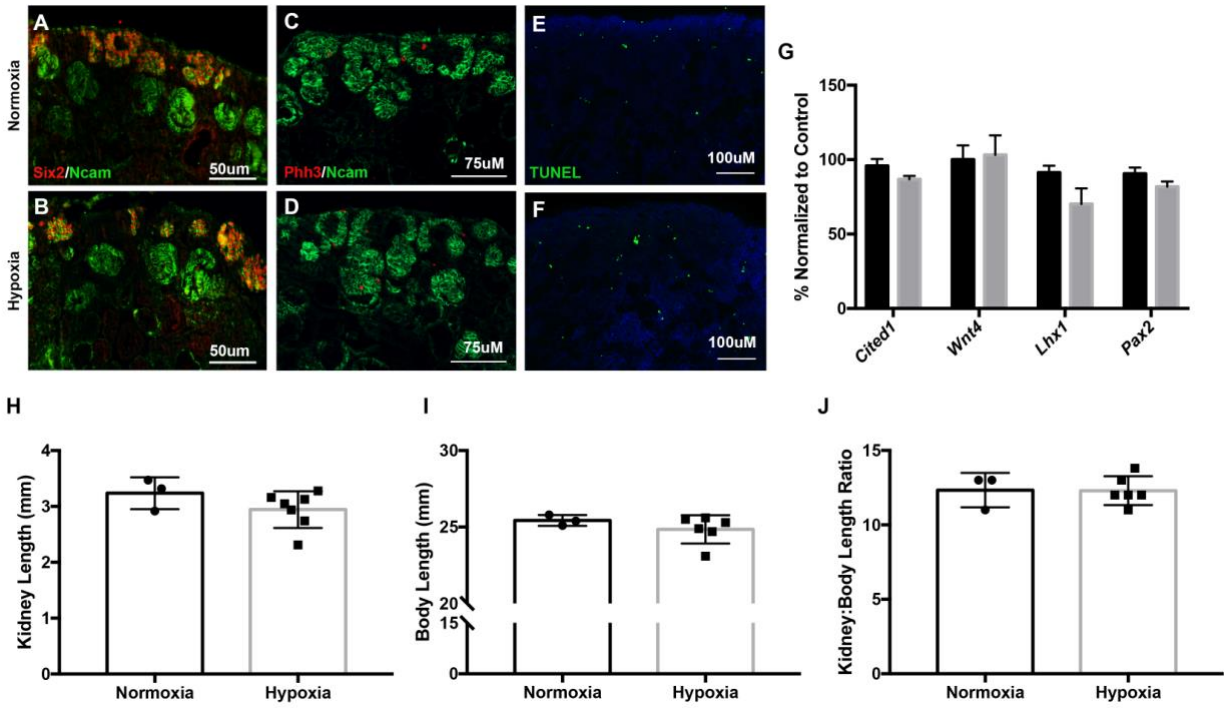

Figure 12: Prenatal hypoxia exposure does not alter development of the kidneys at E18.5
(**A-B**) Immunofluorescent staining with antibodies against Six2 (red) and Ncam (green) show no differences in nephron progenitor differentiation when exposed to prenatal normoxia (top) versus hypoxia (bottom) at E18.5. N=3. (**C-D**) Immunofluorescent staining with antibodies against pHH3 (red) and Ncam (green) reveal no differences in cell proliferation in cells exposed to normoxia (top) and hypoxia (bottom). (**E-F**) TUNEL (green) staining exhibits similar apoptosis levels in hypoxic (top) and normoxic cells (bottom). (**G**) RT-qPCR analysis of genes associated with nephron progenitors (*Cited1, Pax2*) and differentiation (*Wnt4* and *Lhx1*) have similar levels of mRNA expression between prenatal normoxia- (black) and hypoxia- (grey) exposed kidneys. N=4. Error bars indicated as SEM. (**H-J**) No differences in kidney length (P=0.21), body length (P=0.34), or the kidney-to-body length ratio (P=0.96) of E18.5 embryos; Normoxia N=3; Hypoxia N=7.

3.4.2 Prenatal hypoxia alone does not disrupt adult renal function

Next, we assessed renal structure and function at 7 weeks of age. Immunofluorescent staining using LTL and Oat1 (markers of proximal tubule brush borders and proximal tubule epithelial cells, respectively) did not reveal the development of structural abnormalities by 7 weeks of age (Figure 13A-B). There were also no significant differences in glomerular structure (Figure 13C-D) or vascularization (Figure 13E-F) in 7-week mice exposed to prenatal hypoxia compared to normoxia-exposed controls. BUN and creatine measurements were also not significantly altered

in prenatal hypoxia exposed mice (Figure 13G; data not shown). Creatinine levels were all below a detectable 0.5 mg/dL concentration. To confirm that nephrogenesis occurred normally, we quantified the number of glomeruli using unbiased manual counting of glomerular structures. Both mouse cohorts had similar numbers of formed glomeruli (Figure 13H). Further, we quantified the corpuscle and glomerular size, which again did not reveal any differences in nephron development (Figure 13I). Lastly, the weight of the animals did not differ between exposure groups (Figure 13J). Therefore, prenatal hypoxia alone does not lead to major alterations in renal structure or function in C57B/6 adult mouse kidneys.

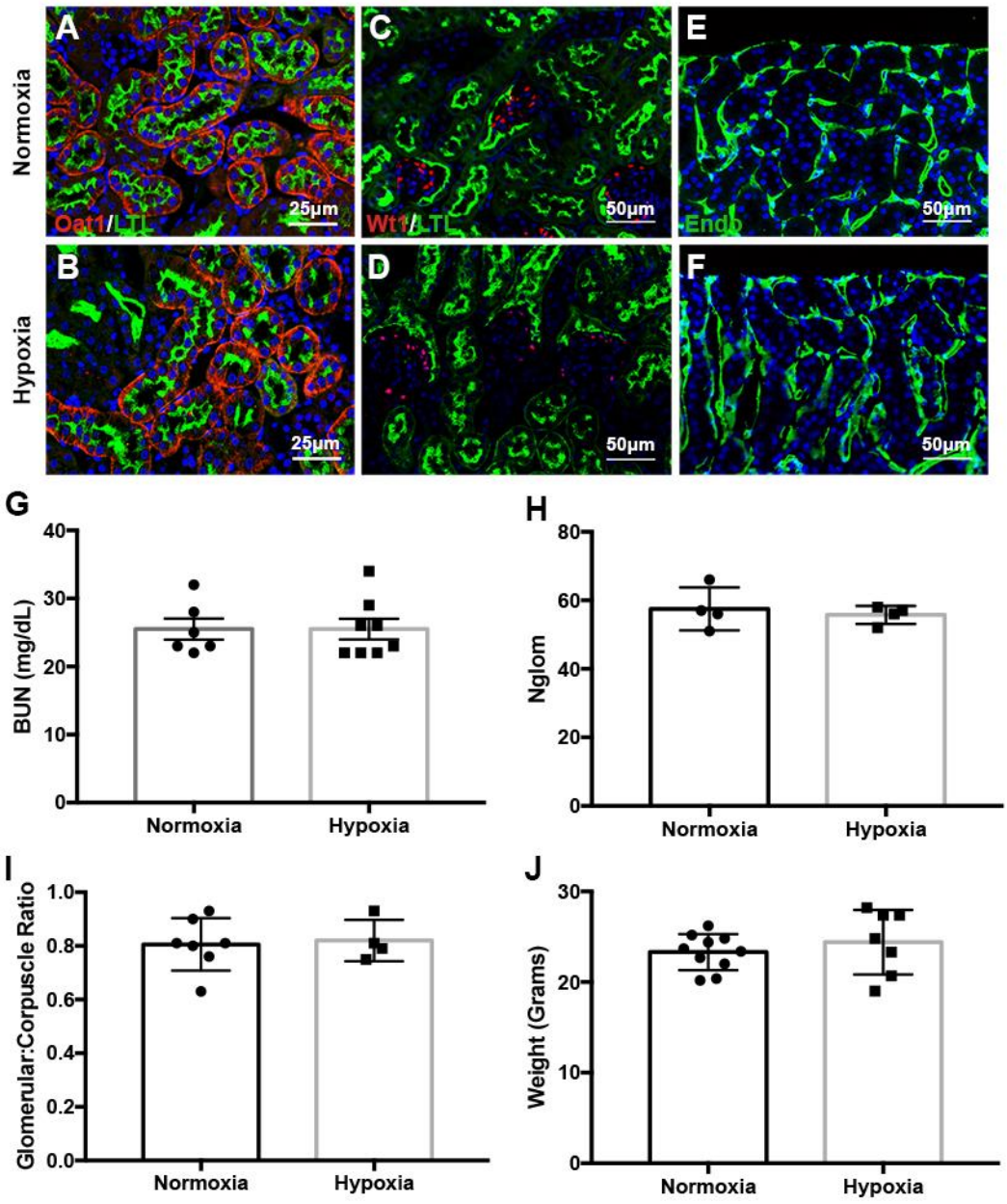

Figure 13: Prenatal hypoxia exposure does not alter structure or function of adult kidneys
(**A-B**) Immunofluorescent staining with antibodies against Oat1 (red) and LTL (green) do not reveal any differences in the proximal tubules of prenatal hypoxia-exposed kidneys (bottom) when compared to normoxia-exposed kidneys (top) at 7 weeks. (**C-D**) Immunofluorescence staining with antibodies against Wt1 (red) and LTL (green) reveal no difference in glomerular structure at 7 weeks. (**E-F**) Immunofluorescence staining with antibodies against endomucin (Endo; green) indicates similar levels of vascularization. (**G**) Levels of renal functional marker, blood urea nitrogen (BUN), is not altered by prenatal hypoxia exposure; Normoxia N=6; Hypoxia N=7; P>0.99. Error bars indicated as SEM. (**H**) Quantification of the glomeruli indicated no differences in nephron number; N=4; P=0.62; Error bars indicated as SEM. (**I**) There were no differences in the size of the glomeruli or corpuscles of animals exposed to prenatal hypoxia compared to controls; Normoxia N=7; Hypoxia N=4; P=0.81. Error bars indicated as SEM. (**J**) There were no differences in the body weight of animals exposed to prenatal hypoxia compared to controls; Normoxia N=10; Hypoxia N=7; P=0.43. Error bars indicated as SEM.

3.4.3 Prenatal hypoxia increases susceptibility to cisplatin-induced AKI

Next, we aimed to determine whether prenatal hypoxia in the absence of structural abnormalities led to increased kidney injury susceptibility. Another cohort of mice that were exposed to prenatal hypoxia were subjected to a single injection of the nephrotoxin cisplatin (20mg/kg bw, ip) and were sacrificed 3 days post injury (3 dpi) (Figure 14A). The prenatal hypoxia kidneys exhibited exacerbated cisplatin-induced injury. Injury included increased formation of proteinaceous casts and severe dilation of the proximal tubules (Figure 14B-E) when compared to normoxia-exposed kidneys. Histopathological scoring revealed a significantly higher level of injury severity (P=0.038). Scoring was done such that a 1 indicated insignificant injury while 5 indicated severe injury. Kidneys that were prenatally exposed to hypoxia had significantly more regions that were designated a 5 compared to normoxia-exposed controls (Figure 14F). Accompanying the tubular injury, these mice exhibited significantly increased levels of blood urea nitrogen (BUN) and creatinine in serum indicating reduced kidney function (Figure 14G-H). Furthermore in the prenatal hypoxia exposed kidneys, immunofluorescent staining with LTL and Oat1 revealed increased frequency of epithelial sloughing and dilation in the proximal tubules (Figure 15A-B). Proximal tubule dilation was quantified and quantification revealed prenatal hypoxia-exposed kidneys treated with cisplatin had significantly increased dilation compared to both baseline hypoxia and prenatal normoxia-exposed kidneys treated with cisplatin (Figure 15C). Hypoxia-exposed kidneys treated with cisplatin also had significantly increased expression of kidney injury marker 1 (Kim1) (Figure 15D-H). Together, this data reveals that although prenatal oxygen levels do not contribute to developmental structural abnormalities, low oxygen conditions prime the kidneys for injury later in life.

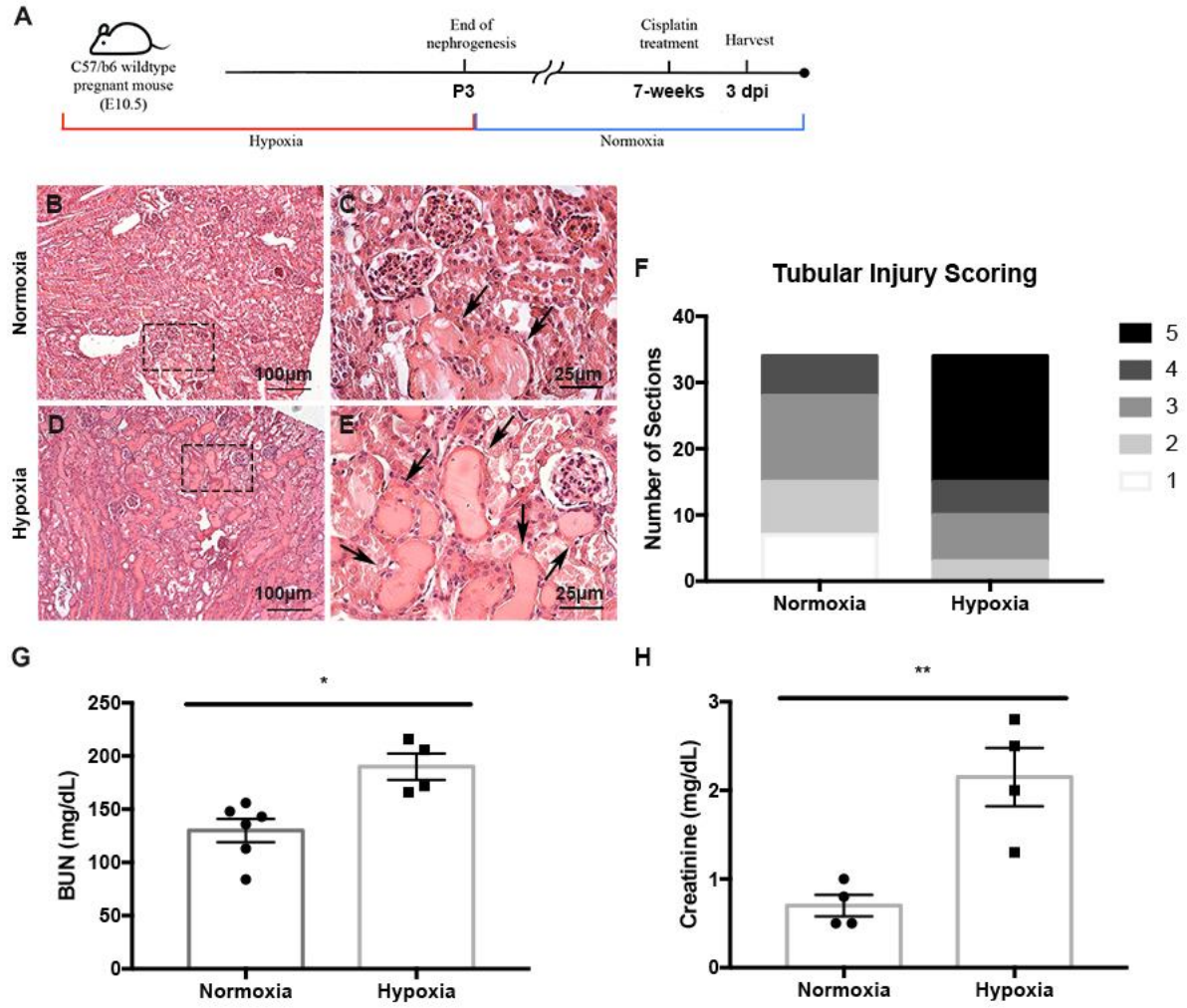

Figure 14: Prenatal hypoxia exposure decreases renal function after cisplatin-induced kidney injury
(**A**) Schematic illustration for mouse model of prenatal hypoxia, coupled with cisplatin-induced AKI in the adult stage. The mice were sacrificed at 3 days post-injury with cisplatin (3 dpi). (**B-E**) H&E staining of kidneys exposed to prenatal hypoxia and treated with cisplatin at 7 weeks (bottom panels) shows increased formation of proteinaceous casts (arrows) and dilation of the proximal tubules compared to prenatal exposure to normoxia with cisplatin treated kidneys (top panels). (**F**) Mice exposed to prenatal hypoxia exhibited a significantly higher injury severity score; $P<0.05$, N=4. (**G**) Hypoxia-exposed mice (grey) have significantly higher BUN levels; Normoxia N=7; Hypoxia N=4. $P<0.05$. Error bars indicated as SEM. (**H**) Hypoxia-exposed mice (grey) show a significant increase in creatinine levels; Normoxia N=4; Hypoxia N=4. $P<0.01$. Error bars indicated as SEM.

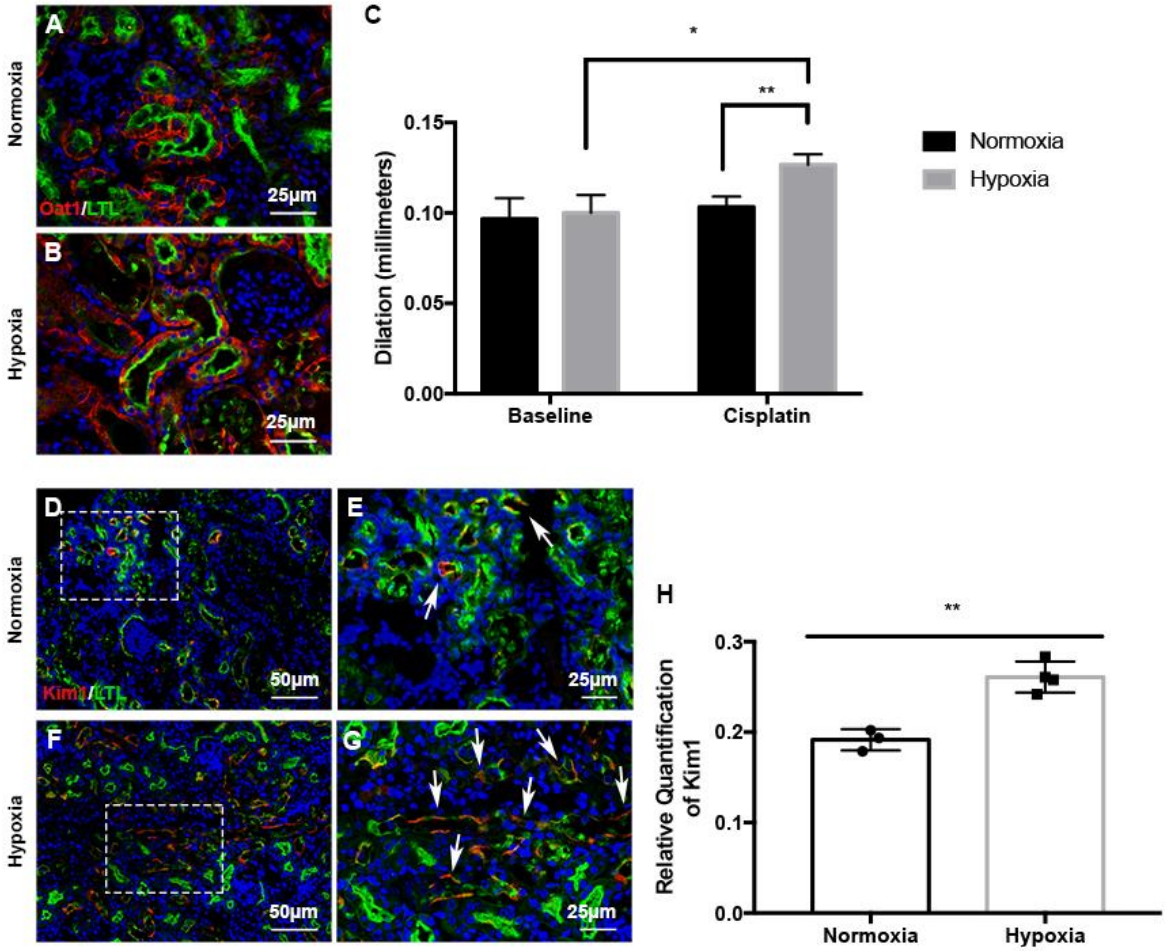

Figure 15: Prenatal hypoxia exposure increases proximal tubular injury after cisplatin-induced kidney injury (**A-B**) Immunofluorescence staining with antibodies against Oat1 (red) and LTL (green) at 3 dpi reveals further increased rate of epithelial sloughing in the proximal tubules in prenatal hypoxia exposed mice after cisplatin treatment. (**C**) Proximal tubule dilation was quantified at baseline and 3dpi. Prenatally hypoxia-exposed mice exhibited significantly increased tubular dilation compared to control animals; ANOVA and student t-test: *P<0.05, **P<0.01; N=3; Error bars indicated as SEM. (**D-G**) Immunostaining with antibodies against Kim1 (red) and LTL (green) at 7 weeks shows further increased injury marker expression (arrows) in prenatal hypoxia-exposed kidneys (bottom). (**H**) Quantification of Kim1-positive area shows further increased Kim1 expression in prenatal hypoxia exposed kidneys (grey); P<0.01, N=3. Error bars indicated as SEM.

3.5 DISCUSSION

Prenatal hypoxia is a multifactorial condition and can be caused by a variety of factors including placental insufficiency, pre-eclampsia, malnutrition, and even high altitude living during pregnancy [163, 182]. Prenatal hypoxia results in decreased blood and nutrient flow to the fetus

leading to decreased oxygen availability in the kidney [139, 161]. In consequence, any complication resulting in prenatal fetal hypoxia can cause changes in fetal growth or organ functionality thereby increasing the risk for diseases later in life [182]. In this study, we interrogated the role of prenatal hypoxia on long-term susceptibility to cisplatin-induced kidney injury.

Our study did not reveal any structural developmental kidney defects in offspring of dams exposed to hypoxia. At both 12% O_2 and ambient oxygen (~21% O_2), the kidneys exhibited a comparable degree of differentiation, proliferation and apoptosis of E16.5 and E18.5 nephron progenitors regardless of oxygen treatment. Although this finding differs slightly from previous investigations utilizing similar hypoxia oxygen concentrations [10, 183, 184], we hypothesize that the lack of developmental defect could be explained by the difference of hypoxic conditions and by the mouse strain used in previous studies. Our study used a modest hypoxia model with an oxygen concentration set at 12% O_2 to maximize survival by treatment. Other studies often use a more severe oxygen concentrations. One study using 12% O_2 and mice with a CD-1 background showed that 12% O_2 was sufficient to mediate structural abnormalities during development, however our investigation utilized mice with a C57B/6 background. The CD-1 mouse strain also exhibits higher mortality in response to hypoxia [185] by activating a maladaptive hypoxia response through HIF-1□□up regulation [186]. Therefore, this is a plausible reason behind the lack of structural abnormalities in our model, thus allowing for an interrogation of physiological reprogramming in the absence of structural abnormalities.

Less is currently known about the sub-pathological role of prenatal hypoxia on organ injury later in life. It has previously been shown that prenatal hypoxia decreases adaptive potential of the brain and subsequently increases the risk of neurodegenerative disorders such as

Parkinson's disease in late adulthood [187, 188]. Further the heart has been shown to undergo physiological reprogramming in relation to *in utero* hypoxia leading to injury susceptibility later in life [125, 189, 190]. However, prenatal hypoxia in the absence of structural defects has not been well studied in kidney injury models.

To precisely dissect the effect from prenatal hypoxia in susceptibility to kidney disease later in life, we challenged the offspring mice that were exposed to prenatal hypoxia with acute nephrotoxicity via a high dose of cisplatin treatment. Mice subjected to prenatal hypoxia displayed increased susceptibility to cisplatin injury despite the absence of clear developmental defects. Cisplatin causes cellular damages in the S3 segment of renal proximal tubular epithelial cells in mice [191]. Our data demonstrated that cisplatin treatment increased expression of proximal tubule specific injury marker, Kim-1, in the group exposed to prenatal hypoxia as well as increased renal functional markers, creatinine and BUN. This study acts as a proof of principle by clearly showing that strict regulation of developmental oxygenation is critical for long-term renal function. Although prenatal hypoxia exposure leads to exacerbated kidney injury, the mechanism leading to this finding is still unclear.

Although this study does not delve into the mechanisms leading to disease, we hypothesize that a physiological reprogramming event occurs during development that primes the kidneys for injury after secondary insult, in this case cisplatin treatment. One possible mechanism that leaves the tubules susceptible to injury may be, at least in part, through stimulation of pathological reactive oxygen species (ROS). ROS is a consequence of incomplete oxygen reduction during mitochondrial respiration [192]. Aberrant ROS production has also been previously implicated as a marker of severe kidney injury and chronic kidney disease [104, 193, 194]. In kidneys after ischemia-reperfusion injury, damaged proximal tubules shift their

major energy production from oxidative phosphorylation to glycolysis as part of the de-differentiation process [74]. There has been some interrogation into the relationship between hypoxia pathways and ROS, however the mechanisms of action are currently inconclusive [147, 195-198]. Although these mechanisms are currently unknown, it is clear that hypoxia and ROS influence adaptive gene expression and may be responsible for the phenotype shown in the present study. Another potential mechanisms that has been implicated in cisplatin-induced kidney injury is the Renin-Angiotensin System. The Renin-Angiotensin System is involved in blood pressure regulation and vascularization and has been previously investigated in prenatal hypoxia and cisplatin studies [199-201]. Independent of vascular roles, cisplatin is known to increase its nephrotoxicity via interaction with Renin-Angiotensin System in T lymphocytes and kidney epithelial cells [201] and could be a pathway of future investigation in developmental physiological reprogramming of the kidneys.

The present study has several limitations and raises a number of questions. It has been previously proposed that age and sex play a role in hypertension pathology after prenatal hypoxia [199]. For this reason, it will be important to evaluate the role of age and sex in susceptibility to cisplatin injury of the offspring after prenatal hypoxia. Further, hypoxia inducible factors (HIFs) and the hypoxia inducible microRNA, miR-210, are regulated in the kidneys after AKI, and thus should also be robustly evaluated [182]. In rats, development of pre-eclampsia-like symptoms of pregnant dam by prenatal hypoxia is mediated by Endothelin-1 (ET-1) signaling [202] and ET-1 interacts with the Renin-Angiotensin system [203]. Therefore, it is also important to assess the role of the Renin-Angiotensin system in pregnant dams and evaluate the effect of this system on developing kidneys in order to explore therapeutic targets.

In conclusion, we show that embryonic hypoxia exposure predisposes mice to enhanced kidney injury after cisplatin treatment during adulthood even in the absence of initial structural abnormalities. This study suggests that sub-pathologically low oxygen concentrations during fetal development may play a critical role in the physiological programming of the nephron in the absence of structural abnormalities and could be used as a prognosticator for kidney disease susceptibility in adults. Further discussion on the future directions and research limitations of this work are described in Chapter 6.2.

4.0 VON HIPPEL LINDAU ACTS AS A METABOLIC SWITCH CONTROLLING NEPHRON PROGENITOR DIFFERENTIATION

This is an adaptation of the author's version of the work. The definitive version is published in

The Journal of the American Society of Nephrology.

"Von Hippel Lindau Acts as a Metabolic Switch Controlling Nephron Progenitor Differentiation"

DOI: 10.1681/ASN.2018111170

Kasey Cargill[1,2], Shelby Hemker[1,2], Andrew Clugston[1,2,3], Anjana Murali[1,2], Elina Mukherjee[1], Daniel Bushnell[1], Jiao Liu[5,6], Andrew Bodnar[1], Zubaida Saifudeen[5,6], Jacqueline Ho[1,2,3], Dennis Kostka[3], Carlton Bates[1,2], Eric Goetzman[2,4], and Sunder Sims-Lucas[1,2 *]

[1]Division of Nephrology, Department of Pediatrics, UPMC Children's Hospital of Pittsburgh, Pittsburgh, PA, USA.

[2]University of Pittsburgh School of Medicine, Pittsburgh, PA, USA.

[3]Department of Developmental Biology, University of Pittsburgh School of Medicine, Pittsburgh, PA, USA.

[4]Division of Medical Genetics, Department of Pediatrics, University of Pittsburgh School of Medicine, Pittsburgh, PA, USA.

[5]Section of Pediatric Nephrology, Department of Pediatrics, Tulane University Health Sciences Center, New Orleans, LA 70112, USA.

[6]The Hypertension and Renal Centers of Excellence, Tulane University Health Sciences Center, New Orleans, LA 70112, USA.

4.1 CHAPTER SUMMARY

Kidney development is a tightly regulated process that is necessary for normal long-term kidney function. Nephron progenitors are a stem cell population that exists within the developing kidney and give rise to the functional unit of the kidney, the nephron. Nephron progenitors are a metabolically active cell population and self-renew under glycolytic conditions. A switch from glycolysis to mitochondrial respiration drives these cells towards differentiation. However, the mechanisms that control this switch are poorly defined. Here, we explore von Hippel Lindau (VHL) as a regulator defining nephron progenitor self-renewal versus differentiation. This investigation reveals a previously unknown mechanism controlling the balance between nephron progenitor self-renewal and differentiation. In nephron progenitor specific *VHL* knockout mice, differentiated nephron progenitors exhibit persistent Six2 expression ultimately leading to decreased nephron endowment and renal dysfunction. Furthermore, we found that nephron progenitors with a VHL deletion favor glycolytic metabolism and rely less on mitochondrial respiration for energy production. This suggests that VHL normally serves to promote a switch from glycolysis towards oxidative phosphorylation, which is critical for nephron progenitors to undergo differentiation.

4.2 INTRODUCTION

Nephron development initially involves reciprocal signaling between the ureteric epithelium (UE) and the cap mesenchyme (CM), a region comprised of renal cells known as nephron progenitors [5]. These nephron progenitors are under strict regulation either to maintain a progenitor state or differentiate [18]. The transcription factor *Six2* plays a major role in the maintenance of the proliferating progenitor population [11, 27, 204]. In self-renewing nephron progenitors, both *Six2* and the cofactor *Cited1* are initially expressed, however *Cited1* expression becomes down regulated at the beginning of differentiation [18, 27, 205, 206]. As nephron progenitors mature, *Six2* also becomes down regulated and the cells begin to express differentiation markers indicating commitment to a mesenchyme to epithelial transition (MET) [11, 31]. This transition, marked by *Wnt4* expression, occurs as CM cells make mature cell-cell contacts and ultimately form functional nephrons [30]. The maturing nephron progenitors give rise to the nephron: a complex structure comprised of a glomerulus and epithelialized tubules that are connected to the collecting duct system [6].

Kidney formation is highly dependent on oxygen concentration [117] and previous studies show that low levels of oxygen (hypoxia) can result in renal malformations including nephron deficit [183, 207]. The kidney initially develops in a relatively hypoxic environment and as the vasculature perfuses, oxygen levels increase [118]. This tightly regulated change in oxygenation coordinates with the inductive signals from the UE to drive proliferation and subsequent differentiation of the nephron progenitors. Hypoxia inducible factors (HIFs) play a large role in mediating cellular responses to oxygen fluctuations. Although there are three HIF isoforms (HIF-1α, HIF-2α, and HIF-3α), HIF-1α is considered the master regulator of developmental responses to hypoxia [109]. HIF-1α is known to stimulate angiogenesis and

maturation of the vasculature, which drives blood flow into hypoxic areas, thereby increasing oxygen concentration [108, 118]. Increases in oxygen facilitate HIF-1α's degradation via recruitment of von Hippel-Lindau (VHL) [108, 118]—a protein component of a ubiquitin ligase complex. If prenatal exposure to pathological hypoxia occurs in the nephron progenitors, VHL is not recruited to degrade HIF-1α allowing for its sustained expression and transcriptional activation of genes containing hypoxia response elements (HREs) [11-13].

Many confirmed HREs are found in genes that encode glycolytic enzymes [11, 12, 14]. High rates of glycolysis allow progenitor cells to rapidly undergo expansion through proliferation and nucleotide generation [15-17]. However as differentiating cells mature, they utilize mitochondrial respiration to maintain energy demands of the cell [120, 121, 144]. HIF-1α is largely responsible for the metabolic profile of progenitor cells and functions in a dual role by promoting glycolysis while suppressing mitochondrial respiration [84, 85, 121]. It has also been shown that nephron progenitors exhibit a gradual, decreased reliance on glycolysis between embryonic day 13.5 (E13.5) and 19.5 (E19.5) [17]. While early stage nephron progenitors rely heavily on glycolysis [17], terminally differentiated nephrons have a unique metabolic profile depending on the particular nephron segment [208]. The proximal tubule segment, which is responsible for a majority of the reabsorption performed by the kidney, utilizes fatty acids, oxidative phosphorylation, and gluconeogenesis to support these critical functions [50, 208, 209]. For these reasons, we hypothesize that the switch from glycolysis to mitochondrial respiration is regulated via VHL-mediated HIF-1α degradation in nephron progenitors during development.

Herein, we report an interrogation into the role of VHL/HIF signaling in mediating nephron progenitor differentiation. Global *VHL* knockout mice are embryonic lethal [108],

suggesting that VHL plays a critical role in embryonic development. To circumvent embryonic lethality, we generated nephron progenitor-specific *VHL* knockout mice (*VHL*$^{NP-/-}$) to interrogate the role of VHL in nephron development. Our investigation reveals that loss of *VHL* results in metabolic dysregulation, which inhibits nephron progenitor differentiation.

4.3 METHODS AND MATERIALS

4.3.1 Experimental mouse model

We bred transgenic Six2EGFPcre mice (JAX009606) [210] with VHL-floxed mice (JAX12933) [211] to generate mice with conditionally deleted VHL in Six2cre+ cells. This generated mice that conditionally delete VHL in the Six2cre-positive nephron progenitors. The University of Pittsburgh Institutional Animal Care and Use Committee approved all experiments (Approval No. 16088935).

4.3.2 Mouse model genotyping

The presence of GFP in the dissected kidneys was visualized with a fluorescent microscope and confirmed using PCR. Embryonic tissue or tail clippings from postnatal animals were collected and genomic DNA was extracted. The primers used for the Six2EGFPcre allele and VHL allele can be found in Appendix C. The cre-positive band is at 350 basepairs while cre-negative mice had no band. The VHL homozygous band is around 500 basepairs and heterozygous bands at 307 base pairs and around 500 basepairs.

4.3.3 Western blotting

Whole kidneys were lysed in radioimmunoprecipitation assay buffer (RIPA buffer; Thermo Scientific) and the homogenates were plated in triplicate to measure protein concentration using a Bradford assay kit (Bio-Rad). Samples were electrophoresed on Bolt™ 4-12% Bis-Tris Plus Gels (ThermoFisher Scientific) for approximately 1 hour at 100V and transferred to 0.2 μm pore size nitrocellulose membranes using the Bolt Western blotting system (ThermoFisher Scientific) for 1 hour at 10V per manufactures guidelines. Antibodies used include (Appendix D): anti-VHL (Santa Cruz Biotechnology, 1:250), anti-HIF-1α (Novus, 1:250), anti-α/β tubulin (Cell Signaling Technology, 1:1000) Secondary antibodies include: anti-IgG rabbit HRP (Cell Signaling Technology, 1:1000) and anti-IgG mouse HRP (Cell Signaling Technology, 1:250). Blots were imaged using a ProteinSimple FluoroChem M System (ProteinSimple) and quantified using ImageJ software (ImageJ/NIH Image).

4.3.4 Tissue collection and histological assessment

Renal histology was assessed at E13.5, E15.5, P1, P21, and P30 in *VHL*$_{NP+/-}$ and *VHL*$_{NP-/-}$ mice. At the indicated time points, embryos (E15.5) or dissected kidneys (P1, P21, P30) were fixed, processed, and sectioned as previously described in 3.3.3. Samples were stained with Hematoxylin and Eosin (H&E) for histological examination or used for immunostaining. The following primary antibodies or lectins were used at a 1:100 dilution unless indicated (Appendix D): anti-Six2 (Proteintech), anti-Ncam (Sigma-Aldrich), anti-Glut1 (Abcam), anti-phospho-histone H3 (pHH3; Cell Signaling), Terminal deoxynucleotide transferase dUTP Nick End Labeling (TUNEL; EMD Millipore), anti-Lef1 (Cell Signaling), anti-Sall1 (Abcam), anti-Wt1

(Santa Cruz Biotechnology), anti-Jag1 (Santa Cruz Biotechnology; 1:20), anti-Pck1 (Proteintech), dolichos biflorus agglutinin (DBA; Vector Laboratories) and lotus tetragonolobus lectin (LTL; Vector Laboratories). Samples were imaged using a Leica microscope (Leica Microsystems) and LAS X software (Leica Microsystems).

4.3.5 3-Dimensional (3D) reconstruction

E13.5 embryos were collected for 3D reconstructions of *VHL*$_{NP+/-}$ and *VHL*$_{NP-/-}$ kidneys. Embryos were fixed as previously described [212]. Five embryos for each genetic group were evaluated via 3D reconstruction as described [212]. A Zeiss Model Axio Imager M1 (Zeiss) microscope with Stereo Investigator Stereology image tracing software (MBF Bioscience) was used for analysis.

4.3.6 Flow cytometry

Kidneys were dissecte from P1 *VHL*$_{NP+/-}$ and *VHL*$_{NP-/-}$ mice. Kidneys were digested using 0.3% collagenase and forced through needlepoint to create a single cell suspension. For cell cycle analysis: Cells were fixed using cold 75% methanol for four hours then stained with Propidium Iodide FxCycle PI/RNase Staining Solution (Thermo Fisher Scientific; Appendix E). For mitochondrial density: 1 x 10_6 cells were stained for 30 minutes at 37°C using 200nM MitoTracker™ Red FM (Thermo Fisher Scientific; Appendix E). The cells were analyzed on a BD LSRFORTESSA cell analyzer (BD Biosciences) (BD Biosciences) through the Flow Cytometry Core at the Rangos Research Center located at the UPMC Children's Hospital of Pittsburgh. Mean fluorescence intensity (MFI) was determined using FlowJo software (v10.1).

4.3.7 Physical dissector/fractionator combination method

P21 kidneys were dissected from *VHL*$_{NP+/-}$ and *VHL*$_{NP-/-}$ mice then fixed and processed as described previously. Embedded samples were completely sectioned at 4 μm thickness. All P1 kidney slides were stained with anti-WT1 (Thermo Fisher Scientific, 1:100) while every 3 slides of P21 samples were subjected to H&E staining [213, 214]. The n_{th} (reference section) and n_{th} + 2 (lookup section) sections were counted for glomeruli as described [213] using Stereo Investigator Stereology Software (MBF Bioscience) on a Zeiss Model Axio Imager M1 (Zeiss) microscope.

4.3.8 Quantification of P1 nephron number

P21 *VHL*$_{NP+/-}$ and *VHL*$_{NP-/-}$ P1 kidneys were dissected, fixed, and processed as described previously. The entire kidney was serially sectioned at 4μm and immunostained with rabbit anti-WT1 antibody and visualized using a Vectastain ABC Kit (Vector Laboratories), per manufacturer's guidelines [215]. For quantification, consecutive sections from every 20 were selected and WT1+ structures were identified using a Wacom drawing tablet (Wacom) and Stereoinvestigator v.9.04 software [215]. Glomerular number was calculated according to the equation by Cullen-McEwen *et al* [213].

4.3.9 Serum analysis

P21 *VHL*$_{NP+/-}$ and *VHL*$_{NP-/-}$ mice were subjected to cardiac puncture for blood collection. Serum was analyzed as previously described in 3.3.4.

4.3.10 RNA-sequencing analysis

RNA sequencing was performed on E17.5 isolated nephron progenitors. E17.5 kidneys were dissected and screened using the GFP expression. Dissected kidneys that expressed GFP were dissociated into single cell suspensions and sorted using a BD FACsaria II cell sorter (Flow Cytometry Core, Rangos Research Center. Each sample consisted of approximately 150,000 pooled control or mutant nephron progenitor cells. RNA was extracted using the miRNeasy Mini Kit (Qiagen). The Health Sciences Sequencing Core at Children's Hospital of Pittsburgh performed library construction and RNA sequencing (single-end reads, 75bp). Bioinformatics quality control was performed using FastQC (version 0.11.5) [216], and adapters were trimmed using BBDuk from the BBMap software package (version 37.41) [217]. Reads were aligned to transcripts assembled from the mm10 genome (GRCm38, GENCODE M17) [218] using the Spliced Transcripts Alignments to a Reference software package (STAR, version 2.5.3a) [219]. Data analysis was performed using the R programming language (version 3.4.3) [220]. Reads aligned to known transcripts were counted using the Bioconductor [221] GenomicAlignments package (version 1.10.1) [221], and differential expression between $VHL_{NP+/-}$ and $VHL_{NP-/-}$ kidney samples was calculated using the DESeq2 R package (version 1.18.1) [222]. Functional annotation analysis was performed using the DAVID database (release 6.8, https://david.ncifcrf.gov/) [223, 224]. Data deposited into Gene Expression Omnibus (GEO Accession Number: GSE122900).

4.3.11 Real-time quantitative polymerase chain reaction (PCR)

E17.5 whole kidney RNA was used to validate the E17.5 isolated nephron progenitor RNA sequencing as described in 2.3.2. The following genes were analyzed: *Pgk1*, *Gapdh*, *Tpi1*, *Bnip3*, *Ddit4*, *Pdk1*, *Eno1*, *Slc16a3, Cited1, Six2, Lef1, Sall1*, *Osr1*, *Eya1*, *Jag1*, *Sox9*, *Foxd1* and *Wnt4*. Primer sequences are listed in Appendix B.

4.3.12 Magnetic activated cell sorting (MACS) nephron progenitor isolation

Nephron progenitors were isolated from *VHL*$_{NP+/-}$ and *VHL*$_{NP-/-}$ kidneys using magnetic-activated cell sorting (MACS, Mitenyi Biotec; [17, 27]). The kidney capsule and ureters were removed from P1 kidneys to expose the nephrogenic zone and washed with Hank's balanced salt solution (HBSS). Kidneys were digested with 0.25% collagenase and 1% pancreatin [27]. Cells were isolated by negative selection via incubation with antibodies against endothelial progenitors (anti-CD105), RBCs and erythroid cells (anti-TER119), cortical interstitium (anti-CD140a), and renal epithelial cells (anti-CD326) following manufactures instruction (Mitenyi Biotec) [27]. Isolated nephron progenitors were seeded in a monolayer on Matrigel-coated (Corning) culture plates at 100,000 cells per well with APEL-based (Stem Cell Technologies) NPME media as previously described [27]. Cells were incubated overnight then subjected to extracellular flux analysis.

4.3.13 Seahorse extracellular flux mitochondrial stress test

Kidneys were pooled from multiple litters for P1 MACS nephron progenitor isolation. Cells were seeded at 100,000 cells per well on Matrigel-coated Seahorse microplates for flux analysis on the XF24 Extracellular Flux Analyzer (Aligent Seahorse Technologies) [17]. *VHL*$_{NP+/-}$ and *VHL*$_{NP-/-}$ nephron progenitors were subjected to a mitochondrial stress test via the sequential administration of specific metabolic pathway inhibitors. The XF sensor cartridges were hydrated overnight at 37° C without carbon dioxide in Seahorse XF calibrant solution. The assay medium was Seahorse XF unbuffered DMEM supplemented with 3-5 mM pyruvate, 5mM D-glucose, and 2 mM L-glutamine (pH 7.4) [17]. Metabolic profiling was performed by measuring basal respiration for 25 minutes followed by the sequential injection of the substrates oligomycin (1 μg/mL; Appendix F), cyanide p-trifluoromethoxy-phenylhydrazone (FCCP, 0.3 μM; Appendix F), and rotenone (0.1 μM; Appendix F) with antimycin A (1μM; Appendix F) [17]. Measurements were taken at eight-minute intervals for 3 hours. Basal respiration, ATP production, maximal respiration, and glycolysis ratios were calculated from a total of three biological data sets done in at least technical duplicate. Data normalized to cell number.

4.3.14 Pyruvate oxidation assay

VHL$_{NP+/-}$ and *VHL*$_{NP-/-}$ P1 mouse kidneys were dissected and homogenized in serum-free Dulbecco's modified Eagle's medium (DMEM) without glucose supplementation. To determine pyruvate oxidation, tissue homogenates were incubated at 37° C with uniformly labeled ^{14}C-pyruvate in sealed in glass tubes sealed with rubber stoppers fitted with hanging baskets. The hanging baskets held 1cm square filter paper inserts soaked in potassium hydroxide (1M). After

30 minutes, perchloric acid (0.5M) was introduced by needle to acidify the media and the reactions were incubated for at 37° C for 1hr to collect ^{14}C-CO_2 [225, 226]. ^{14}C-pyruvate incorporation was measured by scintillation counting and normalized to cellular protein content.

4.3.15 Kidney explant glycolysis inhibition

E13.5 kidneys were cultured on 0.4μm polyethylene terephthalate membrane inserts as previously done [215]. One kidney from each embryo was cultured in improved minimal essential media (IMEM; containing 50 μg/mL transferrin) alone and the other was cultured in media containing 10 μM YN1 inhibitor (Appendix F) [17, 215]. After 72 hours kidneys were fixed in 4% paraformaldehyde for 1 hour. Kidneys were immunostaining with antibodies against Six2 and Jag1 following the previous methods [215].

4.3.16 Statistical analysis

A minimum of 3 biological replicates was used for each experiment in at least technical duplicate. When comparing two sample groups, statistical significance was determined using a two-tailed Student's t test ($\alpha = 0.05$). Significance was defined as *$P<0.05$, **$P<0.01$, and ***$P<0.001$. Where appropriate, data is presented as mean ± standard error of the mean analyzed with figures generated using GraphPad Prism 7.

4.4 RESULTS

4.4.1 *VHL* expression is required for differentiation of nephron progenitors

To determine the functional significance of VHL in nephron progenitors, we conditionally deleted *VHL* from Six2+ nephron progenitors by crossing transgenic *Six2-TGC^{tg}* mice [210] to *VHL$^{lox/lox}$* mice [211] (Figure 16A). This produced *VHL* wild type (*Six2-TGC$^{+/+}$; VHL$^{lox/lox}$* (*VHL$^{NP+/+}$*)), heterozygous knockout (*Six2-TGC $^{tg/+}$; VHL$^{+/lox}$* (*VHL$^{NP+/-}$*)), and homozygous knockout (*Six2-TGC $^{tg/+}$; VHL$^{lox/lox}$* (*VHL$^{NP-/-}$*)) genotypes. *Six2-TGC$^{tg/+}$* embryos enabled GFP visualization in *VHL$^{NP+/-}$* and *VHL$^{NP-/-}$* animals. Due to a slight hypoplastic phenotype associated with the *Six2GFPcre* transgene [227], we used *VHL$^{NP+/-}$* littermate controls for all experiments. VHL protein expression (Figure 16B) and HIF-1α protein stabilization (Figure 15C) in *VHL$^{NP+/-}$* and *VHL$^{NP-/-}$* kidneys confirmed sufficient knockdown and stabilization, respectively. Moreover, subsequent RNA-sequencing analysis (see results below) validated *VHL* knockout specifically in the nephron progenitors.

Histological examination of *VHL$^{NP-/-}$* kidneys did not reveal any significant alterations in development at embryonic day 13.5 (E13.5; Figure 16D-E). However, by E15.5 the *VHL$^{NP-/-}$* kidneys begin to exhibit reduced maturation of the nephron progenitors (Figure 16F-G). By postnatal day 1 (P1) *VHL$^{NP-/-}$* kidneys are smaller and remain developmentally delayed (Figure 16H-I) with fewer nephron progenitor-derived structures (see results below).

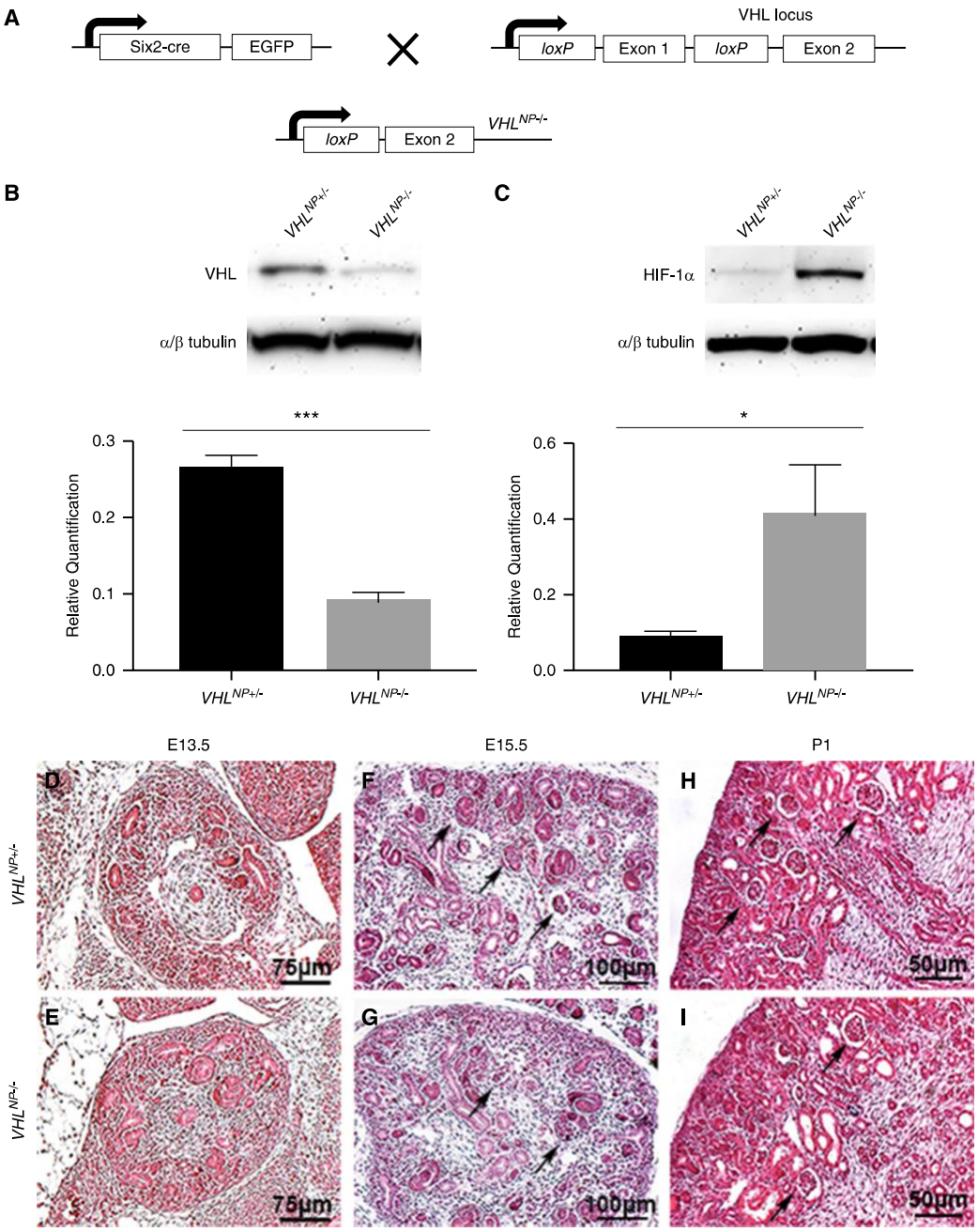

Figure 16: Conditional deletion of *VHL* from Six2+ nephron progenitors
(A) Experimental breeding strategy to obtain successful *VHL* deletion in nephron progenitors using *Six2-TGC*$_{tg}$ and *VHL*$_{lox/lox}$ mice **(B)** Whole kidney homogenates from P1 *VHL*$_{NP+/-}$ and *VHL*$_{NP-/-}$ mice subjected to Western blotting with antibodies against VHL and α/β-tubulin to confirm VHL deletion; ***P<0.0001; *VHL*$_{NP+/-}$ N=3; *VHL*$_{NP-/-}$ N=5. Error bars indicated as SEM. **(C)** Whole kidney homogenates from P1 *VHL*$_{NP+/-}$ and *VHL*$_{NP-/-}$ mice subjected to Western blotting with antibodies against HIF-1α and α/β-tubulin to confirm HIF-1α stabilization; *P<0.05; N=4. Error bars indicated as SEM. **(D-E)** Hematoxylin and Eosin (H&E) staining of kidneys sectioned at E13.5 appears developmentally normal. **(F-I)** H&E staining of kidneys sectioned at E15.5 and P1 exhibit hypoplasia and reduced developing glomeruli (arrows).

To determine the onset of the developmental phenotype, we performed 3-Dimentional (3D) reconstructions of E13.5 kidneys to evaluate kidney size and maturation, which supported the histological examination. The number of glomerular structures, renal vesicles, and immature glomeruli were not significantly altered nor were there differences in kidney volume, ureteric epithelium volume, or glomerular volume (Figure 17A-H).

Next, we evaluated the expression of nephron progenitor and renal vesicle markers through immunofluorescent staining of E15.5 and P1 *VHL*$_{NP+/-}$ and *VHL*$_{NP-/-}$ kidneys as E15.5 is when we first observe a phenotype and P1 is largely an older progenitor population. Staining against the nephron progenitor marker Six2 with Ncam to mark the nascent nephrons at E15.5 (Figure 18A-B) and P1 (Figure 18C-D) revealed that *VHL*$_{NP-/-}$ kidneys have persistent Six2 expression in Ncam+ structures. Further, Ncam expression was also decreased at both E15.5 and P1 suggesting there may be alterations in cell adhesion between nephron progenitors (Figure 18A-D). For these reasons, we quantified the number of Six2+ cells per cap at P1 and found a increase (P=0.006; Figure 18I). Next, we performed immunostaining against Jag1 (differentiating structures) and saw a reduction in the number of Jag1+ structures (P=0.008; Figure 18E-H;J), which further suggests that *VHL*$_{NP-/-}$ kidneys exhibit decreased differentiation.

To evaluate differentiation capacity, we performed unbiased, stereological counting of Wt1+ glomeruli at P1 and found a 30% decrease (P=0.01; Figure 19A). Although there is a significant decrease in the number of nephrons, the kidney-to-body weight ratio at P1 was unchanged between *VHL*$_{NP+/-}$ and *VHL*$_{NP-/-}$ mice (Figure 19B).

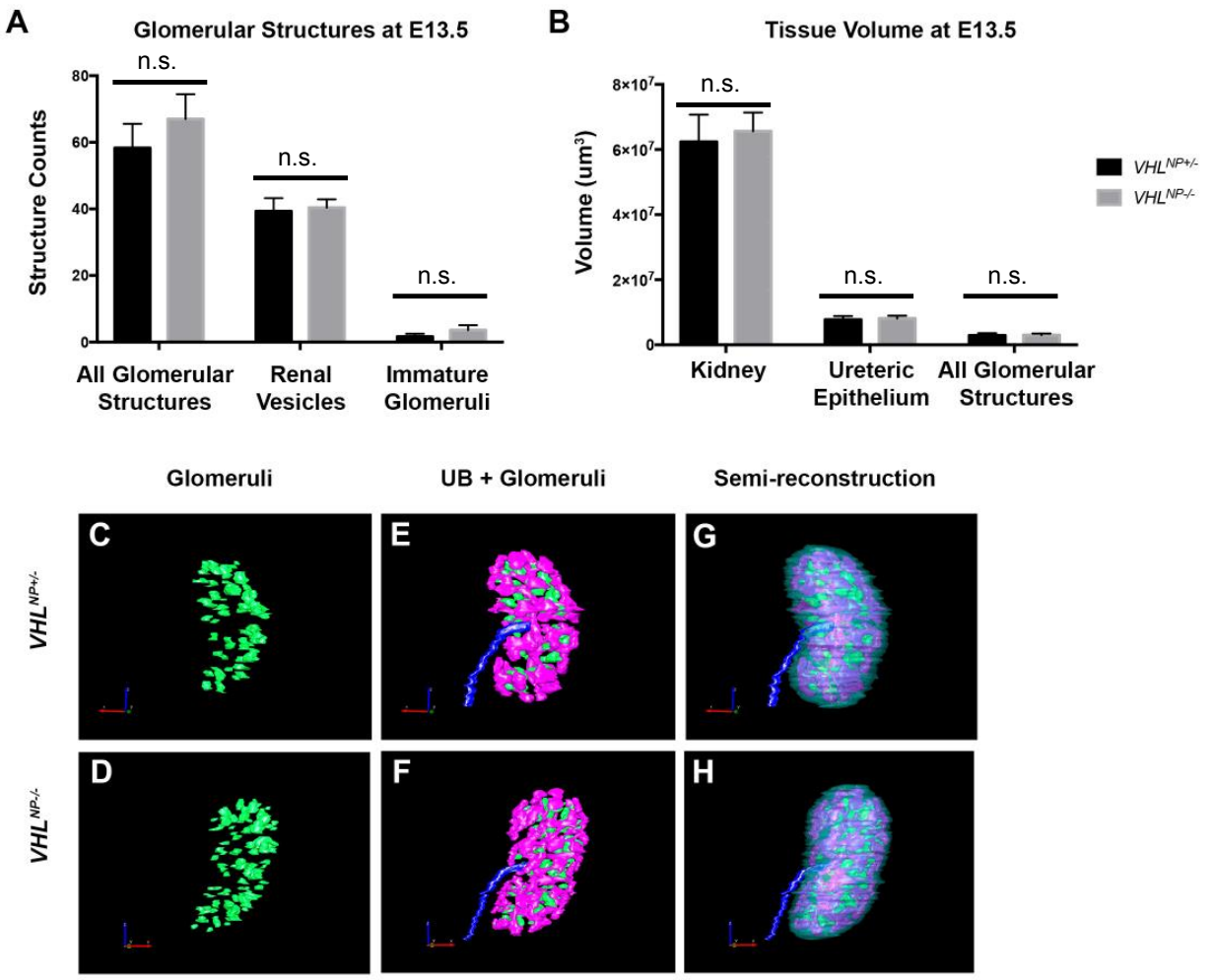

Figure 17: *VHL*$_{NP-/-}$ mice exhibit altered kidney development after E13.5
(A) 3-Dimensional (3D) reconstruction of E13.5 *VHL*$_{NP+/-}$ and *VHL*$_{NP-/-}$ kidneys showing glomerular structure formation. No significant differences in glomerular structure (P=0.47), renal vesicle formation (P=0.81), or immature glomeruli number (P=0.39). *VHL*$_{NP+/-}$ N=3; *VHL*$_{NP-/-}$ N=5. Error bars indicated as SEM. **(B)** 3D reconstruction of E13.5 *VHL*$_{NP+/-}$ and *VHL*$_{NP-/-}$ kidneys showing tissue volume. No significant differences in kidney volume (P=0.75), ureteric epithelium volume (P=0.78), or glomerular volume (P=0.87). *VHL*$_{NP+/-}$ N=3; *VHL*$_{NP-/-}$ N=5. Error bars indicated as SEM. **(C-H)** 3D images depicting all glomerular structures (green), ureteric branching patterns (pink), and a reconstruction of the kidneys.

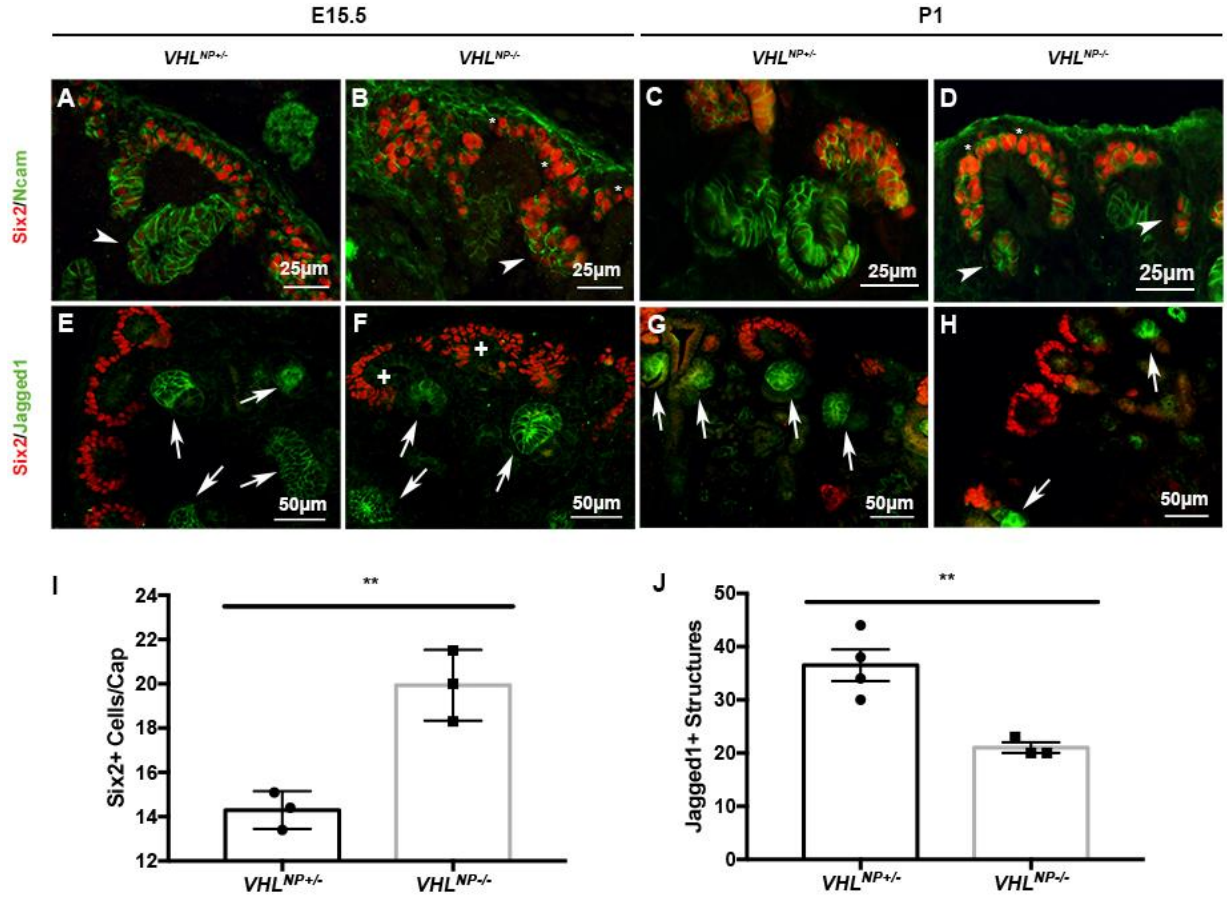

Figure 18: *VHL*$_{NP-/-}$ kidneys exhibit Six2 mis-expression, decreased cell adhesion, and fewer Jagged1+ structures

(A-D) E15.5 and P1 immunofluorescent staining with antibodies against Six2 (red) and Ncam (green) showed prolonged expression of Six2 in Ncam+ structures (arrow head). Reduced Ncam staining was also shown in *VHL*$_{NP-/-}$ kidneys (asterisk). **(E-H)** Six2 (red) and Jag1 (green) staining reveals expansion of Six2+ cells (plus sign) and fewer Jag1+ structures (arrows). **(I)** The number of Six2+ cells per cap was significantly increased in P1 *VHL*$_{NP-/-}$ kidneys. **P<0.01; N=3. Error bars indicated at SEM. **(J)** The number of Jag1+ structures is significantly decreased in P1 *VHL*$_{NP-/-}$ kidneys. **P<0.01; N=3. Error bars indicated as SEM.

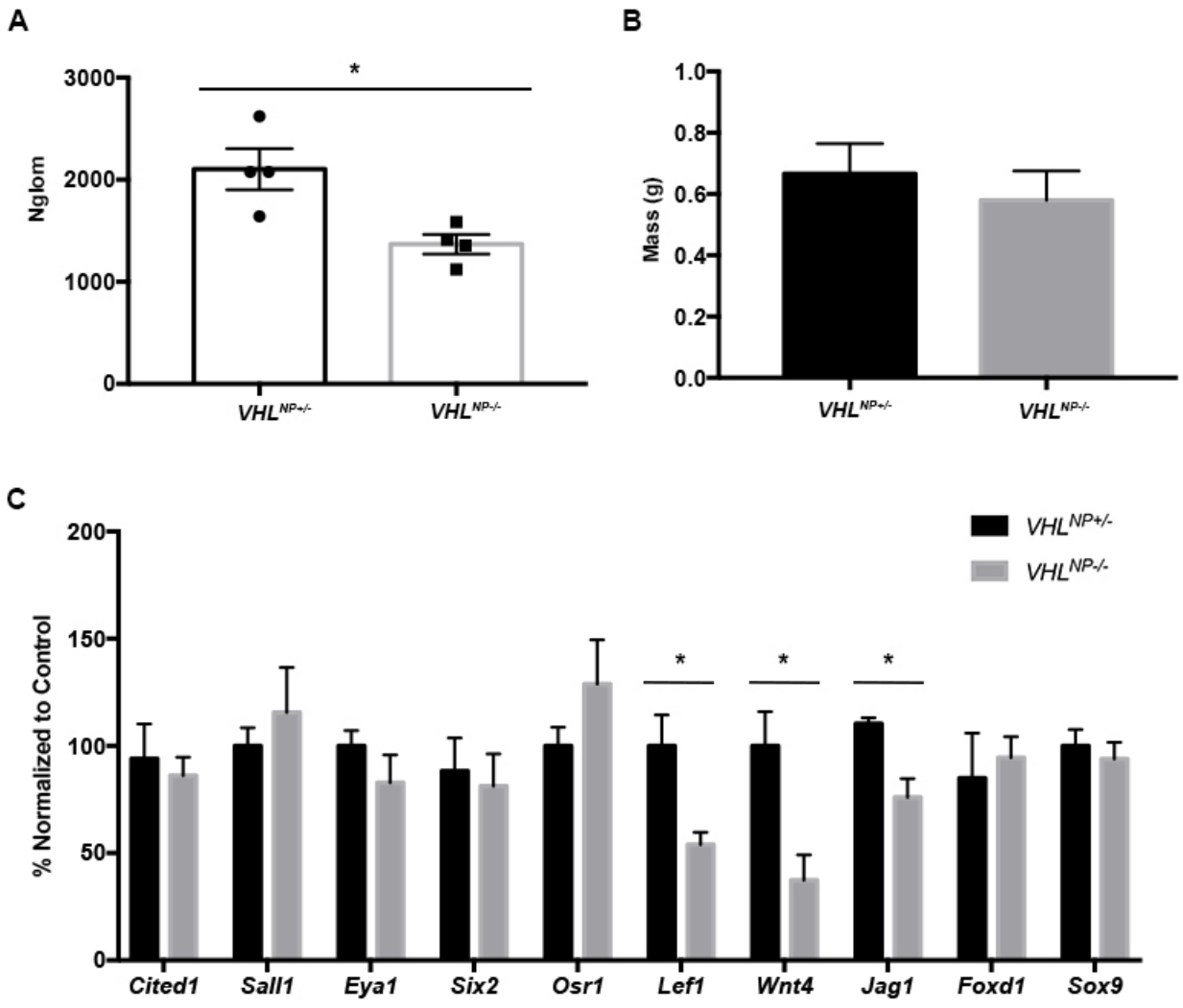

Figure 19: *VHL*$^{NP-/-}$ kidneys have decreased differentiation in nephron progenitors
(A) *VHL*$^{NP-/-}$ kidneys have significantly fewer glomeruli (30% reduction) compared to littermate controls. *P<0.05; N=4. Error bars indicated at SEM. **(B)** No significant differences in the kidney-to-body weight ratio at P1. P=0.33. N=3. **(C)** No significant differences in nephron progenitor gene expression (*Cited1*, *Sall1*, *Eya1*, *Six2*, *Osr1*). Renal vesicle genes (*Lef1*, *Wnt4*, *Jag1*) were all significantly increased. *P<0.05; N=4. Error bars indicated at SEM.

Gene expression analysis of whole E17.5 kidneys showed no differences in several nephron progenitor markers, including *Cited1*, *Sall1*, *Eya1*, *Six2*, and *Osr1* (Figure 19C). Gene expression analysis of the differentiation markers *Lef1*, *Wnt4*, and *Jag1* revealed significant decreases in expression reflecting an inability to properly undergo differentiation (Figure 19C).

There were no changes in *Foxd1* (stromal progenitors) or *Sox9* (ureteric tip identity) gene expression (Figure 19C). Together, this suggests that VHL does not induce profound alterations during the self-renewal phase and likely plays a larger role in the regulation of nephron progenitors that are poised to exit the progenitor niche.

To explore alterations in proliferation and cell death as a possible causes of decreased differentiation, we performed immunofluorescent staining with anti-pHH3 and TUNEL, respectively. There were no differences in proliferation or apoptosis (Figure 20A-P). We also performed cell cycle analysis on P1 nephron progenitors using propidium iodide to investigate potential irregularities in the cell cycle or senescence. Cell cycle analysis showed no differences in G1/G0, S, or G2/M phases (Figure 20Q-R). Collectively, these data indicate that reductions in nephron number do not likely stem from decreased proliferation, increased cell death, cell cycle dysregulation, or cellular senescence prior to cessation of nephrogenesis in *VHL*$_{NP-/-}$ kidneys.

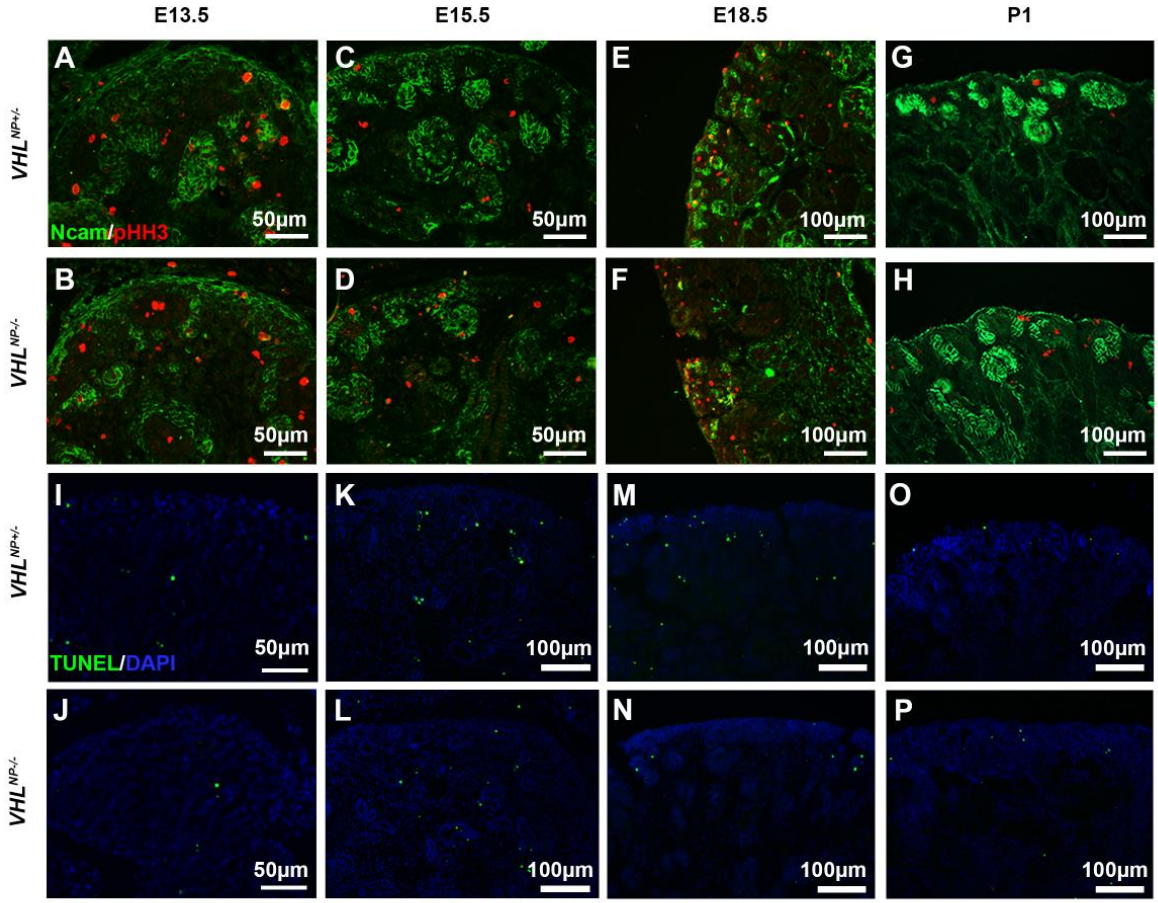

Six2+ Cell Cycle Analysis			
Phase	*VHL NP+/-*	*VHL NP-/-*	*P-value*
G0/G1	76.58 ± 1.70	77.8 ± 2.24	0.717
S	10.35 ± 0.768	8.214 ± 0.982	0.173
G2/M	7.6 ± 0.587	6.343 ± 0.742	0.279
P3	2.05 ± 1.50	2.23 ± 2.23	0.873

Figure 20: *VHL*$_{NP-/-}$ kidneys do not exhibit alterations in proliferation or apoptosis across development
(A-H) Kidneys at E13.5, E15.5, E18.5, and P1 were immunostained for phospho-histone H3 (pHH3; red) and Ncam (green), which did not reveal any alterations in proliferation. **(I-P)** E13.5, E15.5, E18.5, and P1 kidneys were subjected to TUNEL staining (green) and no significant differences were detected. **(Q-R)** P1 *VHL*$_{NP+/-}$ and *VHL*$_{NP-/-}$ kidneys were subjected to cell cycle analysis, which did not reveal any significant differences. *VHL*$_{NP+/-}$ N=4; *VHL*$_{NP-/-}$ N=5.

4.4.2 *VHL*$^{NP-/-}$ nephron progenitors display metabolic gene dysregulation

To better understand the mechanisms underlying how VHL contributes to development, we performed RNA-sequencing (RNA-seq) on E17.5 GFP+ nephron progenitors using FACS. Hierarchical distance clustering and principal component analysis (PCA) showed clear grouping of *VHL*$^{NP+/-}$ and *VHL*$^{NP-/-}$ samples (N=4; Appendix G). Variance and expression of distribution were estimated using DESeq2 and minus-average plotting (Appendix G). We observed a down regulation of *VHL*, confirming efficient deletion of this loxP-flanked fragment by Cre recombinase (Appendix G). Controlling the false discovery rate at 5% and focusing on genes with at least two-fold up or down regulation, we found that 245 known genes were significantly altered: 222 of these genes were up regulated and only 23 were down regulated in *VHL*$^{NP-/-}$ nephron progenitors (Figure 21A). The top most dysregulated genes included *Bnip3l*, *Bnip3*, *Pgm2*, *Fam162a*, *Pfkp*, *Slc2a3*, *Kbtbd11*, *Stc2*, *Adamts13,* and *Mgarp* (Appendix G). Functional enrichment analysis using DAVID (http://david.ncifcrf.gov) generated the top most affected Gene Ontology (GO) term pathways, which included glycolysis (16 genes; 45.7% of KEGG Glycolysis/Gluconeogenesis genes; $P=1.13x10^{-21}$), cellular response to hypoxia (13 genes; 12.6% of KEGG HIF-1 genes; $P=6.65x10^{-10}$), and HIF-1α signaling pathway (12 genes; 11.4% of KEGG HIF-1α genes; $P=3.78x10^{-8}$) among others (Figure 21B). HIFs, the main targets of VHL, are known to transcriptionally activate genes containing HREs. Of which, several were found to be altered including those associated with glycolysis (*Pgk1*, *Gapdh*, and *Tpi1*), hypoxia response (*Bnip3* and *Ddit4*), and HIF-1α signaling (*Pdk1* and *Eno1*) (Figure 21C; Appendix G) in *VHL*$^{NP-/-}$ nephron progenitors. Additionally, we validated several of the RNA-seq data results by real time quantitative PCR using cDNA from *VHL*$^{NP+/-}$ and *VHL*$^{NP-/-}$ whole kidneys (Figure 21D).

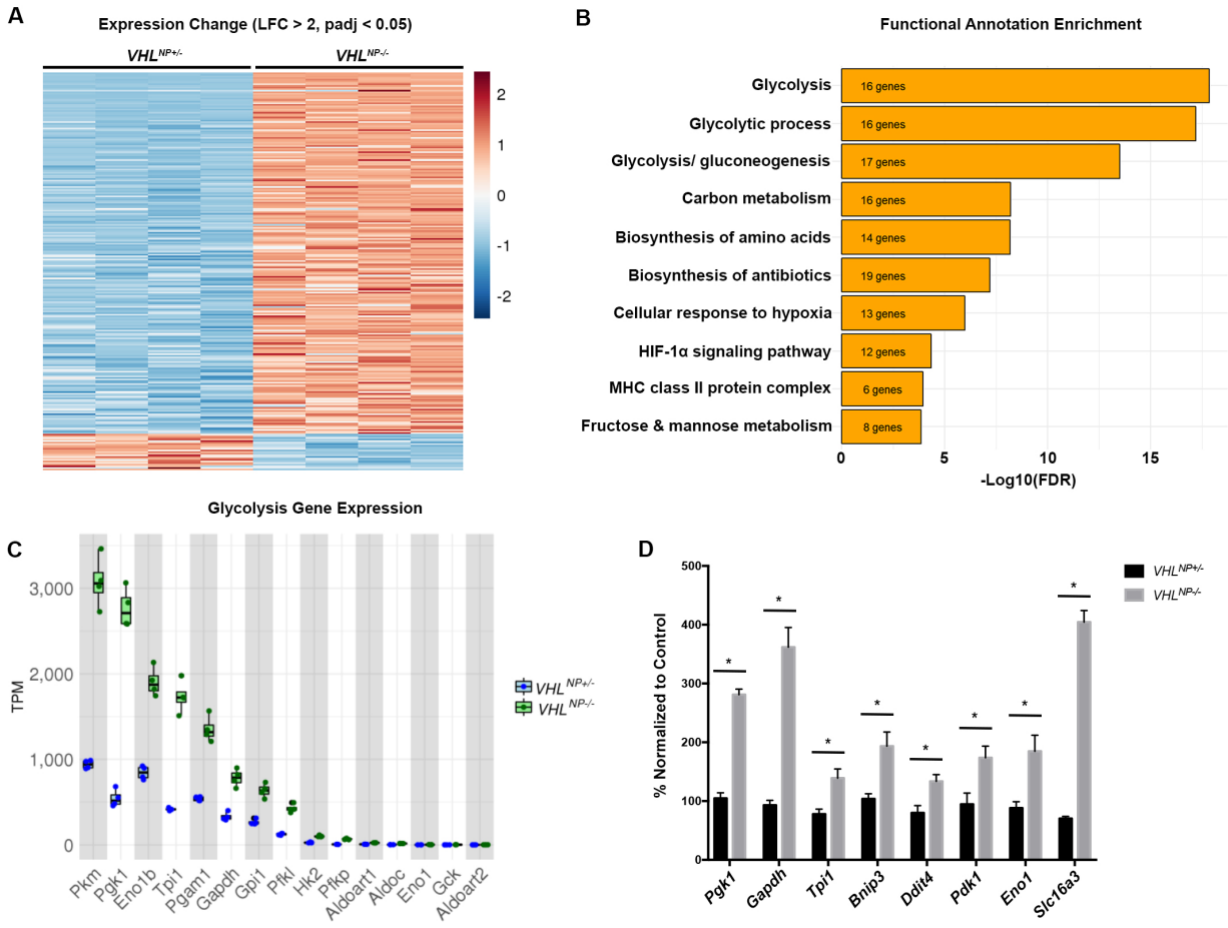

Figure 21: RNA-sequencing reveals genetic dysregulation in isolated *VHL*$^{NP-/-}$ nephron progenitors
(A) Heat map showing differential gene expression in *VHL*$^{NP+/-}$ and *VHL*$^{NP-/-}$ nephron progenitors. Cutoff for significance was set to LFC>2 and P<0.05. **(B)** DAVID functional annotation enrichment analysis showing the pathways associated with the gene expression data. **(C)** Annotation-associated gene expression showing Glycolysis gene dysregulation using DAVID analysis (Gene Ontology terms). **(D)** Real time RT-qPCR validation of significantly dysregulated genes in the glycolysis, cellular response to hypoxia, and HIF-1α signaling pathways. *P<0.05. RNA-sequencing N=4. RT-qPCR validation N=3. Error bars indicated as SEM.

4.4.3 *VHL*$^{NP-/-}$ nephron progenitors exhibit decreased mitochondrial oxygen consumption

RNA-seq data analysis implicated metabolic dysregulation as a potential driver of defective nephron progenitor differentiation in *VHL*$^{NP-/-}$ kidneys. To compare overall mitochondrial function, P1 *VHL*$^{NP+/-}$ and *VHL*$^{NP-/-}$ nephron progenitors were MACS-isolated and subjected to a mitochondrial stress test using a Seahorse XF24 extracellular flux analyzer to measure oxygen

consumption [17, 27]. Oxygen consumption is an indicator of mitochondrial respiration in the presence of a series of metabolic inhibitors and uncoupling agents [225, 228]. Overall oxygen consumption, both before and after substrate addition, resulted in decreased OCR (Figure 22A). Basal oxygen consumption was significantly decreased in *VHL*$^{NP-/-}$ nephron progenitors compared to *VHL*$^{NP+/-}$ littermate controls (Figure 22B). Moreover, mitochondrial ATP-linked respiration was significantly decreased (Figure 22C). Non-mitochondrial respiration was also calculated by averaging the oxygen consumption after addition of rotenone/antimycin A and was increased in *VHL*$^{NP-/-}$ nephron progenitors (P=0.016). This indicates decreased reliance on the mitochondria for energy production. P1 *VHL*$^{NP-/-}$ kidneys also exhibited decreased mitochondrial pyruvate oxidation to CO_2 (Figure 22D), further confirming decreased mitochondrial metabolism. To better understand the decrease in mitochondrial respiration, we analyzed mitochondrial density by flow cytometry using MitoTracker Red. There were no significant differences at P1 in mitochondrial density in the GFP+ cell population (Figure 22E). This data indicates that P1 *VHL*$^{NP-/-}$ nephron progenitors exhibit decreased dependency on mitochondrial ATP for energy production, which is not due to mitochondrial insufficiency.

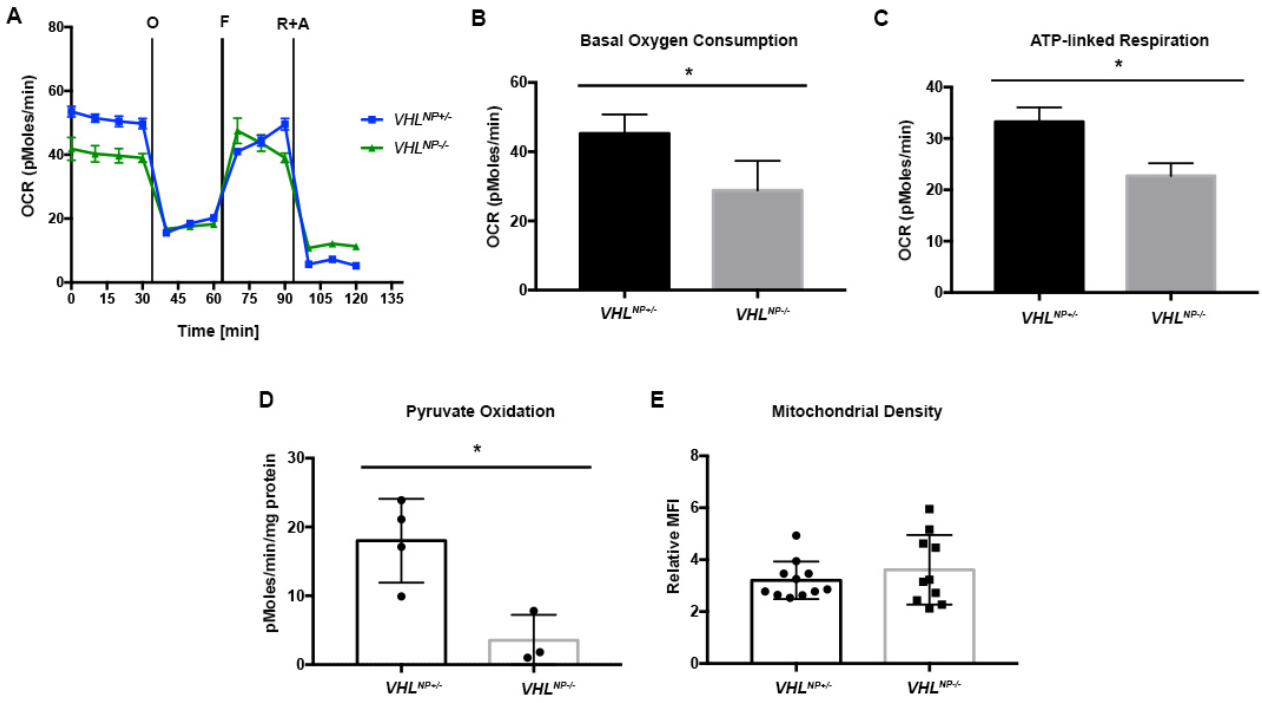

Figure 22: *VHL* deletion suppresses cellular oxygen consumption
(A) P1 MACS-isolated nephron progenitors were subjected to oxygen consumption (OCR) measurements in a Seahorse XF24 extracellular flux analyzer. Measurements of OCR were taken prior to and after sequential administration of the metabolic inhibitors oligomycin (ATP synthase inhibitor), FCCP (mitochondrial oxidative phosphorylation uncoupler), and rotenone/antimycin A (respiratory chain inhibitors). **(B)** The average oxygen consumption over the first 30 minutes produced the basal oxygen consumption, which was significantly decreased in $VHL^{NP-/-}$ nephron progenitors. *P<0.05; N=3. Error bars indicated as SEM. **(C)** ATP-linked respiration was calculated by subtracting basal respiration by the average OCR after oligomycin addition. ATP-linked respiration was significantly decreased in $VHL^{NP-/-}$ nephron progenitors. *P<0.05; N=3. Error bars indicated as SEM. **(D)** Pyruvate oxidation to $^{14}CO_2$ was significantly decreased in $VHL^{NP-/-}$ whole tissue homogenates. *P<0.05; $VHL^{NP+/-}$ N=4; $VHL^{NP-/-}$ N=3. Error bars indicated as SEM. **(E)** Mitochondrial density was not significantly altered P1 nephron progenitors. P=0.39. Error bars indicated as SEM.

4.4.4 $VHL^{NP-/-}$ nephron progenitors exhibit increased glycolysis

In addition to oxygen consumption, the Seahorse XF24 extracellular flux analyzer monitors the extracellular acidification rate (ECAR), as an indicator of anaerobic glycolysis. $VHL^{NP-/-}$ MACS-isolated nephron progenitors demonstrated increased glycolysis both before and after substrate administration (Figure 23A). Basal ECAR was increased (Figure 23B). Moreover, the glycolytic response to oligomycin (mitochondrial respiration inhibitor) was significantly higher in $VHL^{NP-/-}$

nephron progenitors compared to *VHL*$_{NP+/-}$ nephron progenitors demonstrating increased glycolytic capacity (Figure 23C). We evaluated glycolytic dependence by culturing E13.5 kidney explants in media alone or media containing 10μM Y1N (glycolysis inhibitor) for 72 hours. Explants were then subjected to immunostaining against Six2 and Jag1 to mark the nephron progenitors and developing structures, respectively. Visual identification of the number of differentiating structures revealed 1) *VHL*$_{NP-/-}$ kidneys cultured in YN1 were capable of differentiating while *VHL*$_{NP-/-}$ kidneys cultured in media alone underwent minimal differentiation and 2) *VHL*$_{NP+/-}$ and *VHL*$_{NP-/-}$ kidneys cultured in YN1 differentiated similarly (Figure 23D-G). This suggests that the differentiation phenotype arises from an inability of *VHL*$_{NP-/-}$ nephron progenitors to metabolically switch from glycolysis to mitochondrial respiration during nephrogenesis, further validating the importance of VHL during kidney development.

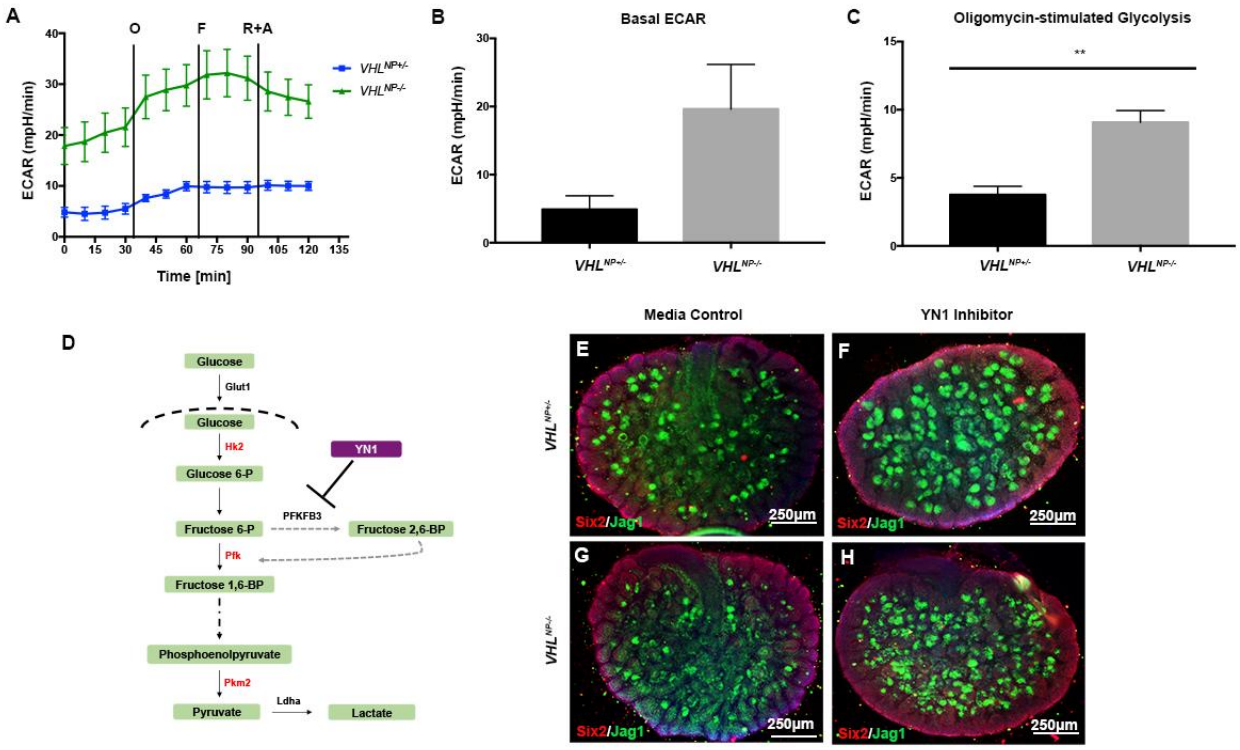

Figure 23: *VHL* deletion leads to increased glycolysis
(A) P1 MACS-isolated nephron progenitors were subjected to extracellular acidification (ECAR) measurements in a Seahorse XF24 extracellular flux analyzer as done in Figure 21. **(B)** Basal glycolysis was determined by averaging the extracellular acidification over the first 30 minutes and exhibited an up-regulated trend (P=0.09) in *VHL*$^{NP-/-}$ nephron progenitors. **(C)** Oligomycin-stimulated glycolysis was calculated by subtracting the basal ECAR from the average of the values obtained after oligomycin addition. Oligomycin-stimulated glycolysis was significantly increased in *VHL*$^{NP-/-}$ nephron progenitors. **P<0.01; N=3. Error bars indicated as SEM. **(D)** Glycolysis pathway showing the target of the glycolysis inhibitor YN1. **(E-H)** Immunofluorescent staining of kidney explants revealed that in media alone *VHL*$^{NP-/-}$ kidneys differentiated less than *VHL*$^{NP+/-}$ kidneys in media alone. When cultured in the presence of the glycolysis inhibitor YN1 both *VHL*$^{NP-/-}$ and *VHL*$^{NP+/-}$ kidneys underwent similar levels of differentiation.

4.4.5 *VHL* deletion results in abnormalities of juvenile mouse kidneys

VHL$^{NP-/-}$ mice experience premature death around P30; therefore we characterized the renal phenotype at P21. To assess renal structure and function of the juvenile (P21) mice, we performed gross and histological examinations, which revealed smaller kidneys with fewer glomerular structures (Figure 24). The *VHL*$^{NP-/-}$ kidneys appeared to have decreased glomeruli and dilation of the proximal tubules (Figure 24A-D), which is likely due to a compensatory

mechanism to overcome the reduction in nephron number [229]. In fact, we found that the *VHL*$_{NP-/-}$ kidneys have a 50% reduction in nephron number ($P<0.0001$; Figure 24I). Although *VHL*$_{NP-/-}$ kidneys were smaller than *VHL*$_{NP+/-}$ kidneys, the kidney-to-body weight ratio was not different (Figure 24K-M). Additionally, blood urea nitrogen (BUN) concentration was significantly increased in *VHL*$_{NP-/-}$ mice (Figure 24J), which we hypothesized was due to glomerular insufficiency and not a result of tubular malfunction. To evaluate this hypothesis, we performed immunostaining against Glut1 (glycolysis) and Pck1 (gluconeogenesis), which did not reveal differences in protein expression between the *VHL*$_{NP+/-}$ and *VHL*$_{NP-/-}$ kidneys (Figure 24E-H), suggesting that the developed tubules are functional.

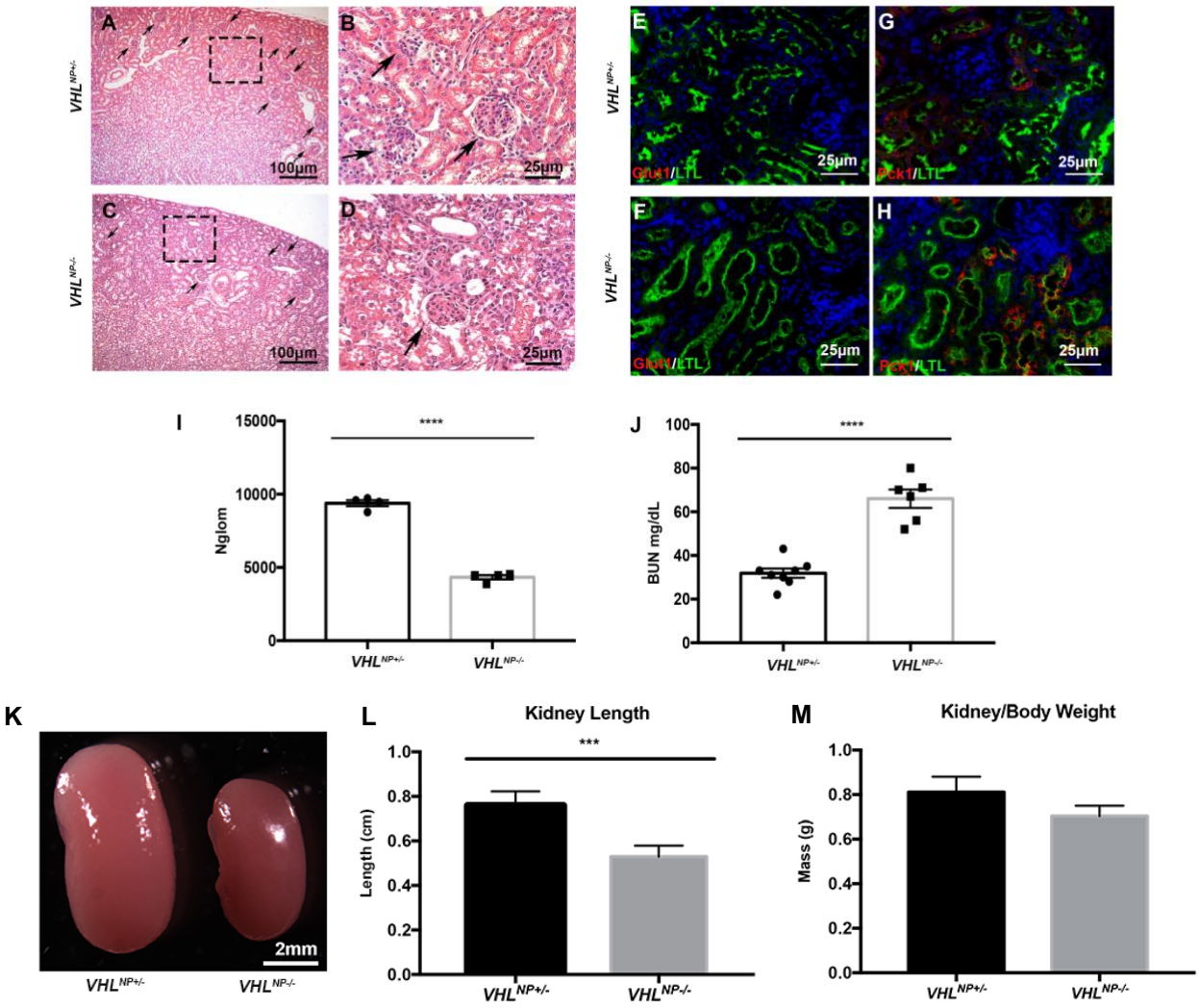

Figure 24: *VHL*$_{NP-/-}$ mice exhibit a glomerular deficit at P21
(A-D) H&E staining of kidneys sectioned at P21 showing reduced nephron number (black arrows). **(E-H)** There are no differences in Glut1 or Pck1 expression in P21 kidneys. LTL staining reveals proximal tubule dilation in *VHL*$_{NP-/-}$ kidneys. **(I)** *VHL*$_{NP+/-}$ and *VHL*$_{NP-/-}$ glomerular counts at P21 revealed approximately 50% reduction in glomerular number. ****P<0.0001; N=4. Error bars indicated as SEM. **(J)** Blood urea nitrogen levels are significantly higher in *VHL*$_{NP-/-}$ mice compared to littermate controls. ****P<0.0001; *VHL*$_{NP+/-}$ N=8; *VHL*$_{NP-/-}$ N=6. Error bars indicated as SEM. **(K)** Gross comparison of kidney size. **(L)** *VHL*$_{NP-/-}$ kidneys are significantly smaller in length at P21. ***P<0.0005; N=4. Error bars indicated as SEM. **(M)** The kidney-to-body weight ratio was similar between control and VHL$_{NP-/-}$ mice. P=0.07. N=4. Error bars indicated as SEM.

4.5 DISCUSSION

From our study it is clear that the VHL/HIF pathway plays a major role in differentiation decisions during nephron progenitor maturation. Our data reveals a previously unknown role for VHL in mediating metabolic switching during kidney development that is broadly applicable to other developing systems. Mechanistically, our data suggests that VHL is required for nephron progenitors to adapt to increasing oxygenation and, in response, alter their primary metabolism from glycolysis to oxidative phosphorylation. Moreover, we propose this metabolic switching is an essential process for differentiating nephron progenitors. Specifically, nephron progenitors lacking VHL exhibit up regulated glycolysis and down regulated mitochondrial respiration. Although mitochondrial respiration was suppressed, mitochondrial density did not differ between *VHL*$^{NP+/-}$ and *VHL*$^{NP-/-}$ nephron progenitors. We conclude that the mitochondria are healthy and retain the ability to function normally, however they lack substrate (i.e. pyruvate) due to the HIF-mediated up regulation of PDK, which effectively blocks pyruvate utilization by the mitochondria. Instead of pyruvate shuttling into the mitochondria, it is preferentially converted into lactate and recycled back into the glycolytic pathway. The profound metabolic alteration leads to decreased differentiation indicated by reduced nephron numbers at both P1 and P21. This model simulates pathological hypoxia, which has previously shown to cause a reduction in nephrons [183], however the underlying mechanisms have not been previously identified.

It is well known that kidney formation is highly dependent on oxygen concentration, which is largely regulated by VHL and HIFs. Of particular interest, *VHL*$^{NP-/-}$ nephron progenitors have access to oxygen, but remain unable to respond to the oxygen. We hypothesize that the *VHL*$^{NP-/-}$ differentiation phenotype is due to prolonged maintenance of a progenitor niche as demonstrated by persistent Six2 and Wt1 expression and decreased nephron number. Six2-

expressing cells represent a multipotent nephron progenitor population expressed throughout kidney development [230, 231] and Six2 must be down regulated to initiate MET [231, 232]. Furthermore, another study has shown that HIF-1α blocks MET [233]—a necessary process for differentiating nephron progenitors—which serves as another potential mechanism leading to decreased nephron number. Although our model has a significant reduction in nephron number, our data suggests that either a subset of nephron progenitors remain capable of maturing into nephrons or that the differentiation process is not as efficient in *VHL*$_{NP-/-}$ mice. Similarly, when *VHL* is deleted from Foxd1-expressing stromal progenitors, the resulting offspring exhibit nephron deficit and postnatal death by 14 days of age, which was attributed to increased HIF expression [234]. Our data shows that the nephrons that do form are either derived from nephron progenitors that underwent differentiation early (prior to E15.5) or due to inefficient nephron progenitor differentiation. The *VHL*$_{NP-/-}$ mice do not exhibit a profound phenotype until E15.5, which we hypothesize is due to the physiologically hypoxic environment the kidneys are subjected to in early development, and is prior to when VHL is critical. Therefore in the absence of VHL prior to E15.5, the nephron progenitors are capable of normal differentiation, however after this time they fail to undergo sufficient differentiation. A previous study by Wang *et al* also investigated renal structure and function in Six2creEGPF-VHL null mice for the purpose of studying renal cell carcinoma [86]. Although our model exhibits profound abnormalities correlating to significantly decreased renal function by P21, their mice are histologically normal and do not exhibit any malformations or dysfunction until approximately 4 months of age [86]. We see an accelerated phenotype, which we attribute to differences in mouse background strains. Our model was generated using a B6/129S4 mixed background, while Wang et al used a BALB/c background. Previous studies have shown that there are significant mouse strain

differences, particularly in the kidney and in the progression of diseases such as renal fibrosis, hypertension, and kidney disease [235-237].

Another significant function of VHL-mediated HIF degradation is the regulation of metabolism. Previous interrogations of HIF implicate it in the regulation of glycolysis and oxidative phosphorylation [121, 144]. While VHL has not been interrogated as a regulator of metabolism in nephron progenitors, HIF-1α is a known mediator in other cell types, suggesting that VHL must also play an important role in regulating the metabolic profile of these progenitors. Moreover, VHL-related cancers exhibit similarly decreased mitochondrial respiration in favor of glycolic metabolism even in the presence of oxygen, a phenomenon known as the Warburg effect [157, 238, 239]. Although our *VHL*$_{NP-/-}$ model is not a cancer model, these mice do exhibit severe alterations in the nephron progenitor metabolic profile consistent with the Warburg effect. In addition to enhanced glycolysis, a previous study investigated the metabolic profiles of E13.5 and P0 nephron progenitors and showed that younger progenitors demonstrate a higher dependence on glycolysis while older progenitors are more dependent on oxidative phosphorylation [17]. Our study suggests that the phenotype associated with the *VHL*$_{NP-/-}$ mice can be attributed to metabolic alterations leading to an inability of the cells to transition from glycolysis to oxidative phosphorylation.

In summary, our study suggests that VHL is crucial for the metabolic switching required during progenitor cell differentiation and validates that strict regulation of oxygenation is vital for cellular differentiation. Thus, VHL is also an essential mediator dictating proliferative, poised, and differentiating nephron progenitors and likely plays a critical role in cell fate decisions. Further discussion on the future directions and research limitations of this work are described in Chapter 6.3.

5.0 VON HIPPEL LINDAU DOES NOT ALTER MITOCHONDRIAL FUNCTION IN THE DEVELOPING KIDNEY

This chapter is an ongoing study and more experimentation is required before it can be considered for publication.

"Von Hippel Lindau and Mitochondrial Function"

Kasey Cargill[1,2], Elina Mukherjee[1], Shiva Yagobian[1], and Sunder Sims-Lucas[1,2]

[1]Division of Nephrology, Department of Pediatrics, UPMC Children's Hospital of Pittsburgh, Pittsburgh, PA, USA.

[2]University of Pittsburgh School of Medicine, Pittsburgh, PA, USA.

5.1 CHAPTER SUMMARY

Von Hippel-Lindau (VHL) is a component of an ubiquitin ligase complex. A major target of VHL is a family of transcription factors known as hypoxia inducible factors (HIFs). One member of the HIF family is HIF-1α, which is highly expressed in the developing kidney. Both VHL and HIFs are critical for development and global deletion of either of these proteins is embryonic lethal. One such process that the VHL/HIF axis has been implicated in is metabolic regulation. HIF-1α has been previously shown to mediate metabolic processes, however the role of VHL in regulating metabolism and mitochondrial function has not been well characterized. A recent study into VHL localization found that VHL directly localizes to the mitochondria, but further characterization of its role in the mitochondria is unknown. This study aims to investigate the role of VHL in mitochondrial function using a mouse model with a conditional deletion of VHL specifically in nephron progenitors (*VHL*$_{NP-/-}$). A previous investigation by our laboratory revealed that the *VHL*$_{NP-/-}$ nephron progenitors exhibit profound metabolic dysregulation glycolysis was up regulated while mitochondrial respiration was significantly down regulated. Herein, we found that in the absence of VHL in the nephron progenitors, mitochondrial density, dynamics, biogenesis, and ROS production are not altered. This suggests that oxidative phosphorylation is inhibited due to HIF-stabilization leading to a lack of substrate availability for normal mitochondrial respiration.

5.2 INTRODUCTION

The tumor suppressor and ubiquitin ligase von Hippel-Lindau (VHL) is most well studied in the context of hypoxia [117, 129], renal cell carcinoma [86, 240, 241], and Von Hippel-Lindau Disease [242]. Many of these pathologies arise from mutations in the *VHL* gene rendering a nonfunctional protein. In a normal cell supplied with ample oxygen, VHL predominantly targets the transcription factor family of hypoxia inducible factors (most notably HIF-1α and HIF-2α) [117]. HIF-1α is highly expressed in developing cells including stem and progenitor cells, however often becomes down regulated (via VHL) for cellular differentiation. Pathologies result from prolonged or inappropriate expression of HIFs due to the up regulation of genes containing hypoxia response elements (HREs). Overexpression of HREs alters cellular processes contributing to cell cycle dysregulation, aberrant proliferation, metabolic irregularities, and immunological reprogramming.

Metabolic dysregulation is a hallmark of many diseases including cancer, autoimmune diseases (diabetes mellitus and rheumatoid arthritis), and kidney disorders (polycystic kidney disease, acute kidney injury, and chronic kidney disease) [152, 208]. Unsurprisingly, the VHL/HIF-1α axis is also commonly disrupted in these diseases. Previous studies have shown that HIF-1α contributes to the metabolic profile of a cell such that high HIF-1α expression results in increased glycolytic metabolism [69, 243]. Additionally, HIF-1α expression also results in the active down regulation of oxidative phosphorylation of the mitochondria [69, 243]. Although the mechanism of HIF-1α in metabolism is well understood, recent studies have also investigated the direct role of VHL in mediating metabolism (as opposed to VHL-mediated HIF-1α metabolic regulation).

A previous study by Shiao *et al* (2000) revealed that, in addition to cytoplasmic localization, VHL localizes to mitochondria in some tissues including the kidney [244]. Moreover, mutated VHL resulted in an abnormal mitochondrial phenotype in adult rat kidneys [244]. Further, another study interrogated the role of VHL in mitochondrial function and found that while oxidative phosphorylation activity and protein content was increased, there were no differences in mitochondrial membrane potential [238]. Although this was an interesting finding, it is likely that the data was due to the regulation of HIFs and not a direct effect of VHL. Studies such as these raise the question: If VHL localizes to the mitochondria, what function does it serve?

To investigate this phenomenon, we used a mouse model (*VHL*$_{NP-/-}$) with a conditional deletion of VHL specifically in the nephron progenitors (self-renewing cell that forms the nephron). A previous study done by our laboratory revealed that *VHL*$_{NP-/-}$ kidneys have prolonged reliance on glycolysis metabolism and inefficiently undergo metabolic switching. Although this was largely attributed to the VHL/HIF-1α pathway, herein we investigate mitochondrial properties contributing to function including: biogenesis, mitophagy, fission/fusion dynamics, ROS, and mitochondrial density. We found that the mitochondria appear healthy and retain the ability to function normally, however they lack substrate (i.e. pyruvate) due to the HIF-mediated up regulation of PDK, which effectively inhibits pyruvate utilization by the mitochondria. Instead of pyruvate migration into the mitochondria, it is preferentially converted into lactate and recycled back into the glycolytic pathway.

5.3 METHODS AND MATERIALS

5.3.1 Experimental mouse model and genotyping

VHL$_{NP+/-}$ and *VHL*$_{NP-/-}$ mice were generated using the same breeding strategy described in 4.3.1. Genotypes were determined as described in 4.3.2.

5.3.2 Real time quantitative polymerase chain reaction (PCR)

E17.5 kidneys were dissected and screened using the GFP expression. Dissected kidneys that expressed GFP were dissociated into single cell suspensions and FACS sorted (Flow Cytometry Core, Rangos Research Center. Each sample consisted of approximately 150,000 pooled control or mutant nephron progenitor cells. RNA isolation and cDNA synthesis was done as previously described in 2.3.3. The following genes were analyzed using this method: *Glut1, Ldha, Pdk1, Tomm20, Tfam, Sirt1, Drp1, Opa1, Bcl2, Lc3, Nox4*. All gene expression was normalized to *Rn18s*. Primer sequences are listed in Appendix B.

5.3.3 Western blotting

Immunoblots were prepared as done in 4.3.3. Antibodies used include (Appendix D): Pgc-1a (Novus), Dnm1l (Thermo Fisher Scientific), Tomm20 (Santa Cruz), and anti-α/β tubulin (Cell Signaling Technology, 1:1000). Secondary antibodies include: anti-IgG rabbit HRP (Cell Signaling Technology, 1:1000) and anti-IgG mouse HRP (Cell Signaling Technology, 1:250).

Blots were imaged using a ProteinSimple FluoroChem M System (ProteinSimple) and quantified using ImageJ software (ImageJ/NIH Image).

5.3.4 Flow cytometry for mitochondrial density

Samples were analyzed using MitoTracker™ Red FM (Thermo Fisher Scientific; Appendix E) as previously described in 4.3.6.

5.3.5 Flow cytometry for reactive oxygen species

Samples were analyzed using MitoSOX™ Red Mitochondrial Superoxide Indicator (Thermo Fisher Scientific; Appendix E) as previously described in 2.3.5.

5.3.6 Flow cytometry for lysosome formation

Kidney tissue was harvested from P1 *VHL*$^{NP+/-}$ and *VHL*$^{NP-/-}$ mice. Kidneys were digested using 0.3% collagenase and forced through needlepoint to create a single cell suspension. 1 x 10^6 cells were stained for 1 hour at 37°C using 50nM LysoTracker™ Red DND-99 (Thermo Fisher Scientific; Appendix E) per manufacturer's guidelines. Cells were analyzed on a BD LSRFORTESSA cell analyzer (BD Biosciences) through the Flow Cytometry Core at the Rangos Research Center located at the UPMC Children's Hospital of Pittsburgh

5.3.7 Immunofluorescent staining

Immunofluorescent staining was performed on paraffin embedded samples as previously described in 3.3.5. Samples were probed using primary antibodies or lectins (1:100; Appendix D) against: Tomm20 (Santa Cruz), LTL (Gibco), and DAPI. Samples were imaged using a Leica microscope (Leica Microsystems) and LAS X software (Leica Microsystems).

5.3.8 Statistical analysis

A minimum of 3 biological replicates was used for each experiment in at least technical duplicate. When comparing two sample groups, statistical significance was determined using a two-tailed Student's t test ($\alpha = 0.05$). Significance was defined as *$P<0.05$, **$P<0.01$, and ***$P<0.001$. Where appropriate, data is presented as mean ± standard error of the mean. Data was analyzed using Microsoft Excel and figures were generated using GraphPad Prism 7.

5.4 RESULTS

To interrogate the role of VHL in mitochondrial function, we utilized our previously published mouse model with a conditional deletion of VHL specifically in nephron progenitors under a Six2cre [245]. This model exhibits profound developmental kidney defects due to an inability to undergo metabolic switching from glycolysis to mitochondrial respiration during nephron progenitor differentiation [245]. We hypothesize that this could be due to three potential

mechanisms: 1) decreased mitochondrial density 2) mitochondrial dysfunction 3) or lack of substrate utilization.

5.4.1 Mitochondrial density is not altered in *VHL$_{NP-/-}$* kidneys

To determine mitochondrial quantity, we performed immunofluorescent staining against Tomm20, an outer mitochondrial membrane protein that can be visualized and quantified as an indicator of mitochondrial mass. Immunofluorescent staining revealed that P1 *VHL$_{NP-/-}$* kidneys appeared to have decreased mitochondrial density (Figure 25A-B). Further, P21 *VHL$_{NP-/-}$* kidneys also exhibited decreases in mitochondrial density (Figure 25C-D). Although there were differences in mitochondrial densities at both P1 and P21, it was previously shown that *VHL$_{NP-/-}$* kidneys have significantly decreased nephron number at both time points, which would lead to a decreased number of proximal tubules [245]. The proximal tubules are highly metabolically active and utilize mitochondrial fatty acid oxidation to a high extent [208]. For this reason, we believe that the decrease in Tomm20 expression in *VHL$_{NP-/-}$* kidneys was due simply to reduced proximal tubule load and not due to inherently decreased mitochondrial density. To test this, we quantified Tomm20 gene and protein expression using real time quantitative PCR and Western blotting. *Tomm20* expression was comparable between FACs sorted nephron progenitors from *VHL$_{NP+/-}$* and *VHL$_{NP-/-}$* kidneys (Figure 25F). Tomm20 protein expression also appeared similar Figure 25E;G). Moreover, we evaluated mitochondrial density by flow cytometry using MitoTracker straining and again did not see any significant differences in mitochondrial density (Figure 25H). Together, this suggests that the reduced mitochondrial utilization by *VHL$_{NP-/-}$* kidneys is not due to decreased mitochondrial density.

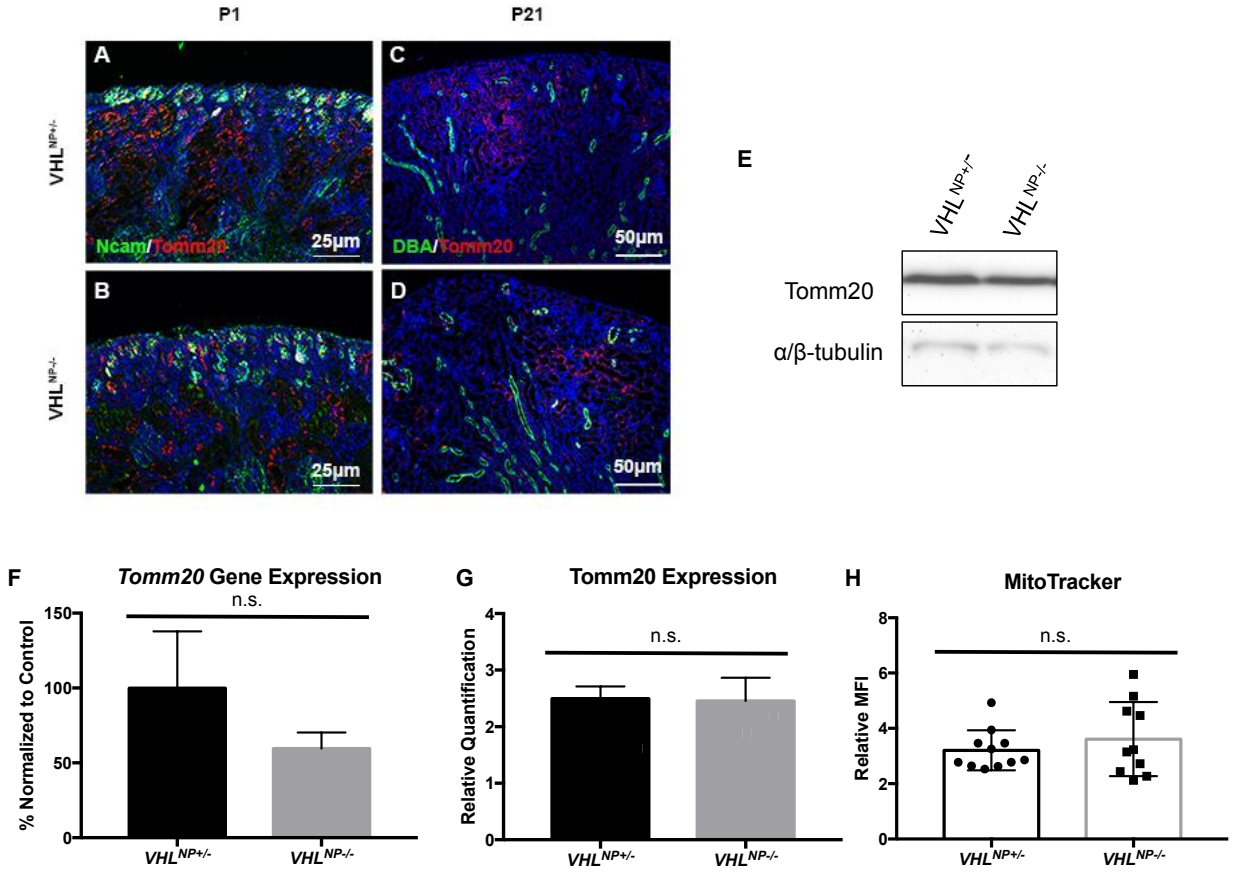

Figure 25: Mitochondrial density is decreased in *VHL*$_{NP-/-}$ kidneys but not in *VHL*$_{NP-/-}$ nephron progenitors
(A-B) P1 kidneys were immunostained against Tomm20 (red) and Ncam (green) and *VHL*$_{NP-/-}$ kidneys appear to have reduced mitochondria indicated by Tomm20 reduction. **(C-D)** Similarly, P21 *VHL*$_{NP-/-}$ kidneys appear to have reduced mitochondria indicated by Tomm20 (red) reduction. No alterations observed in DBA immunostain (green). **(E)** Tomm20 immunoblot against Tomm20 from P1 whole kidney lysates. **(F)** Tomm20 gene expression was not altered in E17.5 isolated nephron progenitors. P=0.09; N=4. Error bars indicated as SEM. **(G)** Quantification of the immunoblot shown in E revealed no difference in protein expression between control and *VHL*$_{NP-/-}$ whole kidney lysates. P=0.93; N=4. Error bars indicated as SEM. **(H)** Mitochondrial density is not different in *VHL*$_{NP-/-}$ nephron progenitors. P=0.39; *VHL*$_{NP+/-}$ N=11; *VHL*$_{NP-/-}$ N=10. Error bars indicated as SEM.

5.4.2 *VHL*$_{NP-/-}$ kidneys do not exhibit mitochondrial dysfunction

Previous hypoxia studies have shown that cells can adapt to oxygen level fluctuations by altering their metabolism [246], which can lead to significant alterations in mitochondrial biogenesis, fission/fusion dynamics, and autophagy. For these reasons, we evaluated gene and protein expression of several key molecules involved in these processes.

Gene expression of the mitochondrial biogenesis genes Tfam and Sirt1 did not show any abnormalities in the rate of mitochondrial formation (Figure 26A) in P1 nephron progenitors. Likewise, Western blotting for PGC-1α, a protein essential for mitochondrial biogenesis, did not reveal any differences in expression (Figure 26B-C) in P1 whole kidney homogenates. Therefore, we do not believe that the mitochondria are undergoing abnormal rates of turnover.

Similarly, we evaluated mitochondrial dynamics in P1 nephron progenitors and kidneys by determining gene and protein expression of Opa1 (inner mitochondrial membrane fusion) and Drp1 (mitochondrial fission). Neither gene nor protein expression of these mitochondrial dynamic markers were altered in *VHL*$_{NP-/-}$ kidneys (Figure 27A-D).

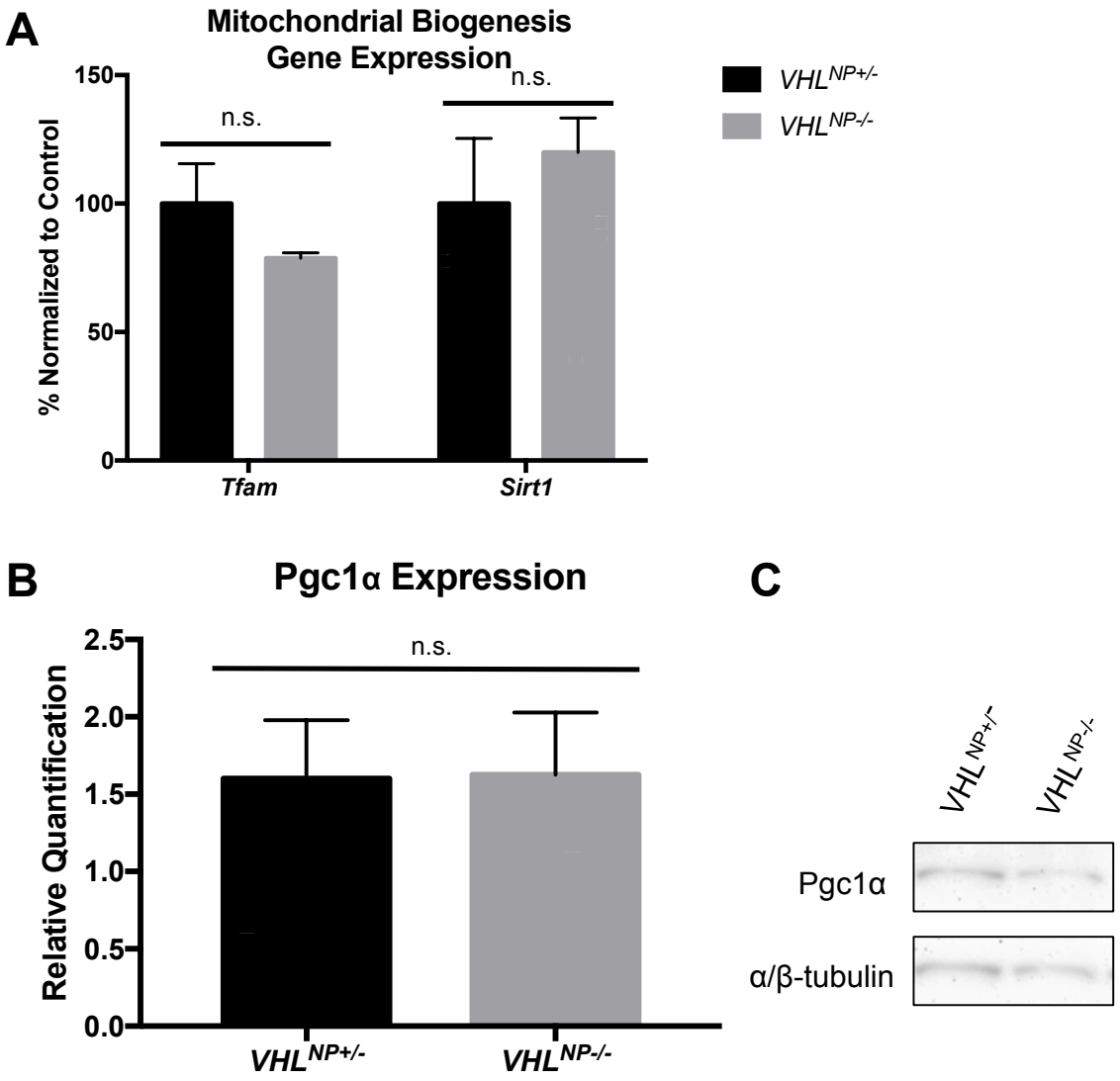

Figure 26: Mitochondrial biogenesis is not altered in *VHL*$^{NP-/-}$ nephron progenitors
(A) Mitochondrial biogenesis genes Tfam and Sirt1 do not exhibit dysregulation in *VHL*$^{NP-/-}$ nephron progenitors at E17.5. *Tfam* P=0.22; *Sirt1* P=0.51; N=4. Error bars indicated as SEM. **(B)** Pgc1α protein quantification did not reveal any significant differences in expression. P=0.94; N=4. Error bars indicated as SEM. **(C)** Immunoblot for Pgc1α shows similar expression both kidneys.

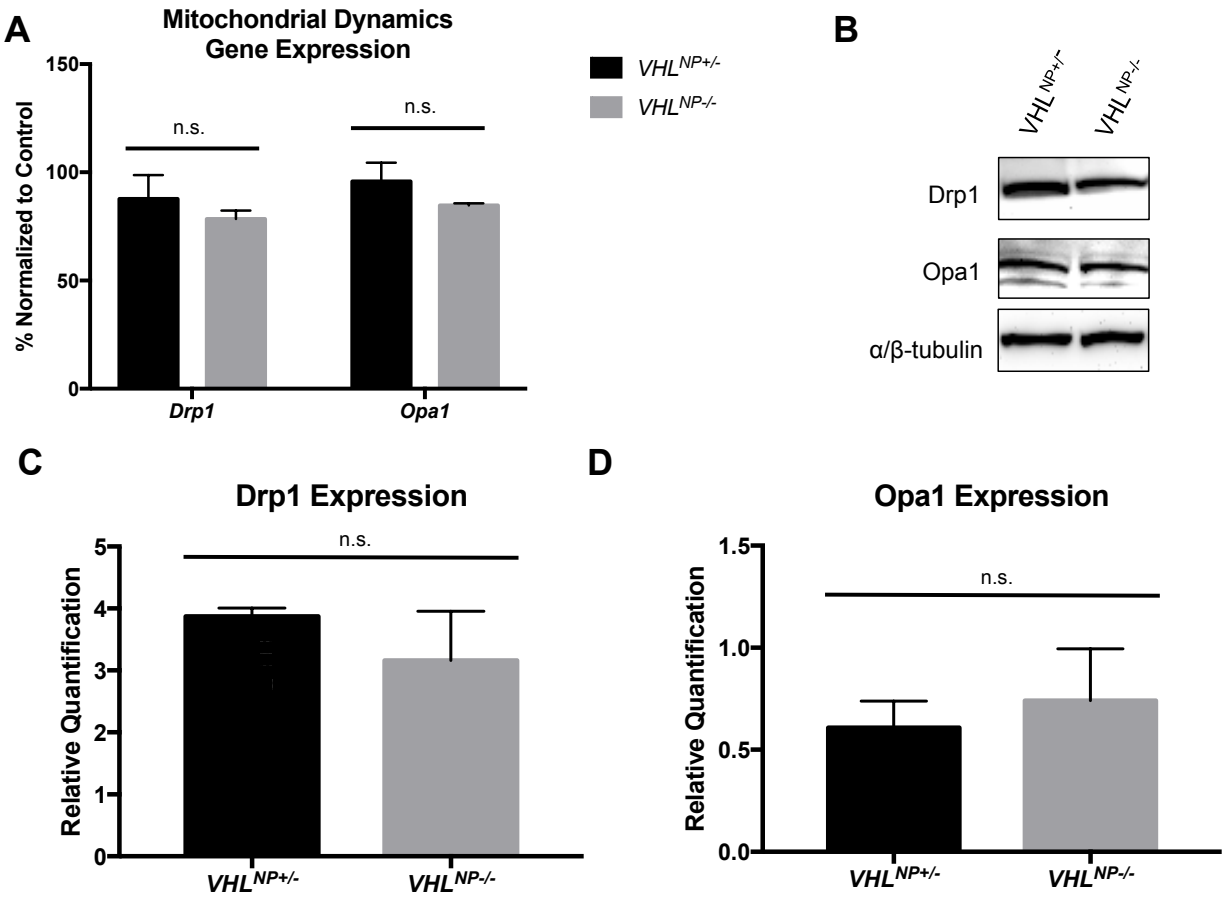

Figure 27: Mitochondrial dynamics are unchanged in *VHL*$_{NP-/-}$ nephron progenitors
(A) Mitochondrial dynamics genes Drp1 (mitochondrial fission; P=0.20) and Opa1 (mitochondrial fusion; P=0.09) are not differentially expressed in *VHL*$_{NP-/-}$ nephron progenitors. N=4. Error bars indicated as SEM. **(B)** Immunoblots of Drp1 and Opa1. **(C-D)** Drp1 (P=0.11) and Opa1 (P=0.66) protein expressions were not significantly altered. N=4. Error bars indicated as SEM.

Next, we performed gene expression analysis to determine whether *VHL*$_{NP-/-}$ kidneys experienced increased mitophagy—mitochondrial degradation by autophagy. We found that *Bcl2* and *Lc3* gene expression were not significantly different (Figure 28A). We also utilized LysoTracker staining and analyzed expression in P1 nephron progenitors by flow cytometry. LysoTracker is a dye that localizes to lysosomes, and during mitophagy the degraded mitochondria are engulfed by autophagosomes that fuse with lysosomes; Therefore, this is a

technique that indicates the level of autophagy that is occurring. There were no differences in lysosomal formation as indicated by LysoTracker flow cytometry (Figure 28B).

Finally, we evaluated ROS generation as an output of mitochondrial dysfunction. *Nox4* (oxidative stress indicator) gene expression was determined to be similar between both *VHL*$_{NP+/-}$ and *VHL*$_{NP-/-}$ kidneys from P1 animals (Figure 29A). Further, MitoSox (ROS indicator) fluorescence as determined by flow cytometry did not reveal any differences between the P1 control and *VHL*$_{NP-/-}$ kidneys (Figure 29B).

Together, this data reveals that in developing nephron progenitors, HIF-1α stabilization does not significantly impact mitochondrial function. Similarly, although it has been shown that VHL may localize to the mitochondrial, it is unlikely that VHL in nephron progenitors plays a significant role in the differentiation process. For these reasons, we believe our data indicates that the mitochondria are functional and capable of performing oxidative phosphorylation, however are not utilized for energy generation due to the preferential conversion of pyruvate to lactate in the cytosol.

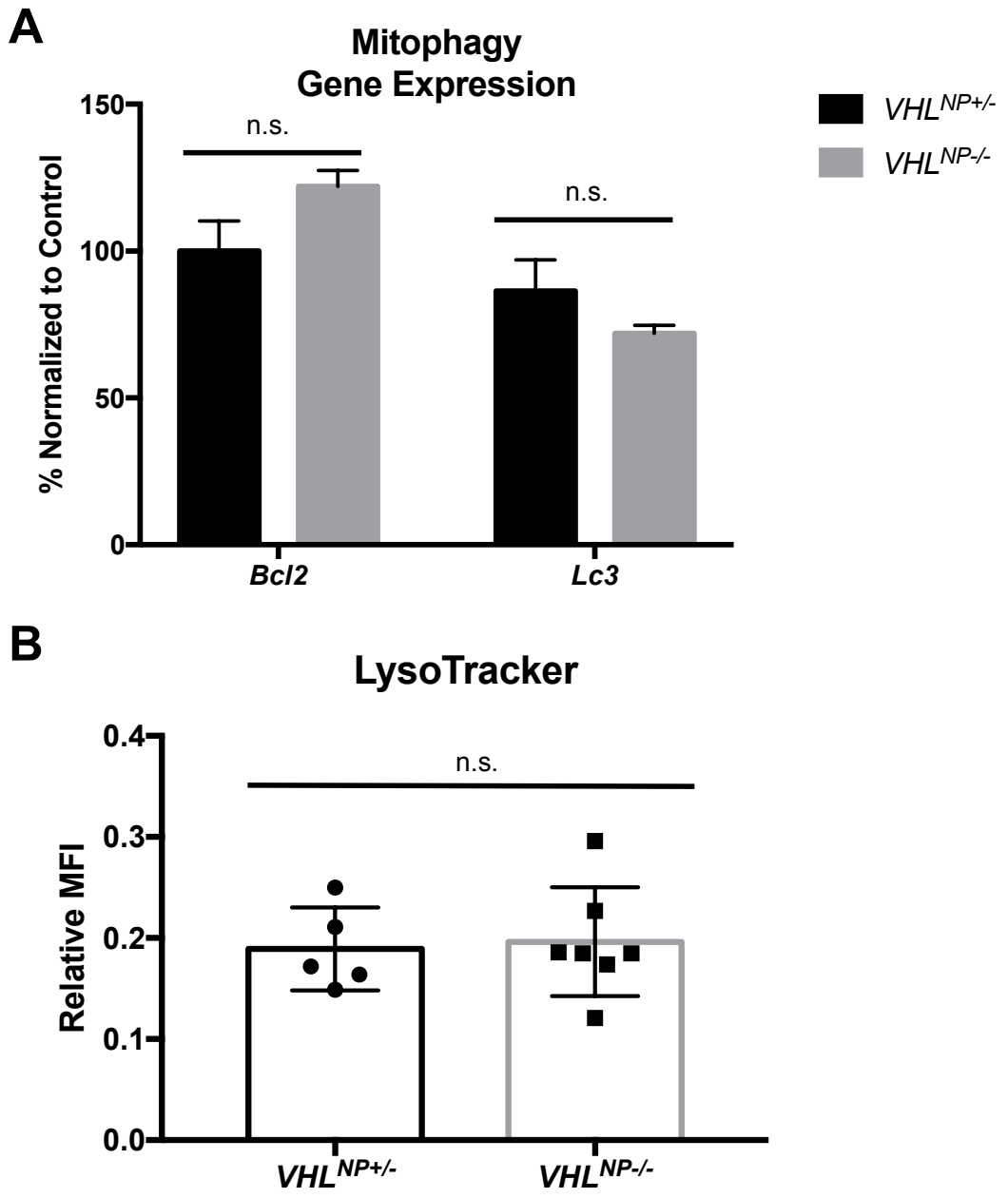

Figure 28: *VHL*$_{NP-/-}$ nephron progenitors have similar levels of autophagy as compared to *VHL*$_{NP+/-}$ nephron progenitors

(A) Mitophagy genes Bcl2 (P=0.11) and Lc3 (P=0.13) are not dysregulated in *VHL*$_{NP-/-}$ nephron progenitors. N=4. Error bars indicated as SEM. **(B)** Lyso tracker analysis by flow cytometry revealed that there is not significant difference in lysosome formation in *VHL*$_{NP-/-}$ nephron progenitors. P=0.81; *VHL*$_{NP+/-}$ N=5; *VHL*$_{NP-/-}$ N=7. Error bars indicated as SEM.

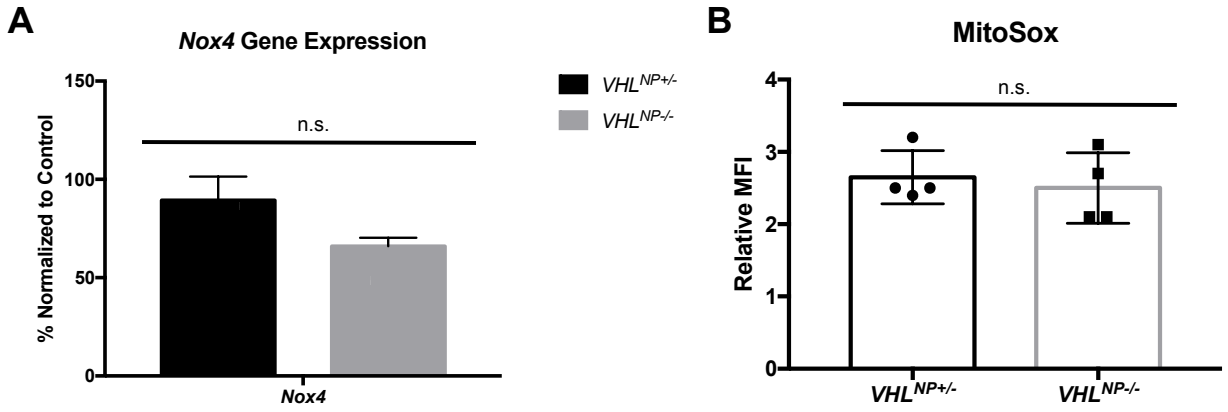

Figure 29: *VHL*$_{NP-/-}$ nephron progenitors do not exhibit aberrant ROS
(A) Nox4 (ROS marker) gene expression was not significantly altered in VHL$_{NP-/-}$ nephron progenitors compared to controls. P=0.06; N=4. Error bars indicated as SEM. **(B)** MitoSox (ROS indicator) staining and flow cytometry analysis did not reveal any differences (student t-test) in ROS generation in VHL$_{NP-/-}$ nephron progenitors. P=0.64; N=4. Error bars indicated as SEM.

5.5 DISCUSSION

Metabolic processes are an important component of normal cellular function. Any disruption in metabolism can lead to reduced energy production, irregularities in cellular function, and ultimately disease pathologies. The kidney functions to eliminate waste and maintain salt-water balance. More than 70% of the kidney's function is performed by the nephron, which is the functional unit of the kidney. The kidney is a highly metabolically active organ and relies on mitochondrial metabolic pathways used by the nephron to filter blood and produce waste (urine). The proximal tubule is one epithelialized segment of the nephron that is involved in filtrate generation and requires an abundance of ATP to transport ions and small molecules from the tubules into the blood system. The required ATP is produced by mitochondria, and as such the proximal tubules are the second most abundant sources of mitochondria in the body. Therefore, mitochondrial function is pertinent to kidney function.

Both developmental processes and normal kidney function utilize ATP, a mechanism that inherently necessitates oxygen since oxygen is considered the final electron acceptor in the electron transport chain. Oxygenation of the kidney occurs during embryonic development and is regulated by the suppression of hypoxia inducible factors (HIFs; particularly HIF-1α) by the ubiquitin ligase Von Hippel-Lindau (VHL). HIF-1α is a known mediator of metabolism by promoting glycolysis and inhibiting mitochondrial respiration. Therefore, as development progresses and renal oxygen availability increases, HIF-1α expression decreases allowing for a metabolic switch from glycolysis to oxidative phosphorylation, which drives nephron progenitor differentiation. Although the occurrence of a metabolic switch is known, the role of the VHL/HIF axis in mitochondrial function has not been well characterized, particularly during kidney development.

Previous studies have shown the VHL directly localizes to the mitochondria [244]. Moreover, another study has shown that loss of VHL in the nephron progenitors leads to suppression of mitochondrial oxygen utilization [245]. In the present study, we interrogated mitochondrial function in nephron progenitors with a VHL deletion. Previous investigations in other organs and disease states have found profound irregularities in mitochondrial biogenesis and autophagy, fission/fusion dynamics, and ROS production. For example, tumorigenic cells—which are often located in a hypoxic environment—exhibit enlarged mitochondria due to decreased fission/increased fusion mediated through interactions with the Bcl-2 family proteins Bnip3 and Bnip3l that serve to protect the cells from undergoing apoptosis [247]. Further, mitochondrial function has been directly related to morphology to allow for optimal cellular energy generation and conservation [53]. In addition to morphological changes during adaptation of cellular activity, many cell types including cancer cells can regulate mitochondrial number

through biogenesis and mitophagy depending on the energy demands and oxygen availability [68]. Since several studies have performed in-depth investigations into mitochondrial function, morphology, and density, we aimed to characterize the mitochondrial phenotype in nephron progenitors with a VHL deletion. We hypothesized that, similarly to cancer cells, we would find mitochondrial abnormalities in the absence of VHL. However, based on gene and protein expression of molecules involved in these processes, those abnormalities do not appear to occur in nephron progenitors lacking VHL. Likewise, we also investigated the role and production of ROS in our model. The current literature is split in terms of the purpose of ROS and it's interactions with HIFs. One study suggests that ROS is an important signaling molecule for HIF activation [248], however another study shows that HIF activity effectively decreases ROS generation [195]. Contradictory studies such as these indicate that the interaction between VHL/HIFs and ROS is multifaceted and likely is cell-type and disease specific. Therefore, conclusions regarding mitochondrial function and hypoxia cannot simply be applied to other model organisms or cell-specific systems without proper interrogation.

Although these previous studies have shown abnormalities in mitochondrial function, we believe that loss of VHL in our model suppresses mitochondrial respiration due to a lack of pyruvate available and transported in the mitochondria. We hypothesize that this is because the nephron progenitors are maintaining a progenitor metabolic profile and are responding to the maintenance cues of their niche. Nephron progenitors are initially exposed to a hypoxic environment and, with the loss of VHL, these cells are programmed to remain in genetically-simulated hypoxia. Other models of VHL loss typically include tumorigenic cells, which are not representative of developmental hypoxia and often experience reprogramming through HIF-2α expression. Although HIF-1α and HIF-2α can act redundantly, an increasing number of studies

are showing that the HIFs have their own unique target genes and can act either synergistically or antagonistically. Moreover HIF-2α behaves as an oncogene while HIF-1α behaves as a tumor suppressor further validating that developmental hypoxia mechanism and pathogenic hypoxia cellular responses are different. Based on these overwhelming differences in hypoxia adaptation, further research is required to characterize the cellular cues of developmental versus pathological hypoxia responses. Further discussion on the future directions and research limitations of this work are described in Chapter 6.4.

6.0 FUTURE DIRECTIONS AND IMPLICATIONS

6.1 ELUCIDATING THE CELLULAR MECHANISMS OF ADAPTATION TO HYPOXIA

6.1.1 Future experimental methodology

This brief project served to characterize the adaptation mechanisms used by kidney cells when exposed to hypoxia. We aimed to determine the proliferative, apoptotic, and metabolic affects of 1% oxygen (O_2) on HEK-293T cells. Although we made some interesting findings—such as hypoxia adaptation is a process that occurs between 24 and 48 hours after initial exposure—we failed to fully characterize the metabolic profile of these cells during the adaptive process. The experiments outlined in Chapter 2 would benefit from an increased sample sizes for gene expression, ROS generation, and lactate determination. Additionally, gene expression data should be confirmed by analysis of protein expression. A time course experiment from 24 to 72 hours should also be done to analyze gene and protein expression every 6 hours and definitively ascertain the adaptation process.

As stated, this project did not fully characterize the metabolic phenotype and although the present data suggests that a metabolic reprogramming even occurs, further experimentation is necessary. Mitochondrial stress tests and glycolysis stress tests using Seahorse extracellular flux

analysis would significantly improve this study. It is known that cells have an innate ability to adapt to low oxygen concentrations using HIF signaling and that one mechanism mediated by HIFs is metabolic reprogramming. Metabolic reprogramming during hypoxia usually consists of a switch from oxidative phosphorylation performed by the mitochondria to cytosolic anaerobic glycolysis. Seahorse extracellular flux would provide information regarding the ability of the mitochondria to function at 1% O_2 in a kidney-derived cell line. Further, a time course assay every 12 hours would allow us to determine whether metabolic switching is necessary for adaptation or whether it is a consequence that occurs after adaptation. Data obtained from the Seahorse should then be confirmed by a pyruvate oxidation assay to quantify the level of pyruvate actively being converted acetyl-CoA and CO_2.

HEK-293T cells are an easily established cell line, which was ideal for the time constraints of the present study. However, the use of human embryonic fetal kidney tissue would greatly benefit the conclusions made from the present investigation. We have preliminary Oroboros data suggesting that human fetal kidneys rely substantially on non-mitochondrial metabolism to meet the energy demands of the developing organ. Repetition of all experiments outlined in Chapter 2 and in this experimental discussion using human fetal kidneys from various gestational ages should be done to determine the ability of primary human kidney cells to adapt to the ever-changing oxygen conditions occurring *in utero*. Additionally, in both HEK-293T and primary human progenitors, it would be advantageous to better understand whether glycolysis is required for cellular maintenance (such as self-renewal of progenitor cells) or if it is merely a consequence of hypoxia. To investigate this mechanistic question, the cells would be treated with a glycolysis inhibitor and then evaluated for basic cellular functions such as cellular proliferation, apoptosis, and metabolism.

Finally, mouse nephron progenitor metabolism has been well studied [11, 17, 245], however other renal progenitor cell metabolism and the role of hypoxia has not been as extensively studied. It has previously been shown *in vivo* that maternal exposure to hypoxia (<7.5% O_2) significantly reduces ureteric branching and β-catenin signaling in the ureteric tree [10] suggesting that hypoxia does contribute to alterations in early ureteric epithelium development. Further, renal stromal progenitors with *Vhl* depletion under a Foxd1:cre results in impairment of kidney development and postnatal death that can be rescued by co-depletion of *Vhl* and *Hif-2α* [234]. The drastic phenotypes that appear in *Vhl*-depleted stromal progenitors and in hypoxia-exposed ureteric epithelium have been well characterized, however further insight into the mechanism driving these phenotypes should be aimed at metabolic profiling of the specific cell types. The work herein serves as a basis for future hypoxia investigations and suggests that metabolism plays a major role in normal progenitor cell development.

6.1.2 Expected outcomes and research limitations

Based on our current experimental data, we would predict that glycolytic metabolism would be favored during extended hypoxia exposure, which would be indicated by increased glycolysis gene and protein expression as well as increased lactate secretion in the media supernatants. Therefore, it is expected that a metabolic switching event between 24 and 48 would be confirmed using the rigorous additional experimentation outlined above. This metabolic switch likely occurs as a protective mechanism for the cells to evade apoptosis as previously shown [53, 246, 247, 249].

One major limitation to the present study is the small sample sizes. Although we reached a samples size of three per condition group of each experiment, additional samples should be

generated to determine whether significance would be reached for the experiments that were conducted.

Additionally, another major limitation was due to the use of HEK-293T cells. This cell line was originally established in 1973 from normal human embryonic kidney cells. Through decades of propagation, it is likely that these cells have acquired mutations allowing them to easily grow. Cellular division utilizes numerous mechanisms to produce the required nucleotides and proteins to sustain life, and some of these mechanisms are likely metabolic in nature. Immortalized cell lines often resemble other cell lineages or tumorigenic cells and HEK cells in particular have been shown to have dysregulated apoptotic mechanisms and cell cycle dysregulation [250]. Moreover, due to the abnormal karyotype, expression of cancer-associated proteins, and neuronal cell characteristics [250, 251], the behavior of these cells may not be entirely indicative of how the kidney would respond and adapt to hypoxia. Genomic investigation has previously shown that the HEK cell transcriptome shows expression of adrenal, kidney, and pituitary tissue [251] and expresses genes such as *NF-L*, *NF-M*, *Vim*, and several neuronal *keratins* [252]. Further, the adrenal tissue is of neural crest origin, which is hypothesized to be the reason that HEK cells has a unique "neuronal" phenotype compared to kidney specific cells lines. For these reasons, the experiments outlined in Chapter 2 and above should be repeated in more suitable cells such as MK3, MK4, or primary human kidney cells, which would be more indicative of developmental renal cell behavior.

6.1.3 Global implications

Intrauterine hypoxia is a common gestational stressor that can lead to developmental abnormalities of the fetus. Placental insufficiency is one type of intrauterine hypoxia-related

condition and is characterized by fetal oxygen deprivation [139, 253]. Moreover, placental insufficiency is a leading cause of Intrauterine Growth Restriction (IUGR) [254]. IUGR is a condition that affects 12% of deliveries and causes 75% of perinatal deaths in the United States. When disorders such as these present in the clinic, one concern of the physician is failure to thrive and decreased organ development due to the preferential redirection of blood and oxygen to the brain and heart [139, 161]. The kidney is a highly perfused organ that requires oxygen to develop and function normally. If prenatal hypoxia exposure occurs, the risk for long-term kidney disease is significantly increased. Due to the high prevalence of gestational hypoxia disorders and prenatal complications, research into the effect of hypoxia on kidney development and disease is critical.

Not only is oxygen availability important for kidney development, but also it is critical for normal kidney function. The kidney is a highly metabolically active organ and requires an abundance of oxygen to supply mitochondrial energy and facilitate blood filtration. Without oxygen, the kidney cannot transport ions and small molecules across the epithelium, thus leading to damage of the renal tubules. The nephron is the functional unit of the kidney and is comprised of the proximal and distal tubules among other segments. These tubular segments perform more than 70% of all renal function; therefore damage greatly increases susceptibility to kidney disease and injury. In fact, hypoxia is considered a major driver of chronic kidney disease and end stage renal failure (ESRF) [255]. Causes of hypoxia-induced kidney disease include: anemia, hyperglycemia, hypertension, hypercholesterolemia, sleep apnea, and environmental factors (cigarette smoking and air pollution) [255]. Unfortunately, there is no known cure for kidney disease and the treatment options include dialysis or kidney transplant, both of which significantly reduce lifespan. Current investigations into alternative treatments are aimed at

oxygenation such as erythropoietin injections, renal angioplasty, whole body oxygen chambers, and various drug therapies [255].

6.2 INTERROGATING PHYSIOLOGICAL REPROGRAMMING IN THE KDINEYS AFTER HYPOXIA EXPOSURE

6.2.1 Future experimental methodology

The focus of Chapter 3 was to characterize the phenotype, both pre- and post-natally, of mice that were exposed to hypoxia *in utero*. Previous investigations into the effect of hypoxia failed to determine the role of strict oxygenation on embryonic development, or more specifically on kidney development. Some studies have suggested that hypoxia exposure may lead to decreased nephron endowment and structural abnormalities in the kidney and other organs, but a complete characterization has not currently been done. We aimed to determine the effect of prenatal hypoxia exposure on kidney development by housing pregnant dams in hypoxia (12% O_2) or normoxia (ambient oxygen) during nephrogenesis. Although we evaluated renal histology, developmental gene expression, protein expression, and renal function our sample sizes were not ideal and several additional parameters should be assessed.

Future work should first focus on repeating the experiments outlined in Chapter 3. Numbers should be increased to four pregnant dams per condition group and time point—normoxia embryonic development, hypoxia embryonic development, normoxia P1 development, hypoxia P1 development, normoxia baseline 7 week, hypoxia baseline 7 week, normoxia cisplatin treated, and hypoxia cisplatin treated. During the oxygenation treatment period (E10.5-

P3), maternal parameters such as food intake, water intake, urine output, weight gain, litter sizes, and placental weights should all be measured. At the appropriate embryonic and postnatal collection periods, pup weight, kidney weight, pup length, and kidney length should be determined. To better define the lack of structural abnormalities, glomerular number should be quantified at all time periods, as should proximal tubule and corpuscle parameters. Moreover, this study primarily utilized male mice for post-natal characterization at baseline and after injury. In future experiments, ideally both males and females should be used, particularly because kidney injury is know to have sex-related differences [199, 256-258].

Additionally, as our laboratory has previously shown that the major developmental hypoxia pathway (VHL/HIF) mediates metabolism [245], the HIF pathway should be interrogated for its contribution in priming a physiological reprogramming response that increases kidney injury susceptibility, especially since hypoxia has been correlated to kidney disease incidence [255]. It is likely that the HIF pathway, or HIF-mediated mechanisms leading to alterations in post-translational modifications, is at play in the physiological adaptation and priming of the offspring to a secondary insult later in life. To further this investigation, HIF protein expression should be evaluated through Western blotting and immunohistochemistry to determine both quantity and localization in the kidneys. Since the proximal tubules perform a majority of blood filtration and because cisplatin preferentially targets the proximal tubules, it would be interesting to assess localization of HIF expression.

6.2.2 Expected outcomes and research limitations

Our experimental design utilizes moderate hypoxia as a maternal stressor during gestation. It is possible that 12% O_2 is not severe enough to induce structural abnormalities in the offspring of

dams exposed to the hypoxia. However, this also leads to a potential limitation of the study in that a more severe prenatal hypoxia model (which may cause structural lesions) could lead to death. For this reason, we selected the more modest oxygen dosing. However, increasing the number of samples and the parameters assessed in the study should not change the fundamental conclusions that were previously drawn in Chapter 3.

In the present study, one drawback to using hypoxia is that this treatment must be done in a contained apparatus. These devices are small, thus making it difficult to collect the maternal parameters such as food/water intake and urine output, which must be done using individual metabolic cages. Additionally, another potential drawback to the study is the use of cisplatin, however we elected to use this method of injury because we did not want to use both primary and secondary hypoxia-based injury models (ischemic reperfusion injury) so that we could attribute any differences in phenotype to developmental hypoxia exposure. Further, cisplatin usage at an incorrect dosage has been shown to cause systemic toxicity, which can occur when an incorrect dosage or evaluation time is selected [259]. Therefore, a baseline study should have first been conducted to ensure optimal dosing and timing was chosen for C57BL/6 mice.

The final major limitation to this investigation was that a mechanism was not established. In addition to an interrogation into the hypoxia pathways, several other mechanisms could be contributing to the phenotype and should be evaluated. Pathological ROS have been previously implicated in severe kidney injury and kidney disease [104, 193, 194]. The role of ROS in contributing to the robust injury found in the prenatal hypoxia-exposed mice should be conducted. Further, the Renin-Angiotensin System should be of primary interest in this investigation as the regulation of blood pressure by Renin-Angiotensin System can play an important role in cisplatin susceptibility after prenatal hypoxia. In humans, lower blood pressure

and the use of Renin-Angiotensin system inhibitors have also been associated with incidence of cisplatin nephrotoxicity [200]. Therefore based on the current literature, these pathways should be investigated for their potential role in physiological priming of injury after hypoxia exposure.

6.2.3 Global implications

This investigation has important implications in the study of placental insufficiency and IUGR even though our model was not specifically evaluated for placental abnormalities due to hypoxia. Further, our model may be more indicative of "preplacental" hypoxia, which has been shown to changes in placental blood flow, oxygenation, and nutrient availability [260]. This preplacental maternal hypoxia can also lead to alterations such as epigenetic modifications and developmental delay, both of which contribute to increased disease susceptibility [260]. Causes of preplacental hypoxia include: maternal diabetes, cardiovascular disease, anemia, asthma, and others. Although there are several causes of maternofetal hypoxia, it is best exemplified in studies investigating high altitude living. Previous studies interested in individuals residing at high altitudes have shown that for every 1,000-meter altitude increase, the resulting offspring have a 100-gram decrease in birth weight [260, 261]. Further, the placental-to-fetal weight ratio is also skewed in these populations [260]. These statistics solidify the importance of research into maternal and prenatal hypoxia exposure and its effect on offspring development.

6.3 UTILIZING THE VHL/HIF AXIS TO REGULATE METABOLISM AND NEPHRON DEVELOPMENT

6.3.1 Future experimental methodology

Chapter 4 investigated the role of VHL in kidney development. We found that VHL is critical for normal nephron differentiation and its loss leads to decreased nephron endowment. Further, we revealed that the decreased nephron endowment associated with VHL loss was due to a failure of nephron progenitors to switch their metabolic profile to induce differentiation. Although the work done in this project went through several revisions and reviewer critiques prior to its publication, further experiments could be done to utilize our findings as precursors to therapeutics and disease prevention.

We propose that future investigations should be aimed at rescuing the characterized phenotype of *VHL*$^{NP-/-}$ mice. This includes utilizing both pharmacological and genetic rescue techniques. In the present study, we performed an *in vitro* rescue on whole kidney explants using the glycolysis inhibitor YN1. This experiment allowed us to show that *VHL*$^{NP-/-}$ kidneys do not undergo sufficient differentiation, however when glycolysis is inhibited the nephron progenitors can differentiate to a similar extent as the control kidneys. The first experiment that should be done in this rescue investigation is to metabolically profile the nephron progenitors after glycolysis is inhibited in culture to determine whether these cells switched to mitochondrial energy generation. Next, similar experimentation *in vivo* should be conducted. Glycolysis inhibitors—including YN1—have been previously studied as cancer therapies to inhibit high rates of glycolysis [262, 263]. This treatment could also be used as a potential strategy to enhance nephron number in individuals with VHL mutations. A preclinical trial using *VHL*$^{NP-/-}$

mice should be done using a low dose of YN1 in an attempt to enhance nephrogenesis. Optimization of dosing and timing of treatment would first need to be conducted, however, if possible this should be done postnatally but prior to P3 (the conclusion of nephrogenesis) to reduce maternal side effects.

Another important rescue experiment that should be done is a genetic rescue using a mouse model with both a nephron progenitor-specific VHL deletion as well as a double deletion with HIF-1α knocked out as well. This would help us more definitively determine whether HIF-1α stabilization is resulting in the observed phenotype. However, one apparent drawback to this model is that there is a possibility that HIF-2α could compensate for HIF-1α loss [264, 265]. Although there is also literature that suggests there is not redundancy between the two HIF molecules [266, 267], this still may be a concern of the outlined experiment.

6.3.2 Expected outcomes and research limitations

The present study shows that nephron progenitors require a metabolic switch from glycolysis to mitochondrial respiration in order to undergo normal differentiation. Therefore, the addition of the experiments outlined above would serve to further validate the mechanistic pathway and necessitate the occurrence of a metabolic switch. We hypothesize that glycolysis inhibition *in vitro* will force the $VHL_{NP-/-}$ nephron progenitors to switch from glycolysis to oxidative metabolism, which would be shown through metabolic profiling using Seahorse extracellular flux analysis. Moreover, we would expect that *in vivo* treatment of newborn pups with YN1 would promote nephron differentiation, which could be quantified by stereological counting of the glomeruli. Although this appears feasible, pup treatment would likely have several limitations including maternal rejection and pup death. If the experiment were manageable,

further drawbacks of using systemic YN1 treatment may be failure to thrive and cell cycle arrest leading to organ failure and disease. Due to these potential complications, optimal dosing and treatment strategy would need to be determined.

6.3.3 Global implications

Previous work aimed at understanding the metabolic requirements of nephron progenitors revealed that self-renewing progenitors relied more heavily on glycolysis while progenitors poised to exit the niche preferred oxidative metabolism [17]. This study aimed to attribute the metabolic profiles to a mechanism. We found that hypoxia is a likely contributor to the metabolic switching event that occurs. Similar to nephron progenitors, other stem and progenitor cells also reside in a hypoxic environment prior to differentiation [124, 234, 243, 268]. Further, stem cell metabolism has also been readily studied and these studies have attributed metabolic regulation to hypoxia [32, 269]. Although the role of hypoxia and metabolism in stem cell population has been greatly studied, with the kidney being a particularly metabolic organ with high developmental HIF expression, it was crucial to interrogate these conditions in relation to nephron progenitor maintenance and differentiation cues. More broadly however, this study shows the importance of oxygen in cellular differentiation and is likely applicable to other models. Further, diseases—such as VHL disease, ccRCC, and end stage renal disease—may be preventable in the future based on data from hypoxia studies such as this. Identification of critical HIF targets aberrantly expressed in these disease systems could be offered as therapeutic targets, however further investigation should be done to characterize potential targets.

6.4 DETERMINING THE FUNCTIONAL ROLE OF VHL IN THE MITOCHONDRIA

6.4.1 Future experimental methodology

One study has previously shown that VHL localizes to the mitochondria [244]. Based on this finding and our interest in the role of VHL in metabolism, we hypothesized that if VHL localizes to the mitochondria then it must serve a function in the mitochondria. The present study investigated this hypothesis by defining mitochondrial density, dynamics, biogenesis, death, and ROS production and did not find any significant differences between $VHL_{NP+/-}$ and $VHL_{NP-/-}$ mitochondrial properties. Additional experimentation that should be included in this study is confirmation of VHL localization to the mitochondria in nephron progenitors. This could be done following the same experimental outline as in Shiao *et al* (2000) such as immunofluorescent staining of VHL and mitochondria or gold bead-tagged VHL visualized by electron microscopy [244]. Further, electron microscopy should be used to phenotype mitochondrial morphology, another characterization that was not analyzed in the interrogation outlined in Chapter 5.

6.4.2 Expected outcomes and research limitations

In this study, we examined several characteristics of mitochondrial health and function and did not reveal any significant findings. This led us to conclude that the mitochondria are functional in $VHL_{NP-/-}$ nephron progenitors but not utilized due to the up regulation of HIF-mediated glycolysis. Performing the experiments outlined above would likely confirm that VHL does

indeed localize to the mitochondria. In cancer cell lines, VHL's role in mitochondrial function has been shown to be dependent on the specific mutation and cell type [270], therefore we do not believe that it serves a prominent functional role in differentiating nephron progenitors.

One limitation of this portion of the study is the abundance of literature describing VHL, HIF, and metabolism. Although several of these studies were done in cancer cell lines, many of them are contradictory suggesting that this pathway may behave differently (or different VHL targets are implicated) depending on the specific cell type analyzed. It is also known that VHL has non-HIF related targets. Although HIFs re the most well characterized and hypothesized to be the major targets of VHL, non-HIF signaling could also be involved in regulating mitochondrial function in certain cell types. Several online databases, such as VHLdb, currently monitor published VHL target proteins and catalogue the function of those proteins [271]. Future work on this project should take these alternative pathways into consideration, as it would be beneficial to the investigation to explore other target pathways for involvement in mitochondrial metabolism.

6.4.3 Global implications

Similarly to the previous VHL/HIF chapter, this study has important implications in disease treatment for conditions including VHL disease and cancer. These diseases arise from mutations in the *VHL* gene leading to a nonfunctional VHL protein. One study aimed to determine whether VHL mutations in ccRCC resulted in mitochondrial dysfunction or if the other accumulated mutations in tumorigenic cells lead to the mitochondrial phenotype [238]. It was shown that when VHL was present, mitochondrial DNA and oxidative metabolism was utilized and therefore in diseases with abnormal VHL expression oxidative phosphorylation was inhibited

[238]. One limitation of this study was that it was conducted using commercially available cell lines. We believe that our mouse model offers a more translational approach to investigate VHL's role in mitochondrial function even though our model does not develop renal cancer. Wang *et al* (2014) also interrogated VHL and renal cancer and found that VHL deletion (in nephron progenitors) alone was not sufficient to cause a renal cancer phenotype, and they concluded that renal cancer arises from the accumulation of multiple mutations [86]. Although there is not cancer presentation by one month of age in our *VHL*$^{NP-/-}$ model, we can still effectively characterize the mitochondria. Further interrogation into a mitochondrial phenotype should be done using VHL-specific knockout mouse models and in primary human renal cancer cells in order to delineate VHL's role in cancer progression and treatment resistance. An investigation such as this should also be aimed at defining potential therapeutic targets, which may include use of antimetabolites (category of drug used to inhibit metabolism).

6.5 SUMMARY AND CONCLUSION

Our investigation aims to elucidate the connection between hypoxia, metabolism, and kidney development. We utilized cell lines and mouse models of developmental and genetic hypoxia in order to establish the role of the major hypoxia pathway—the VHL/HIF pathway—in regulating metabolism and ultimately nephron differentiation. We found that exposure to hypoxia *in vitro* promotes glycolysis and inhibits mitochondrial respiration and we mirrored those experiments and conclusions *in vivo* using the VHL$^{NP-/-}$ mouse model. The experiments performed *in vivo* highlight the importance of strict oxygen regulation during development and show the necessity for proper nephron formation. Although our work is not without limitation, we believe that our

hypoxia studies have laid the foundation for future work in developmental biology, disease etiology, and therapeutic investigations.

APPENDIX A

LIST OF ABBREVIATIONS

2-DG – 2-Deoxyglucose

3D – Three-dimensional

Acetyl-coA – Acetyl-coenzyme A

Acyl-coA – Acyl-coenzyme A

ADAMTS13 – A disintegrin-like and metalloprotease with thrombospondin type 1 motif 13

AKI – Acute kidney injury

AMPKα – Protein kinase AMP-activated catalytic subunit alpha 1

ATP – Adenosine triphosphate

BAP1 – BRCA1 associated protein 1

BCL2 – B cell lymphoma 2

BNIP3 – BCL2 interacting protein 3

BUN – Blood urea nitogen

CAKUT – Congenital anomalies of the kidney and urinary tract

CASP3 – Caspase 3

ccRCC – Clear cell renal cell carcinoma

cDNA – Complementary DNA

CITED1 – Cbp/P300 interacting transactivator with Glu/Asp rich carboxy-terminal domain 1

CKD – Chronic kidney disease

CO1 – Cytochrome c oxidase subunit I

CO_2 – Carbon dioxide

DAVID – The database for annotation, visualization and integrated discovery

DDIT4 – DNA damage inducible transcript 4

DMEM – Dulbecco's modified eagle media

DNA – Deoxyribonucleic acid

DNM1L/DRP1 – Dynamin family member proline-rich carboxyl-terminal domain less

ENO1 – Enolase 1

ESRD – End stage renal disease

ETC – Electron transport chain

FACS – Fluorescence-activated cell sorting

FADH/$FADH_2$ – Flavin adenine dinucleotide

FAM162A – Family with sequence similarity 162 member A

FBS – Fetal bovine serum

FCCP – Carbonyl cyanide-p-trifluoromethoxyphenylhydrazone

Fe2+ – Ferrous cation (iron)

FIS1 – Mitochondrial fission 1 protein

GAPDH – Glyceraldehyde-3-phosphate dehydrogenase

GDNF – Glial cell derived neurotrophic factor

GFP – Green fluorescent protein

GO – Gene ontology

H&E – Hematoxylin and eosin

H_2O – Dihydrogen monoxide (water)

HBSS – Hank's balanced salt solution

Hek293 – Human embryonic kidney 293 cell line

Hif1α – Hypoxia-inducible factor 1α

Hif1β – Hypoxia-inducible factor 1β

Hif2α – Hypoxia-inducible factor 2α

Hif2β – Hypoxia-inducible factor 2β

Hif3α – Hypoxia-inducible factor 3α

HIFs – Hypoxia-inducible factors

HK2 – Hexokinase 2

HREs – Hypoxia response elements

HRP – Horseradish peroxidase

KBTBD11 – Kelch repeat and BTB domain containing 11

KI67 – Protein phosphatase 1, regulatory subunit 105: protein marker protein Ki-67

LC3 I/MAP1LC3A – Microtubules associated protein 1 light chain 3 alpha

LC3 II/MAP1LC3B – Microtubule associated protein 1 light chain 3 beta

LDHA – Lactate dehydrogenase A

LEF1 – Lymphoid enhancer binding factor 1

LHX1 – LIM homeobox protein 1

MACS – Magnetic-activated cell sorting

MET – Mesenchyme to epithelial transition

MFN1 – Mitofusin 1

MFN2 – Mitofusin 2

MGARP – Mitochondria localized glutamic acid rich protein

MM – Metanephric mesenchyme

mtDNA – Mitochondrial DNA

NAD/NADH – Nicotinamide adenine dinucleotide

NCAM – Neural cell adhesion molecule

nDNA – Nuclear DNA

NDUFV1 – NADH:ubiquinone oxioreductase core subunit V1

NIX/BNIP2L – BCL2 interacting protein 3 like

NOX4 – kidney superoxide-producing NADPH oxidase

pAMPKα – Phosphorylated protein kinase AMP-activated catalytic subunit alpha 1

PCA –Principal component analysis

PCR – Polymerase chain reaction

PDK1 – Pyruvate dehydrogenase kinase 1

PFKFB3 – 6-Phosphofructo-2-kinase/Fructose-2,6-biphosphtase 3

PFKP – Phosphofructokinase, platelet-isoform

PGK1 – Phosphoglycerate kinase 1

PHD genes – Prolyl hydroxylase domain containing proteins

pHH3 – Phosphohistone H3

PI – Propidium iodide

PPARGC-1α/PGC-1α – Peroxisome proliferator-activated receptor gamma coactivator 1 alpha

PPARγ – Peroxisome proliferator-activated receptor gamma

RBCs – Red blood cells

RCC – Renal cell carcinoma

RIPA – Radioimmunoprecipitation

RN18S – 18s ribosomal RNA

RNA – Ribonucleic acid

ROS – Reactive oxygen species

SIX2 – Sine oculis homeobox homolog 2

SLC16A3/MCT4 – Solute carrier family 16 member 3 (Monocarboxylate transporter 3)

SLC2A1/GLUT1 – Solute carrier family 2 member 1 (Glucose transporter type 1)

SLC2A3 – Solute carrier family 2 member 3 (Glut3)

TCA – Tricarboxylic acid

TFAM – Transcription factor A, mitochondrial

TMRM – Tetramethylrhodamine, methyl ester, perchlorate

TPI1 – Triosephosphate isomerase 1

TUNEL – Terminal deoxynucleotidyl transferase dUTP Nick-End Labeling

UB – Ureteric bud

UE – Ureteric epithelium

VHL – Von Hippel Lindau

WNT4 – Wingless-type MMTV integration site family member 4

APPENDIX B

LIST OF REAL TIME PCR PRIMERS

Table 2: List of real time PCR primers

Gene	Species	Sense Primer	Antisense Primer
18S	Human	TCGATGCTCTTAGCTGAGTGTC	TGGCAAATGCTTTCGCTCTG
CASP3	Human	ATTATTCAGGCCTGCCGTGG	GACTGGATGAACCAGGAGCC
GAPDH	Human	AAAATCAAGTGGGGCGATGC	TCTCATGGTTCACACCCATGAC
IDH1	Human	TCCATTTTTGCCTGGACCAG	TCAGAACGTTGCACATTGGG
KI67	Human	TCCAAAGAAGGCTGAGGACA	TGAAGCCGATTCAGACCCAG
LDHA	Human	TCTCCCACCCTGCTTTTTCTG	AAGCATTCAAATGCAGCGTATC
NOX4	Human	TTTGCCATGAAGCAGGACTC	ACGGTCATCTTGCCACATTC
SIRT3	Human	CTGCTCATCAACCGGGACTT	TGGTCCATCAAGCTTCCCAG
TOMM20	Human	AGGCTTCGAGAACGAAGAAAGA	TGTCAGATGGTCTACGCCCT
Bcl2	Mouse	GAGGCTGGGATGCCTTTGT	GCAGGTTTGTCGACCTCACT
Bnip3	Mouse	TTTAAACACCCGAAGCGCAC	CCAATGTAGATCCCCAAGCCA
Cited1	Mouse	CCAACCAGGAGATGAACT	AGAGCCTATTGGAGATGTC
Ddit4	Mouse	AGGAATTTCTGTGGTGGAGACC	AAGCCTGTGTGACTCCTAAGC
Drp1	Mouse	TTCTGAGCTATGCGGTGGTG	CTCATGGACCAGCTCCACAC

Table 2 Continued: List of real time PCR primers

Gene	Species	Sense Primer	Antisense Primer
Eno1	Mouse	CTACCCAGTGGTGTCCATCG	TTACACGCCTGCAGGGATTC
Eya1	Mouse	GGAATGCTATTATGAGGTAGAA	ATCCTTGTTGACACTTGAC
Foxd1	Mouse	TGTGGAGAACTTTACTGCTA	AAATAGATGGACCCTCTGAG
Gapdh	Mouse	AACCTGCCAAGTATGATGA	GGAGTTGCTGTTGAAGTC
Jag1	Mouse	ACAACACCACCAACAATG	GTCATCCTCCTCCACTTC
Lc3	Mouse	GAACCGCAGACGCATCTCT	ATGATCACCGGGATCTTACTGG
Ldha	Mouse	TGGAGTGGTGTGAATGTTGC	ATGGTGGAAATGGGATGCAC
Lef1	Mouse	AGCTTGTTGAAACCCCAGAC	TTTTTGGAAGTCGGCGCTTG
Lhx1	Mouse	CTACATCATAGACGAGAACAAG	TCATTACTACCACCTTCCTTAT
Nox4	Mouse	TCAAACAGCTGTGCTATGCC	ATCAACAGCGTGCGTCTAAC
Opa1	Mouse	CTTGCCAGTTTAGCTCCCGA	GTCTGACACCTTCCTGTAATGCT
Osr1	Mouse	ACTGATGAGCGACCTTAC	TTGTGAGTGTAGCGTCTT
Pax2	Mouse	GCTAAGGAAAGGACTTTGTG	TAGGCAGTTCAGGTGGAT
Pdk1	Mouse	GCGAGGAGGATCTGACTGTG	GATAACCGCATCTGTCCCGT
Pgk1	Mouse	AGAAATATGCCGAGGCTGTG	TGTGTTCCATTTGGCACAGC
Rn18s	Mouse	GACAGGATTGACAGATTGATAG	CCAGAGTCTCGTTCGTTA
Sall1	Mouse	GGACTATGAACTACACTATGAAG	CAACTTGCGATTGCCATA
Six2	Mouse	GCAGGACTCCATACTCAA	GATACCGAGCAGACCATT
Slc2a1	Mouse	ACTTCATTGTGGGCATGTGC	TCGGGTGTCTTGTCACTTTG
Sox9	Mouse	AAGGAAGGAAGGAAGGAAG	AGGCACAGTGAATGTTCTA
Tfam	Mouse	AAGTCTTGGGAAGAGCAGATGGCT	AGACCTAACTGGTTTCTTGGGCCT
Wnt4	Mouse	TCTCTGCTCATTGTCCAT	TGCTGAACTAAGTCTACCA

APPENDIX C

LIST OF GENOTYPING PRIMERS

Table 3: List of genotyping primers

Gene	Sense Primer	Antisense Primer
Six2-TGC$_{tg}$ allele	ATGCTCATCCGGAGTTCCGTATG	CACCTTGTCGCCTTGCGTATAA
Vhl allele	AAGAGCACGCAGCTTAGGAG	TTTCTGAGTCCTGGGGATTG

APPENDIX D

LIST OF ANTIBODIES AND LECTINS

Table 4: List of antibodies and lectins

Protein/antibody	Company	Catalog #	Concentration
α/β tubulin	Cell Signaling Technology	2148	1:1000
CD105	R&D Systems	AF1320	1:10
CD140a	R&D Systems	AF1061	1:10
CD326	BD Biosciences	552370	1:50
DAPI	Thermo Fisher Scientific	D1306	1:3000
DBA	Vector Laboratories	B-1035	1:!00
Dnm1l	Thermo Fisher Scientific	PA1-16987	1:250
Donkey anti-mouse	Jackson ImmunoResearch Laboratories	715-475-150	1:200
Donkey anti-rabbit	Rockland antibodies & assays	612-446-026	1:200
Endomucin	Santa Cruz Biotechnology	sc-65495	1:100
Glut1	Abcam	ab652	1:100
Hif-1α	Novus Biologicals	NB100-105	1:250

Table 4 Continued: List of antibodies and lectins

Protein/antibody	Company	Catalog #	Concentration
Protein/antibody	Company	Catalog #	Concentration
IgG-Mouse-HRP	Cell Signaling Technology	7076	1:1000
IgG-Rabbit-HRP	Cell Signaling Technology	7074	1:1000
Jagged1	Santa Cruz Biotechnology	sc-390177	1:20
Lef1	Cell Signaling	2230	1:100
LTL	Vector Laboratories	L-1320	1:100
Ncam	Millipore Sigma	C9672	1:100
Oat1	Alpha Diagnostic International	OAT11-A	1:100
Pck1	Proteintech	16754-1-AP	1:100
pHH3	Cell Signaling Technology	9701	1:100
Pgc-1α	Novus Biologicals	4676	1:250
Sall1	Abcam	ab31526	1:100
Six2	Proteintech	11562-1-AP	1:100
TER119	R&D Systems	MAB1125	1:10
Tomm20	Santa Cruz Biotechnology	sc-11415	1:500
Vhl	Santa Cruz Biotechnology	sc-5575	1:250
Wt1	Santa Cruz Biotechnology	sc-393498	1:100

APPENDIX E

LIST OF FLUORESCENT DYES

Table 5: List of fluorescent dyes

Dye	Concentration	Company	Catalog #
LysoTracker	65nM	Thermo Fisher Scientific	L7528
MitoSox	5μM	Thermo Fisher Scientific	M36008
MitoTracker	200nM	Thermo Fisher Scientific	M22425
Propidium Iodide	0.5mL	Thermo Fisher Scientific	F10797
VPD450	1mM	BD Biosciences	562158

APPENDIX F

LIST OF INHIBITORS

Table 6: List of inhibitors

Inhibitor	Concentration	Company	Catalog #
Antimycin A	1μM	Agilent	103015-100
Cisplatin	20mg/kg bw	APP NDC	63323-103-64
FCCP	0.3 μM	Agilent	103015-100
Oligomycin	1 μg/mL	Agilent	103015-100
Rotenone	0.1 μM	Agilent	103015-100
YN1	10 μM	Millipore Sigma	CAS 75187-63-2

APPENDIX G

SUPPLEMENTAL DATA

RNA-sequencing supplemental data

Table 7: Complete list of significantly dysregulated genes

ID	Definition
mmu:100042025	K00134 glyceraldehyde 3-phosphate dehydrogenase [EC:1.2.1.12] | (RefSeq) Gapdh-ps15, Gm20899
mmu:105244208	K02991 small subunit ribosomal protein S6e | (RefSeq) 40S ribosomal protein S6
mmu:10805	K04515 calcium/calmodulin-dependent protein kinase (CaM kinase) II [EC:2.7.11.17] | (RefSeq) Camk2d
mmu:112405	K09592 hypoxia-inducible factor prolyl hydroxylase [EC:1.14.11.29] | (RefSeq) Egln1, AI503754, C1orf
mmu:112406	K09592 hypoxia-inducible factor prolyl hydroxylase [EC:1.14.11.29] | (RefSeq) Egln2, 0610011A13Rik
mmu:112407	K09592 hypoxia-inducible factor prolyl hydroxylase [EC:1.14.11.29] | (RefSeq) Egln3, 2610021G09Rik
mmu:11600	K05465 angiopoietin 1 | (RefSeq) Angpt1, 1110046O21Rik, Ang-1, Ang1; angiopoietin 1
mmu:11601	K05466 angiopoietin 2 | (RefSeq) Angpt2, Agpt2, Ang-2, Ang2; angiopoietin 2
mmu:11602	K05467 angiopoietin 4 | (RefSeq) Angpt4, ANG-3, ANG-4, Agpt4, Ang3; angiopoietin 4
mmu:11651	K04456 RAC serine/threonine-protein kinase [EC:2.7.11.1] | (RefSeq) Akt1, Akt, LTR-akt, PKB, PKB/Akt
mmu:11652	K04456 RAC serine/threonine-protein kinase [EC:2.7.11.1] | (RefSeq) Akt2, 2410016A19Rik, AW554154
mmu:11674	K01623 fructose-bisphosphate aldolase, class I [EC:4.1.2.13] | (RefSeq) Aldoa, Aldo-1, Aldo1; aldolase
mmu:11863	K09097 aryl hydrocarbon receptor nuclear translocator | (RefSeq) Arnt, D3Ertd557e, Drnt, ESTM42, Hif
mmu:12043	K02161 apoptosis regulator Bcl-2 | (RefSeq) Bcl2, AW986256, Bcl-2, C430015F12Rik, D630044D05Rik, D83
mmu:12322	K04515 calcium/calmodulin-dependent protein kinase (CaM kinase) II [EC:2.7.11.17] | (RefSeq) Camk2a
mmu:12323	K04515 calcium/calmodulin-dependent protein kinase (CaM kinase) II [EC:2.7.11.17] | (RefSeq) Camk2b
mmu:12325	K04515 calcium/calmodulin-dependent protein kinase (CaM kinase) II [EC:2.7.11.17] | (RefSeq) Camk2g
mmu:12575	K06625 cyclin-dependent kinase inhibitor 1A | (RefSeq) Cdkn1a, CAP20, CDKI, CIP1, Cdkn1, P21, SDI1
mmu:12576	K06624 cyclin-dependent kinase inhibitor 1B | (RefSeq) Cdkn1b, AA408329, AI843786, Kip1, p27, p27Kip
mmu:12914	K04498 E1A/CREB-binding protein [EC:2.3.1.48] | (RefSeq) Crebbp, AW558298, CBP, CBP/p300, KAT3A, p30
mmu:13058	K21421 NADPH oxidase 2 [EC:1.-.-.-] | (RefSeq) Cybb, C88302, CGD91-phox, Cgd, Cyd, Nox2, gp91-1, gp9
mmu:13614	K16366 endothelin-1 | (RefSeq) Edn1, ET-1, PPET1, preproET; endothelin 1
mmu:13645	K04357 epidermal growth factor | (RefSeq) Egf, AI790464; epidermal growth factor
mmu:13649	K04361 epidermal growth factor receptor [EC:2.7.10.1] | (RefSeq) Egfr, 9030024J15Rik, AI552599, Erbb
mmu:13684	K03259 translation initiation factor 4E | (RefSeq) Eif4e, EG668879, Eif4e-ps, If4e, eIF-4E; eukaryot
mmu:13685	K07205 eukaryotic translation initiation factor 4E binding protein 1 | (RefSeq) Eif4ebp1, 4e-bp1, AA
mmu:13806	K01689 enolase [EC:4.2.1.11] | (RefSeq) Eno1, 0610008I15, AL022784, Eno-1, MBP-1; enolase 1
mmu:13807	K01689 enolase [EC:4.2.1.11] | (RefSeq) Eno2, AI837106, D6Ertd375e, Eno-2, NSE; enolase 2
mmu:13808	K01689 enolase [EC:4.2.1.11] | (RefSeq) Eno3, Eno-3, MSE; enolase 3, beta muscle
mmu:13856	K05437 erythropoietin | (RefSeq) Epo; erythropoietin
mmu:13866	K05083 receptor tyrosine-protein kinase erbB-2 [EC:2.7.10.1] | (RefSeq) Erbb2, Erbb-2, HER-2, HER2
mmu:14254	K05096 FMS-like tyrosine kinase 1 [EC:2.7.10.1] | (RefSeq) Flt1, AI323757, Flt-1, VEGFR-1, VEGFR1, s
mmu:14433	K00134 glyceraldehyde 3-phosphate dehydrogenase [EC:1.2.1.12] | (RefSeq) Gapdh, Gapd; glyceraldehyde
mmu:15251	K08268 hypoxia-inducible factor 1 alpha | (RefSeq) Hif1a, AA959795, HIF-1-alpha, HIF1-alpha, HIF1alpha

Table 7 Continued: Complete list of significantly dysregulated genes

mmu:15275	K00844 hexokinase [EC:2.7.1.1] | (RefSeq) Hk1, BB404130, Hk-1, Hk1-s, dea, mHk1-s; hexokinase 1
mmu:15277	K00844 hexokinase [EC:2.7.1.1] | (RefSeq) Hk2, AI642394, HKII; hexokinase 2
mmu:15368	K00510 heme oxygenase 1 [EC:1.14.14.18] | (RefSeq) Hmox1, D8Wsu38e, HO-1, HO1, Hemox, Hmox, Hsp32
mmu:15978	K04687 interferon gamma | (RefSeq) Ifng, IFN-g, Ifg; interferon gamma
mmu:15979	K05132 interferon gamma receptor 1 | (RefSeq) Ifngr1, CD119, IFN-gammaR, Ifgr, Ifngr, Nktar
mmu:15980	K05133 interferon gamma receptor 2 | (RefSeq) Ifngr2, Ifgr2, Ifgt; interferon gamma receptor 2
mmu:16000	K05459 insulin-like growth factor 1 | (RefSeq) Igf1, C730016P09Rik, Igf-1, Igf-I
mmu:16001	K05087 insulin-like growth factor 1 receptor [EC:2.7.10.1] | (RefSeq) Igf1r, A330103N21Rik, CD221
mmu:16193	K05405 interleukin 6 | (RefSeq) Il6, Il-6; interleukin 6
mmu:16194	K05055 interleukin 6 receptor | (RefSeq) Il6ra, CD126, IL-6R, IL-6R-alpha, IL-6RA, Il6r
mmu:16333	K04526 insulin | (RefSeq) Ins1, Ins-1, Ins2-rs1
mmu:16334	K04526 insulin | (RefSeq) Ins2, AA986540, Ins-2, InsII, Mody, Mody4; insulin II
mmu:16337	K04527 insulin receptor [EC:2.7.10.1] | (RefSeq) Insr, 4932439J01Rik, CD220, D630014A15Rik
mmu:16828	K00016 L-lactate dehydrogenase [EC:1.1.1.27] | (RefSeq) Ldha, Ldh1, Ldhm, l7R2; lactate dehydrogenase
mmu:17000	K03159 lymphotoxin beta receptor TNFR superfamily member 3 | (RefSeq) Ltbr, AI256028, LTbetaR, Ltar
mmu:170768	K01103 6-phosphofructo-2-kinase / fructose-2,6-biphosphatase 3 [EC:2.7.1.105 3.1.3.46] | (RefSeq) Pf
mmu:17346	K04372 MAP kinase interacting serine/threonine kinase [EC:2.7.11.1] | (RefSeq) Mknk1, 2410048M24Rik
mmu:17347	K04372 MAP kinase interacting serine/threonine kinase [EC:2.7.11.1] | (RefSeq) Mknk2, 2010016G11Rik
mmu:18033	K02580 nuclear factor NF-kappa-B p105 subunit | (RefSeq) Nfkb1, NF-KB1, NF-kappaB, NF-kappaB1, p105
mmu:18126	K13241 nitric-oxide synthase, inducible [EC:1.14.13.39] | (RefSeq) Nos2, MAC-NOS, NOS-II, Nos-2
mmu:18127	K13242 nitric-oxide synthase, endothelial [EC:1.14.13.39] | (RefSeq) Nos3, 2310065A03Rik, Nos-3
mmu:18597	K00161 pyruvate dehydrogenase E1 component alpha subunit [EC:1.2.4.1] | (RefSeq) Pdha1, Pdha-1
mmu:18598	K00161 pyruvate dehydrogenase E1 component alpha subunit [EC:1.2.4.1] | (RefSeq) Pdha2, Pdhal
mmu:18641	K00850 6-phosphofructokinase 1 [EC:2.7.1.11] | (RefSeq) Pfkl, AA407869, ATP-PFK, PFK-B, PFK-L
mmu:18655	K00927 phosphoglycerate kinase [EC:2.7.2.3] | (RefSeq) Pgk1, Pgk-1; phosphoglycerate kinase 1
mmu:18706	K00922 phosphatidylinositol-4,5-bisphosphate 3-kinase catalytic subunit alpha/beta/delta
mmu:18707	K00922 phosphatidylinositol-4,5-bisphosphate 3-kinase catalytic subunit alpha/beta/delta
mmu:18708	K02649 phosphoinositide-3-kinase regulatory subunit alpha/beta/delta | (RefSeq) Pik3r1, PI3K
mmu:18709	K02649 phosphoinositide-3-kinase regulatory subunit alpha/beta/delta | (RefSeq) Pik3r2, p85beta
mmu:18710	K02649 phosphoinositide-3-kinase regulatory subunit alpha/beta/delta | (RefSeq) Pik3r3, AA414954
mmu:18750	K02677 classical protein kinase C alpha type [EC:2.7.11.13] | (RefSeq) Prkca, AI875142, Pkca
mmu:18751	K19662 classical protein kinase C beta type [EC:2.7.11.13] | (RefSeq) Prkcb, PKC-B, PKC-Beta, Pkcb
mmu:18752	K19663 classical protein kinase C gamma type [EC:2.7.11.13] | (RefSeq) Prkcg, PKCgamma, Pkcc, Prkcc
mmu:18787	K03982 plasminogen activator inhibitor 1 | (RefSeq) Serpine1, PAI-1, PAI1, Planh1
mmu:18803	K01116 phosphatidylinositol phospholipase C, gamma-1 [EC:3.1.4.11] | (RefSeq) Plcg1, AI894140, Cded
mmu:19697	K04735 transcription factor p65 | (RefSeq) Rela, p65, p65_NF-kappa_B, p65_NFkB
mmu:20104	K02991 small subunit ribosomal protein S6e | (RefSeq) Rps6, S6R; ribosomal protein S6
mmu:20525	K07299 MFS transporter, SP family, solute carrier family 2 (facilitated glucose transporter)
mmu:20848	K04692 signal transducer and activator of transcription 3 | (RefSeq) Stat3, 1110034C02Rik, AW109958
mmu:212032	K00844 hexokinase [EC:2.7.1.1] | (RefSeq) Hk3, HK_III, HK-III; hexokinase 3
mmu:216019	K00844 hexokinase [EC:2.7.1.1] | (RefSeq) Hkdc1, BC016235; hexokinase domain containing 1
mmu:21687	K05121 endothelial-specific receptor tyrosine kinase [EC:2.7.10.1] | (RefSeq) Tek, AA517024, Cd202b
mmu:218268	K03259 translation initiation factor 4E | (RefSeq) Eif4e1b, Eif4eloo, Gm273
mmu:21857	K16451 metallopeptidase inhibitor 1 | (RefSeq) Timp1, Clgi, EPA, TIMP-1, TPA-S1, Timp
mmu:21898	K10160 toll-like receptor 4 | (RefSeq) Tlr4, Lps, Ly87, Ran/M1, Rasl2-8; toll-like receptor 4
mmu:22041	K14736 transferrin | (RefSeq) Trf, AI266983, Cd176, HP, Tf, Tfn, hpx
mmu:22042	K06503 transferrin receptor | (RefSeq) Tfrc, 2610028K12Rik, CD71, E430033M20Rik, Mtvr1, TFR, TFR1
mmu:22339	K05448 vascular endothelial growth factor A | (RefSeq) Vegfa, Vegf, Vpf
mmu:22346	K03871 von Hippel-Lindau disease tumor supressor | (RefSeq) Vhl, Vhlh, pVHL; von Hippel-Lindau tumor
mmu:226265	K01689 enolase [EC:4.2.1.11] | (RefSeq) Eno4, 6430537H07Rik; enolase 4
mmu:228026	K12077 pyruvate dehydrogenase kinase isoform 1 [EC:2.7.11.2] | (RefSeq) Pdk1, B830012B01, D530020C15
mmu:230899	K12334 natriuretic peptide A | (RefSeq) Nppa, ANP, Anf, Pnd; natriuretic peptide type A
mmu:234779	K05859 phosphatidylinositol phospholipase C, gamma-2 [EC:3.1.4.11] | (RefSeq) Plcg2, PLC-gamma-2
mmu:23797	K04456 RAC serine/threonine-protein kinase [EC:2.7.11.1] | (RefSeq) Akt3, AI851531, D930002M15Rik
mmu:26395	K04368 mitogen-activated protein kinase kinase 1 [EC:2.7.12.2] | (RefSeq) Map2k1, MAPKK1, MEKK1
mmu:26396	K04369 mitogen-activated protein kinase kinase 2 [EC:2.7.12.2] | (RefSeq) Map2k2, AA589381, MEK2
mmu:26413	K04371 mitogen-activated protein kinase 1/3 [EC:2.7.11.24] | (RefSeq) Mapk1, 9030612K14Rik
mmu:26417	K04371 mitogen-activated protein kinase 1/3 [EC:2.7.11.24] | (RefSeq) Mapk3, Erk-1, Erk1, Ert2
mmu:26987	K03259 translation initiation factor 4E | (RefSeq) Eif4e2, 2700069E09Rik, AI036339, AV129531
mmu:328572	K04498 E1A/CREB-binding protein [EC:2.3.1.48] | (RefSeq) Ep300, A430090G16, A730011L11, KAT3B, p300

Table 7 Continued: Complete list of significantly dysregulated genes

mmu:433182	K01689 enolase [EC:4.2.1.11] | (RefSeq) Eno1b, EG433182, Eno-1, Eno1, Gm5506, NNE; enolase 1B
mmu:56438	K03868 RING-box protein 1 [EC:2.3.2.32] | (RefSeq) Rbx1, 1500002P15Rik, AA517855, ROC1
mmu:56717	K07203 serine/threonine-protein kinase mTOR [EC:2.7.11.1] | (RefSeq) Mtor, 2610315D21Rik, AI327068
mmu:58988	K04688 ribosomal protein S6 kinase beta [EC:2.7.11.1] | (RefSeq) Rps6kb2, S6K-beta-2, S6K2
mmu:67673	K03873 elongin-B | (RefSeq) Elob, 0610040H15Rik, Tceb2
mmu:67923	K03872 elongin-C | (RefSeq) Eloc, 2610043E24Rik, 2610301I15Rik, AA407206, AI987979, AW049146, Tceb1
mmu:68263	K00162 pyruvate dehydrogenase E1 component beta subunit [EC:1.2.4.1] | (RefSeq) Pdhb, 2610103L06Rik
mmu:71745	K03870 cullin 2 | (RefSeq) Cul2, 1300003D18Rik, 4932411N15Rik, AI327301, mKIAA4106
mmu:71775	K14736 transferrin | (RefSeq) 1300017J02Rik, Ica, mICA
mmu:72508	K04688 ribosomal protein S6 kinase beta [EC:2.7.11.1] | (RefSeq) Rps6kb1, 2610318I15Rik, AA959758
mmu:74769	K00922 phosphatidylinositol-4,5-bisphosphate 3-kinase catalytic subunit alpha/beta/delta

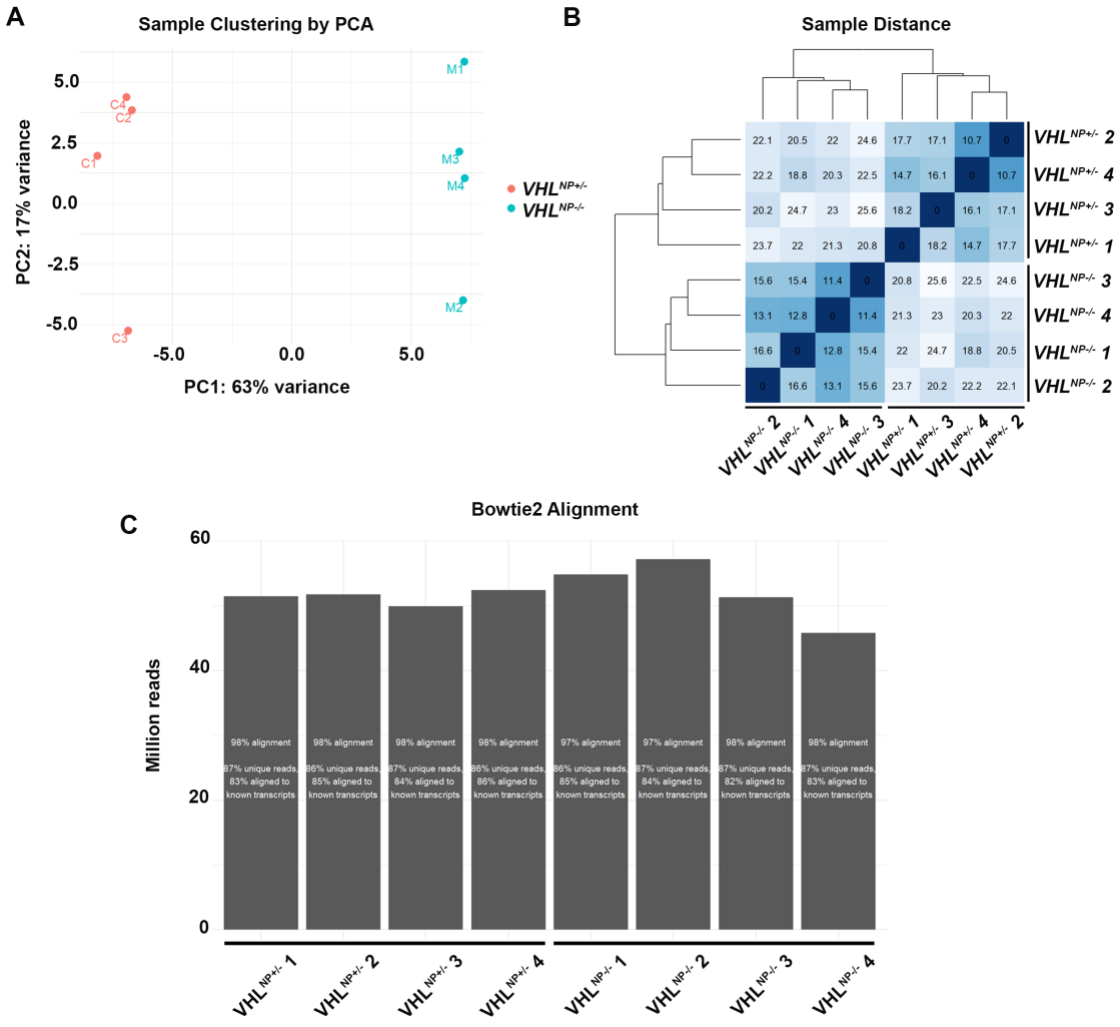

Figure 30: RNA-sequencing gene expression clustering
(A) Sample clustering by Principal Component Analysis shows clear grouping of samples based on genotype. **(B)** Sample distance heat map shows clustering of samples based on genotype. **(C)** Library sizes are consistent between samples with a high percentage of unique reads aligned to known transcripts. N=4.

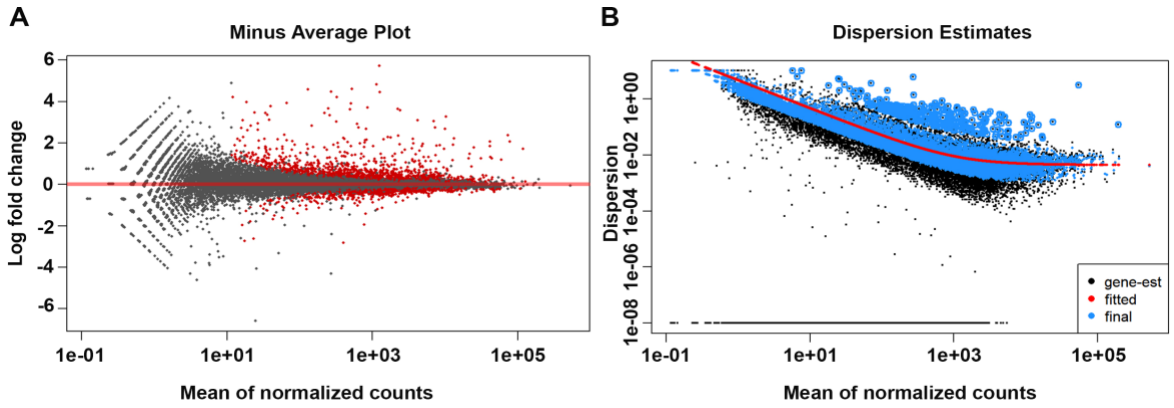

Figure 31: RNA-sequencing gene dispersion
(A) Minus average plot showing the distribution of expression changes versus total expression. Red dots indicate significance while black dots are not significant. **(B)** Dispersion estimates by DESeq2 to estimate variance of a given gene based on expression level. Red line indicates expected variance of a given gene. Black dots indicate actual variance of each gene and blue dots indicate DESeq2 correction. N=4.

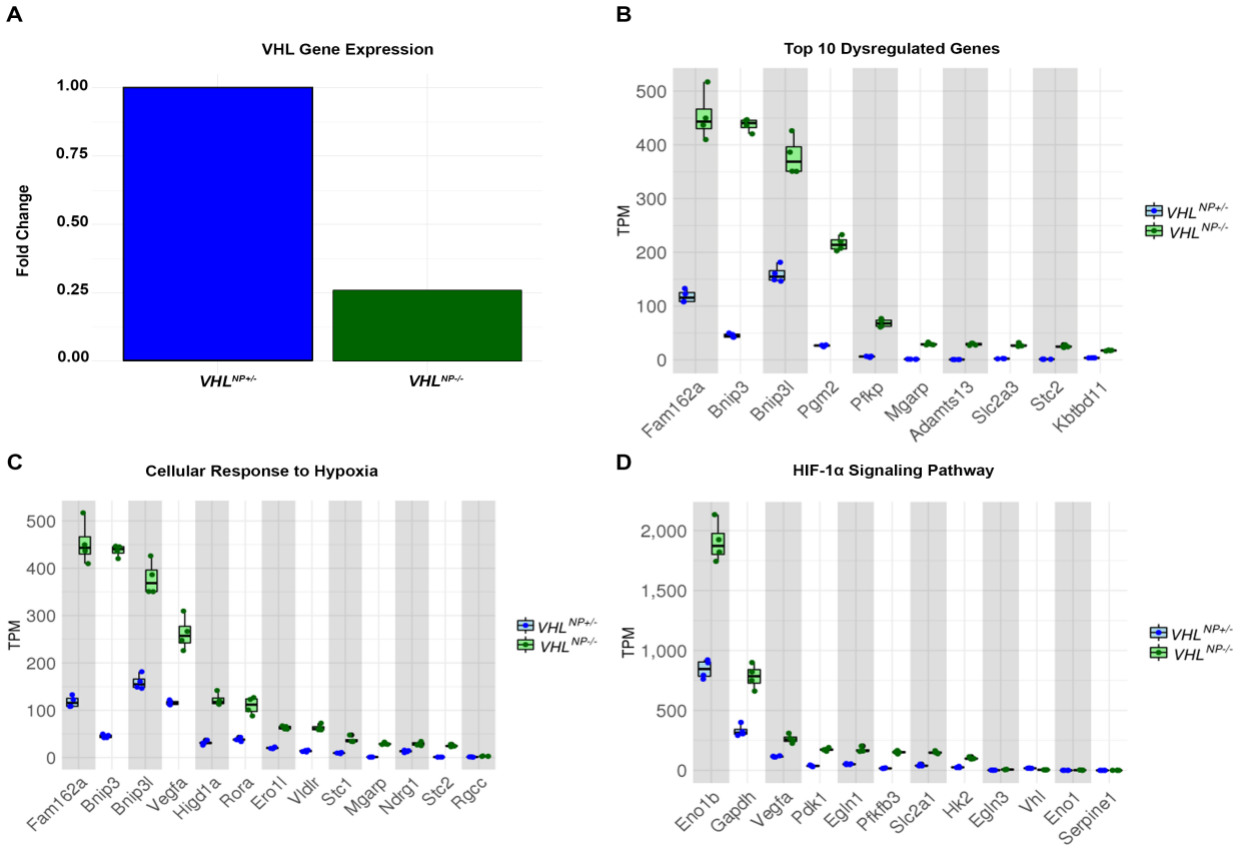

Figure 32: RNA-sequencing gene expression
(A) Mean read counts showing decreased VHL gene expression in isolate nephron progenitors from *VHL*$^{NP-/-}$ mice. **(B)** Plot showing the top 10 most dysregulated genes. **(C)** Annotation-associated gene expression showing cellular response to hypoxia (GO term) genes using DAVID analysis. **(D)** Annotation-associated gene expression showing HIF-1α signaling pathway (GO term) genes using DAVID analysis. N=4

BIBLIOGRAPHY

1. Gilbert, S.F., *Intermediate Mesoderm*, in *Developmental Biology*. 2000, Sinauer Associates, Inc: Sunderland, MA.

2. Davidson, A.J., *Mouse Kidney Development*, in *StemBook*, K.R. Chien, Editor. 2009, The Stem Cell Research Community.

3. Little, M.H., et al., *Kidney Development: Two Tales of Tubulogenesis*, in *Current Topics in Developmental Biology*. 2010, Elsevier. p. 193-229.

4. Lechner, M.S. and G.R. Dressler, *The molecular basis of embryonic kidney development.* Mech Dev, 1997. **62**(2): p. 105-20.

5. Hatini, V., et al., *Essential role of stromal mesenchvme in kidnev morphogenesis revealed' by targeted di&upCion of Winged Helix transcription factor BF-2.* Genes & Development, 1996. **10**: p. 1467-1478.

6. Little, M.H. and A.P. McMahon, *Mammalian kidney development: principles, progress, and projections.* Cold Spring Harb Perspect Biol, 2012. **4**(5).

7. O'Brien, L.L. and A.P. McMahon, *Induction and patterning of the metanephric nephron.* Semin Cell Dev Biol, 2014. **36**: p. 31-8.

8. Dressler, G.R., *The cellular basis of kidney development.* Annu Rev Cell Dev Biol, 2006. **22**: p. 509-29.

9. Keller, G., et al., *Nephron number in patients with primary hypertension.* N Engl J Med, 2003. **348**(2): p. 101-8.

10. Wilkinson, L.J., et al., *Renal developmental defects resulting from in utero hypoxia are associated with suppression of ureteric beta-catenin signaling.* Kidney Int, 2015. **87**(5): p. 975-83.

11. Li, Y., et al., *p53 Enables metabolic fitness and self-renewal of nephron progenitor cells.* Development, 2015. **142**(7): p. 1228-41.

12. Seikaly, M.G., et al., *Chronic renal insufficiency in children: the 2001 Annual Report of the NAPRTCS.* Pediatr Nephrol, 2003. **18**(8): p. 796-804.

13. Smith, J.M., et al., *Contributions of the Transplant Registry: The 2006 Annual Report of the North American Pediatric Renal Trials and Collaborative Studies (NAPRTCS).* Pediatr Transplant, 2007. **11**(4): p. 366-73.

14. Saran, R., B. Robinson, and V. Shahinian, *US Renal Data System 2015 Annual Data Report: epidemiology of kidney disease in the United States.* Am J Kidney Dis, 2016. **67**(3).

15. Pannabecker, T.L., *Structure and Function of the Thin Limbs of the Loop of Henle.* Comprehensive Physiology, 2012. **2**(3): p. 2063-2086.

16. Takasato, M. and M.H. Little, *The origin of the mammalian kidney: implications for recreating the kidney in vitro.* Development, 2015. **142**(11): p. 1937-47.

17. Liu, J., et al., *Regulation of Nephron Progenitor Cell Self-Renewal by Intermediary Metabolism.* J Am Soc Nephrol, 2017. **28**(11): p. 3323-3335.

18. Cebrian, C., et al., *The number of fetal nephron progenitor cells limits ureteric branching and adult nephron endowment.* Cell Rep, 2014. **7**(1): p. 127-37.

19. Liu, S., et al., *Effect of Hypoxia on the Differentiation and the Self-Renewal of Metanephrogenic Mesenchymal Stem Cells.* Stem Cells Int, 2017. **2017**: p. 7168687.

20. Nwankwo, T., et al., *Hypertension among adults in the United States: National Health and Nutrition Examination Survey, 2011–2012.* NCHS data brief, 2013(133).

21. (CDC), C.f.D.C.a.P., *National Chronic Kidney Disease Fact Sheet: General Information and National Estimates on Chronic Kidney Disease in the United States, 2014.* 2014.

22. Bertram, J.F., et al., *Human nephron number: implications for health and disease.* Pediatr Nephrol, 2011. **26**(9): p. 1529-33.

23. QueiBer-Luft, A., et al., *Malformations in newborn: results based on 30940 infants and fetuses from the Mainz congenital birth defect monitoring system (1990-1998).* Arch Gynecol Obstet, 2002. **266**: p. 163-167.

24. Sanna-Cherchi, S., et al., *Renal outcome in patients with congenital anomalies of the kidney and urinary tract.* Kidney Int, 2009. **76**(5): p. 528-33.

25. Moritz, K.M., et al., *Developmental programming of a reduced nephron endowment: more than just a baby's birth weight.* Am J Physiol Renal Physiol, 2008. **296**: p. 1-9.

26. Costantini, F. and R. Kopan, *Patterning a complex organ: branching morphogenesis and nephron segmentation in kidney development.* Dev Cell, 2010. **18**(5): p. 698-712.

27. Brown, A.C., S.D. Muthukrishnan, and L. Oxburgh, *A synthetic niche for nephron progenitor cells.* Dev Cell, 2015. **34**(2): p. 229-41.

28. Saifudeen, Z., et al., *p53 regulates metanephric development.* J Am Soc Nephrol, 2009. **20**(11): p. 2328-37.

29. Karner, C.M., et al., *Canonical Wnt9b signaling balances progenitor cell expansion and differentiation during kidney development.* Development, 2011. **138**(7): p. 1247-57.

30. Tanigawa, S., et al., *Wnt4 induces nephronic tubules in metanephric mesenchyme by a non-canonical mechanism.* Dev Biol, 2011. **352**(1): p. 58-69.

31. Nagalakshmi, V.K. and J. Yu, *The ureteric bud epithelium: morphogenesis and roles in metanephric kidney patterning.* Mol Reprod Dev, 2015. **82**(3): p. 151-66.

32. Ito, K. and T. Suda, *Metabolic requirements for the maintenance of self-renewing stem cells.* Nat Rev Mol Cell Biol, 2014. **15**(4): p. 243-56.

33. Gray, L.R., S.C. Tompkins, and E.B. Taylor, *Regulation of pyruvate metabolism and human disease.* Cell Mol Life Sci, 2014. **71**(14): p. 2577-604.

34. Li, X.B., J.D. Gu, and Q.H. Zhou, *Review of aerobic glycolysis and its key enzymes - new targets for lung cancer therapy.* Thorac Cancer, 2015. **6**(1): p. 17-24.

35. McCommis, K.S. and B.N. Finck, *Mitochondrial pyruvate transport: a historical perspective and future research directions.* Biochem J, 2015. **466**(3): p. 443-54.

36. Rogatzki, M.J., et al., *Lactate is always the end product of glycolysis.* Front Neurosci, 2015. **9**: p. 22.

37. Vander Heiden, M.G., L.C. Cantley, and C.B. Thompson, *Understanding the Warburg effect: the metabolic requirements of cell proliferation.* Science, 2009. **324**(5930): p. 1029-33.

38. Singer, K., et al., *Warburg phenotype in renal cell carcinoma: high expression of glucose-transporter 1 (GLUT-1) correlates with low CD8(+) T-cell infiltration in the tumor.* Int J Cancer, 2011. **128**(9): p. 2085-95.

39. Spencer, N.Y. and R.C. Stanton, *Glucose-6-phosphate dehydrogenase and the kidney.* Nephrology and Hypertension, 2017. **26**(1): p. 43-49.

40. Steer, K.A., et al., *Regulation of pathways of glucose metabolism in kidney.* FEBS Letters, 1982. **150**(2): p. 494-498.

41. Socher, M., S. Kunjara, and P. McLean, *Regulation of Pathways of Glucose Metabolism on the Kidney.* Hormone and Metabolic Research, 1988. **20**: p. 676-681.

42. Guder, W.G. and G. Wirthensohn, *Metabolism of isolated kidney tubules.* Eur. J. Biochem., 1979. **99**: p. 577-584.

43. Wirthensohn, G. and W.G. Guder, *Triacyiglycerol Metabolism in Isolated Rat Kidney Cortex Tubules.* Biochem. J., 1980. **186**(317-324).

44. Mather, A. and C. Pollock, *Glucose handling by the kidney.* Kidney Int Suppl, 2011(120): p. S1-6.

45. Triplitt, C.L., *Understanding the kidneys' role in blood glucose regulation.* Am J Manag Care, 2012. **18**(1): p. S11-16.

46. Stumvoll, M., et al., *Role of glutamine in human carbohydrate metabolism in kidney and other tissues.* Kidney Int, 1999. **55**(3): p. 778-92.

47. Engelking, L., *Gluconeogenesis*, in *Textbook of Veternary Physiology*. 2015, Academic Press. p. 225-230.

48. Gerich, J.E., et al., *Renal Gluconeogenesis.* Diabetes Care, 2001. **24**(2).

49. Poirier, Y., et al., *Peroxisomal beta-oxidation--a metabolic pathway with multiple functions.* Biochim Biophys Acta, 2006. **1763**(12): p. 1413-26.

50. Forbes, J.M., *Mitochondria-Power Players in Kidney Function?* Trends Endocrinol Metab, 2016. **27**(7): p. 441-2.

51. Houten, S.M. and R.J. Wanders, *A general introduction to the biochemistry of mitochondrial fatty acid beta-oxidation.* J Inherit Metab Dis, 2010. **33**(5): p. 469-77.

52. Ramday, R.R., R.D. Gandour, and F.R. van der Leij, *Molecular enzymology of carnitine transfer and transport.* Biochimica et Biophysica Acta, 2001: p. 21-43.

53. Wai, T. and T. Langer, *Mitochondrial Dynamics and Metabolic Regulation.* Trends Endocrinol Metab, 2016. **27**(2): p. 105-17.

54. Qian, W. and B. Van Houten, *Alterations in bioenergetics due to changes in mitochondrial DNA copy number.* Methods, 2010. **51**(4): p. 452-7.

55. Bratic, I. and A. Trifunovic, *Mitochondrial energy metabolism and ageing.* Biochim Biophys Acta, 2010. **1797**(6-7): p. 961-7.

56. Gautheron, D.C., *Mitochondrial Oxidative Phosphorylation and Respiratory Chain: Review.* J. Inher. Metab. Dis., 1984. **7**(1): p. 57-61.

57. Guder, W.G., S. Wagner, and G. Wirthensohn, *Metabolic fuels along the nephron: Pathways and intracellular mechanisms of interaction.* Kidney International, 1986. **29**: p. 41-45.

58. Schmidt, U. and W.G. Guder, *Sites of enzyme activity along the nephron.* Kidney International, 1976. **9**(3): p. 233-242.

59. Cecchini, G., *Function and Structure of Complex II of the Respiratory Chain.* Annual Reviews, 2003. **72**(77).

60. Ramsay, R.R., D.J. Steenkamp, and M. Husain, *Reactions of electron-transfer flavoprotein and electron-transfer flavoprotein ubiquinone oxidoreductase.* Biochem. J. , 1987. **241**: p. 883-892.

61. Berry, E.A., et al., *Structure and Function of Cytochrome bc Complexes.* Annu. Rev. Biochem., 2000. **69**: p. 1005-10075.

62. Nelson, N., et al., *The cellular biology of proton-motive force generation by v-ATPases.* The Journal of Experimental Biology, 2000. **203**: p. 89-95.

63. Held, P., *An Introduction to Reactive Oxygen Species.* BioTek, 2015.

64. Joshi, D.C. and J.C. Bakowska, *Determination of mitochondrial membrane potential and reactive oxygen species in live rat cortical neurons.* J Vis Exp, 2011(51).

65. Dikalov, S.I. and Z. Ungvari, *Role of mitochondrial oxidative stress in hypertension.* Am J Physiol Heart Circ Physiol, 2013. **305**(10): p. H1417-27.

66. Mittler, R., *ROS Are Good.* Trends Plant Sci, 2017. **22**(1): p. 11-19.

67. Niaudet, P., *Mitochondrial disorders and the kidney.* Arch Dis Child, 1998. **78**: p. 387-390.

68. Che, R., et al., *Mitochondrial dysfunction in the pathophysiology of renal diseases.* Am J Physiol Renal Physiol, 2014. **306**: p. 367- 378.

69. Suda, T., K. Takubo, and G.L. Semenza, *Metabolic regulation of hematopoietic stem cells in the hypoxic niche.* Cell Stem Cell, 2011. **9**(4): p. 298-310.

70. Gordan, J.D., C.B. Thompson, and M.C. Simon, *HIF and c-Myc sibling rivals for control of cancer cell metabolism and proliferation.* Cancer Cell, 2007. **12**(2): p. 108-113.

71. Kobayashi, H., et al., *Hypoxia-inducible factor prolyl-4-hydroxylation in FOXD1 lineage cells is essential for normal kidney development.* Kidney Int, 2017. **92**(6): p. 1370-1383.

72. Berkers, C.R., et al., *Metabolic regulation by p53 family members.* Cell Metab, 2013. **18**(5): p. 617-33.

73. Kung, C.P. and M.E. Murphy, *The role of the p53 tumor suppressor in metabolism and diabetes.* J Endocrinol, 2016. **231**(2): p. R61-R75.

74. Lan, R., et al., *Mitochondrial Pathology and Glycolytic Shift during Proximal Tubule Atrophy after Ischemic AKI.* J Am Soc Nephrol, 2016. **27**(11): p. 3356-3367.

75. Bonventre, J.V. and L. Yang, *Cellular pathophysiology of ischemic acute kidney injury.* J Clin Invest, 2011. **121**(11): p. 4210-21.

76. *Cancer Facts & Figures 2016*, 2016, American Cancer Society: Atlanta, Ga.

77. Kreidberg, J.A., *WT1 and kidney progenitor cells.* Organogenesis, 2010. **6**(2): p. 61-70.

78. Aminzadeh, S., et al., *Energy metabolism in neuroblastoma and Wilms tumor.* Transl Pediatr, 2015. **4**(1): p. 20-32.

79. Feichtinger, R.G., et al., *Heterogeneity of mitochondrial energy metabolism in classical triphasic Wilms' tumor.* Front Biosci, 2011. **3**: p. 187-193.

80. Hammer, E., et al., *Kidney protein profiling of Wilms' tumor patients by analysis of formalin-fixed paraffin-embedded tissue samples.* Clin Chim Acta, 2014. **433**: p. 235-41.

81. Zawacka-Pankau, J., et al., *Inhibition of glycolytic enzymes mediated by pharmacologically activated p53: targeting Warburg effect to fight cancer.* J Biol Chem, 2011. **286**(48): p. 41600-15.

82. Dungwa, J.V., L.P. Hunt, and P. Ramani, *Overexpression of carbonic anhydrase and HIF-1alpha in Wilms tumours.* BMC Cancer, 2011. **11**: p. 390.

83. Leisz, S., et al., *Distinct von Hippel-Lindau gene and hypoxia-regulated alterations in gene and protein expression patterns of renal cell carcinoma and their effects on metabolism.* Oncotarget, 2015. **6**(13): p. 11395-11406.

84. Baldewijns, M.M., et al., *VHL and HIF signalling in renal cell carcinogenesis.* J Pathol, 2010. **221**(2): p. 125-38.

85. LaGory, E.L., et al., *Suppression of PGC-1alpha Is Critical for Reprogramming Oxidative Metabolism in Renal Cell Carcinoma.* Cell Rep, 2015. **12**(1): p. 116-127.

86. S.S., W., et al., *Bap1 is essential for kidney function and cooperates with Vhl in renal tumorigenesis.* PNAS, 2014. **111**(46): p. 16538-16543.

87. Granchi, C. and F. Minutolo, *Anticancer agents that counteract tumor glycolysis.* ChemMedChem, 2012. **7**(8): p. 1318-50.

88. Ishimoto, Y. and R. Inagi, *Mitochondria: a therapeutic target in acute kidney injury.* Nephrol Dial Transplant, 2016. **31**(7): p. 1062-9.

89. Basu, R.K., et al., *Assessment of Worldwide Acute Kidney Injury, Renal Angina and Epidemiology in critically ill children (AWARE): study protocol for a prospective observational study.* BMC Nephrol, 2015. **16**: p. 24.

90. Carafa, V., et al., *Sirtuin functions and modulation: from chemistry to the clinic.* Clin Epigenetics, 2016. **8**: p. 61.

91. Yamamoto, H., K. Schoonjans, and J. Auwerx, *Sirtuin functions in health and disease.* Mol Endocrinol, 2007. **21**(8): p. 1745-55.

92. Tran, M.T., et al., *PGC1alpha drives NAD biosynthesis linking oxidative metabolism to renal protection.* Nature, 2016. **531**(7595): p. 528-32.

93. Wakino, S., K. Hasegawa, and H. Itoh, *Sirtuin and metabolic kidney disease.* Kidney Int, 2015. **88**(4): p. 691-8.

94. Kitada, M., S. Kume, and D. Koya, *Role of sirtuins in kidney disease.* Curr Opin Nephrol Hypertens, 2014. **23**(1): p. 75-9.

95. Rowe, I. and A. Boletta, *Defective metabolism in polycystic kidney disease: potential for therapy and open questions.* Nephrol Dial Transplant, 2014. **29**(8): p. 1480-6.

96. Baum, M., *Overview of polycystic kidney disease in children.* Curr Opin Pediatr, 2015. **27**(2): p. 184-5.

97. Rowe, I., et al., *Defective glucose metabolism in polycystic kidney disease identifies a new therapeutic strategy.* Nat Med, 2013. **19**(4): p. 488-93.

98. Ishimoto, Y., et al., *Mitochondrial Abnormality Facilitates Cyst Formation in Autosomal Dominant Polycystic Kidney Disease.* Mol Cell Biol, 2017.

99. Flowers, E.M., et al., *Lkb1 deficiency confers glutamine dependency in polycystic kidney disease.* Nat Commun, 2018. **9**(1): p. 814.

100. *Kidney Disease: Inproving Global Outcomes (KDIGO) CKD work group. KDIGO 2012 clinical practice guideline for the evaluation and management of chronic kidney disease.* . Kidney Int Suppl, 2013. **3**: p. 1-150.

101. Plantinga, L.C., D.S. Tuot, and N.R. Powe, *Awareness of chronic kidney disease among patients and providers.* Adv Chronic Kidney Dis, 2010. **17**(3): p. 225-36.

102. Becherucci, F., et al., *Chronic kidney disease in children.* Clin Kidney J, 2016. **9**(4): p. 583-91.

103. Zhao, J., et al., *Genomic integration of ERRγ-HNF1β regulates renal bioenergetics and prevents chronic kidney disease.* PNAS, 2018. **115**(7): p. E4910-E4919.

104. Granata, S., et al., *Mitochondrial dysregulation and oxidative stress in patients with chronic kidney disease.* BMC Genomics, 2009. **10**: p. 388.

105. Granata, S., et al., *Mitochondria: a new therapeutic target in chronic kidney disease.* Nutr Metab (Lond), 2015. **12**: p. 49.

106. Han, S.H., et al., *PGC-1alpha Protects from Notch-Induced Kidney Fibrosis Development.* J Am Soc Nephrol, 2017. **28**(11): p. 3312-3322.

107. Portilla, D., et al., *Alterations of PPARalpha and its coactivator PGC-1 in cisplatin-induced acute renal failure.* Kidney Int, 2002. **62**(4): p. 1208-18.

108. Iyer, N.V., et al., *Cellular and developmental control of O2 homeostasis by hypoxia-inducible factor 1 alpha.* Genes Dev, 1998. **12**(2): p. 149-62.

109. Majmundar, A.J., W.J. Wong, and M.C. Simon, *Hypoxia-inducible factors and the response to hypoxic stress.* Mol Cell, 2010. **40**(2): p. 294-309.

110. Gunaratnam, L. and J.V. Bonventre, *HIF in Kidney Disease and Development.* Journal of the American Society of Nephrology, 2008. **20**(9): p. 1877-1887.

111. Haase, V.H., *The VHL/HIF oxygen-sensing pathway and its relevance to kidney disease.* Kidney Int, 2006. **69**(8): p. 1302-7.

112. Tanimoto, K., et al., *Mechanism of regulation of the hypoxia-inducible factor 1a by the von Hippel-Lindau tumor suppressor protein.* 19, 2000. **16**(4298-4309).

113. Dunwoodie, S.L., *The role of hypoxia in development of the Mammalian embryo.* Dev Cell, 2009. **17**(6): p. 755-73.

114. Semenza, G.L., *Hypoxia-inducible factor 1: regulator of mitochondrial metabolism and mediator of ischemic preconditioning.* Biochim Biophys Acta, 2011. **1813**(7): p. 1263-8.

115. Semenza, G.L., *Regulation of metabolism by hypoxia-inducible factor 1.* Cold Spring Harb Symp Quant Biol, 2011. **76**: p. 347-53.

116. Tsuji, K., S. Kitamura, and H. Makino, *Hypoxia-inducible factor 1alpha regulates branching morphogenesis during kidney development.* Biochem Biophys Res Commun, 2014. **447**(1): p. 108-14.

117. Hemker, S.L., S. Sims-Lucas, and J. Ho, *Role of hypoxia during nephrogenesis.* Pediatr Nephrol, 2016.

118. Bernhardt, W.M., et al., *Expression of hypoxia-inducible transcription factors in developing human and rat kidneys.* Kidney Int, 2006. **69**(1): p. 114-22.

119. Freeburg, P.B., et al., *Podocyte expression of hypoxia-inducible factor (HIF)-1 and HIF-2 during glomerular development.* J Am Soc Nephrol, 2003. **14**(4): p. 927-38.

120. Shyh-Chang, N., G.Q. Daley, and L.C. Cantley, *Stem cell metabolism in tissue development and aging.* Development, 2013. **140**(12): p. 2535-47.

121. Papandreou, I., et al., *HIF-1 mediates adaptation to hypoxia by actively downregulating mitochondrial oxygen consumption.* Cell Metab, 2006. **3**(3): p. 187-97.

122. Freeburg, P.B. and D.R. Abrahamson, *Hypoxia-inducible factors and kidney vascular development.* J Am Soc Nephrol, 2003. **14**(11): p. 2723-30.

123. Freeburg, P.B., *Hypoxia-Inducible Factors and Kidney Vascular Development.* Journal of the American Society of Nephrology, 2003. **14**(11): p. 2723-2730.

124. Lin, Q., Y.J. Lee, and Z. Yun, *Differentiation arrest by hypoxia.* J Biol Chem, 2006. **281**(41): p. 30678-83.

125. Li, G., et al., *Effect of fetal hypoxia on heart susceptibility to ischemia and reperfusion injury in the adult rat.* J Soc Gynecol Investig, 2003. **10**(5): p. 265-274.

126. Kobayashi, H., et al., *Distinct subpopulations of FOXD1 stroma-derived cells regulate renal erythropoietin.* J Clin Invest, 2016. **126**(5): p. 1926-38.

127. Bakker, W.J., I.S. Harris, and T.W. Mak, *FOXO3a is activated in response to hypoxic stress and inhibits HIF1-induced apoptosis via regulation of CITED2.* Mol Cell, 2007. **28**(6): p. 941-53.

128. Benita, Y., et al., *An integrative genomics approach identifies Hypoxia Inducible Factor-1 (HIF-1)-target genes that form the core response to hypoxia.* Nucleic Acids Res, 2009. **37**(14): p. 4587-602.

129. Liu, W., et al., *Hypoxia and cell cycle regulation of the von Hippel-Lindau tumor suppressor.* Oncogene, 2011. **30**(1): p. 21-31.

130. Kotch, L.E., et al., *Defective Vascularization of HIF-1a-Null EmbryosIs Not Associated with VEGF Deficiencybut with Mesenchymal Cell Deat.* Developmental Biology, 1999. **209**.

131. Ricketts, C.J., D.R. Crooks, and W.M. Linehan, *Targeting HIF2a in Clear-Cell Renal Cell Carcinoma.* Cancer Cell, 2016. **30**: p. 515-517.

132. Chen, Y.B., et al., *Molecular analysis of aggressive renal cell carcinoma with unclassified histology reveals distinct subsets.* Nat Commun, 2016. **7**: p. 13131.

133. Gnarra, J.R., et al., *Defective placental vasculogenesis causes embryonic lethality in VHL-deficient mice.* Proc Natl Acad Sci U S A, 1997. **94**(17): p. 9102-7.

134. Kapitsinou, P.P. and V.H. Haase, *The VHL tumor suppressor and HIF: insights from genetic studies in mice.* Cell Death Differ, 2008. **15**(4): p. 650-9.

135. Chen, Y.H., et al., *von Hippel-Lindau gene plays a role during zebrafish pronephros development.* In Vitro Cell Dev Biol Anim, 2015. **51**(10): p. 1023-32.

136. van Rooijen, E., et al., *Zebrafish mutants in the von Hippel-Lindau tumor suppressor display a hypoxic response and recapitulate key aspects of Chuvash polycythemia.* Blood, 2009. **113**(25): p. 6449-60.

137. Okazaki, K.M. and E. Maltepe, *Oxygen, epigenetics and stem cell fate.* Regenerative Medicine, 2005. **1**(1).

138. Mohyeldin, A., T. Garzon-Muvdi, and A. Quinones-Hinojosa, *Oxygen in stem cell biology: a critical component of the stem cell niche.* Cell Stem Cell, 2010. **7**(2): p. 150-61.

139. Cosmi, E., et al., *Consequences in infants that were intrauterine growth restricted.* J Pregnancy, 2011. **2011**: p. 364381.

140. Eleftheriades, M., G. Creatsas, and K. Nicolaides, *Fetal growth restriction and postnatal development.* Ann N Y Acad Sci, 2006. **1092**: p. 319-30.

141. Kingdom, J., et al., *Development of the placental villous tree and its consequences for fetal growth.* Eur J Obstet Gynecol Reprod Biol, 2000. **92**(1): p. 35-43.

142. Hutter, D., J. Kingdom, and E. Jaeggi, *Causes and mechanisms of intrauterine hypoxia and its impact on the fetal cardiovascular system: a review.* Int J Pediatr, 2010. **2010**: p. 401323.

143. Romo, A., R. Carceller, and J. Tobajas, *Intrauterine growth retardation (IUGR): epidemiology and etiology.* Pediatr Endrocrinol Rev, 2009. **3**: p. 332-336.

144. Formenti, F., et al., *Regulation of human metabolism by hypoxia-inducible factor.* Proc Natl Acad Sci U S A, 2010. **107**(28): p. 12722-7.

145. Hsu, S.H., C.T. Chen, and Y.H. Wei, *Inhibitory effects of hypoxia on metabolic switch and osteogenic differentiation of human mesenchymal stem cells.* Stem Cells, 2013. **31**(12): p. 2779-88.

146. Schonenberger, M.J. and W.J. Kovacs, *Hypoxia signaling pathways: modulators of oxygen-related organelles.* Front Cell Dev Biol, 2015. **3**: p. 42.

147. Hervouet, E., et al., *HIF and reactive oxygen species regulate oxidative phosphorylation in cancer.* Carcinogenesis, 2008. **29**(8): p. 1528-37.

148. Zhang, H., et al., *HIF-1 inhibits mitochondrial biogenesis and cellular respiration in VHL-deficient renal cell carcinoma by repression of C-MYC activity.* Cancer Cell, 2007. **11**(5): p. 407-20.

149. Wei, P., et al., *The Force Is Strong with This One: Metabolism (Over)powers Stem Cell Fate.* Trends Cell Biol, 2018. **28**(7): p. 551-559.

150. Semenza, G.L., *HIF-1 mediates metabolic responses to intratumoral hypoxia and oncogenic mutations.* J Clin Invest, 2013. **123**(9): p. 3664-71.

151. Onnis, B., A. Rapisarda, and G. Melillo, *Development of HIF-1 inhibitors for cancer therapy.* J Cell Mol Med, 2009. **13**(9A): p. 2780-6.

152. Phan, A.T. and A.W. Goldrath, *Hypoxia-inducible factors regulate T cell metabolism and function.* Mol Immunol, 2015. **68**(2 Pt C): p. 527-35.

153. Menrad, H., et al., *Roles of hypoxia-inducible factor-1alpha (HIF-1alpha) versus HIF-2alpha in the survival of hepatocellular tumor spheroids.* Hepatology, 2010. **51**(6): p. 2183-92.

154. Schodel, J., et al., *Hypoxia, Hypoxia-inducible Transcription Factors, and Renal Cancer.* Eur Urol, 2016. **69**(4): p. 646-657.

155. Lian, X., et al., *The changes in glucose metabolism and cell proliferation in the kidneys of polycystic kidney disease mini-pig models.* Biochem Biophys Res Commun, 2017. **488**(2): p. 374-381.

156. Riwanto, M., et al., *Inhibition of Aerobic Glycolysis Attenuates Disease Progression in Polycystic Kidney Disease.* PLoS One, 2016. **11**(1): p. e0146654.

157. Lu, H., R.A. Forbes, and A. Verma, *Hypoxia-inducible factor 1 activation by aerobic glycolysis implicates the Warburg effect in carcinogenesis*. J Biol Chem, 2002. **277**(26): p. 23111-5.

158. Cao, Y., J.C. Rathmell, and A.N. Macintyre, *Metabolic reprogramming towards aerobic glycolysis correlates with greater proliferative ability and resistance to metabolic inhibition in CD8 versus CD4 T cells.* PLoS One, 2014. **9**(8): p. e104104.

159. Underwood, A.H. and E.A. Newsholme, *Control of glycolysis and gluconeogenesis in rat kidney cortex slices.* Biochem J, 1967. **104**(1): p. 300-5.

160. Thompson, L., et al., *Intrauterine hypoxia: clinical consequences and therapeutic perspectives.* Research and Reports in Neonatology, 2015: p. 79.

161. Battista, M.C., et al., *Intrauterine growth restriction in rats is associated with hypertension and renal dysfunction in adulthood.* Am J Physiol Endocrinol Metab, 2002. **283**: p. E124-E131.

162. Hemker, S.L., S. Sims-Lucas, and J. Ho, *Role of hypoxia during nephrogenesis.* Pediatr Nephrol, 2016. **31**(10): p. 1571-7.

163. Patterson, A.J. and L. Zhang, *Hypoxia and Fetal Heart Development.* Curr Mol Med, 2010. **10**(7): p. 653-666.

164. Peyronnet, J., et al., *Prenatal hypoxia impairs the postnatal development of neural and functional chemoafferent pathway in rat.* Journal of Physiology, 2000. **524**(2): p. 525-537.

165. Patterson, A.J., et al., *Chronic prenatal hypoxia induces epigenetic programming of PKC{epsilon} gene repression in rat hearts.* Circ Res, 2010. **107**(3): p. 365-73.

166. Bagby, S.P., *Developmental origins of renal disease: should nephron protection begin at birth?* Clin J Am Soc Nephrol, 2009. **4**(1): p. 10-3.

167. Nishinakamura, R., *Stem cells and renal development in 2015: Advances in generating and maintaining nephron progenitors.* Nat Rev Nephrol, 2016. **12**(2): p. 67-8.

168. Jensen, G.M. and L.G. Moore, *The effect of high altitude and other risk factors on birthweight: independent or interactive effects?* Am J Public Health, 1997. **87**(6): p. 1003-1007.

169. Boubred, F., et al., *The magnitude of nephron number reduction mediates intrauterine growth-restriction-induced long term chronic renal disease in the rat. A comparative study in two experimental models.* J Transl Med, 2016. **14**(1): p. 331.

170. Newsome, A.D., G.K. Davis, and B.T. Alexandar, *Intrauterine Growth Restriction Programs Greater Susceptibility to Chronic Kidney Injury in Male and Female Aged Rats.* FASEB Journal, 2017. **31**(1).

171. Walton, S.L., et al., *Prolonged prenatal hypoxia selectively disrupts collecting duct patterning and postnatal function in male mouse offspring.* J Physiol, 2018. **596**(23): p. 5873-5889.

172. Ozkok, A. and C.L. Edelstein, *Pathophysiology of cisplatin-induced acute kidney injury.* Biomed Res Int, 2014. **2014**: p. 967826.

173. Basile, D.P., M.D. Anderson, and T.A. Sutton, *Pathophysiology of acute kidney injury.* Comprehensive Physiology, 2012. **2**(2): p. 1303-1353.

174. Hsu, R.K. and C.Y. Hsu, *The Role of Acute Kidney Injury in Chronic Kidney Disease.* Semin Nephrol, 2016. **36**(4): p. 283-292.

175. Ostermann, M. and K. Liu, *Pathophysiology of AKI.* Best Pract Res Clin Anaesthesiol, 2017. **31**(3): p. 305-314.

176. Miller, R.P., et al., *Mechanisms of Cisplatin nephrotoxicity.* Toxins (Basel), 2010. **2**(11): p. 2490-518.

177. Barnett, L.M.A. and B.S. Cummings, *Nephrotoxicity and Renal Pathophysiology: A Contemporary Perspective.* Toxicol Sci, 2018. **164**(2): p. 379-390.

178. Oh, G.S., et al., *Cisplatin-induced Kidney Dysfunction and Perspectives on Improving Treatment Strategies.* Electrolyte Blood Press, 2014. **12**(2): p. 55-65.

179. Coca, S.G., *Acute kidney injury in elderly persons.* Am J Kidney Dis, 2010. **56**(1): p. 122-131.

180. He, L., et al., *AKI on CKD: heightened injury, suppressed repair, and the underlying mechanisms.* Kidney Int, 2017. **92**(5): p. 1071-1083.

181. Ho, J., *The regulation of apoptosis in kidney development: implications for nephron number and pattern?* Front Pediatr, 2014. **2**: p. 128.

182. Ducsay, C.A., et al., *Gestational Hypoxia and Developmental Plasticity.* Physiol Rev, 2018. **98**: p. 1241-1334.

183. Gonzalez-Rodriguez, P., Jr., et al., *Fetal hypoxia results in programming of aberrant angiotensin ii receptor expression patterns and kidney development.* Int J Med Sci, 2013. **10**(5): p. 532-8.

184. Xia, S., et al., *Prenatal exposure to hypoxia induced Beclin 1 signaling-mediated renal autophagy and altered renal development in rat fetuses.* Reprod Sci, 2015. **22**(2): p. 156-64.

185. Zwemer, C.F., et al., *Strain differences in response to acute hypoxia: CD-1 versus C57BL/6J mice.* J Appl Physiol, 2007. **102**(1): p. 286-293.

186. Li, Q., et al., *Strain differences in behavioral and cellular responses to perinatal hypoxia and relationships to neural stem cell survival and self-renewal: Modeling the neurovascular niche.* Am J Pathol, 2009. **175**(5): p. 2133-46.

187. Golan, H. and M. Huleihel, *The effect of prenatal hypoxia on brain development: short- and long-term consequences demonstrated in rodent models.* Developmental Science, 2006. **9**(4): p. 338-349.

188. Nalivaeva, N.N., A.J. Turner, and I.A. Zhuravin, *Role of Prenatal Hypoxia in Brain Development, Cognitive Functions, and Neurodegeneration.* Front Neurosci, 2018. **12**: p. 825.

189. Xue, Q. and L. Zhang, *Prenatal hypoxia causes a sex-dependent increase in heart susceptibility to ischemia and reperfusion injury in adult male offspring: role of protein kinase C epsilon.* J Pharmacol Exp Ther, 2009. **330**(2): p. 624-32.

190. Xu, Y., et al., *Hypoxia or nutrient restriction during pregnancy in rats leads to progressive cardiac remodeling and impairs postischemic recovery in adult male offspring.* FASEB Journal, 2006. **20**(8): p. 1251-1253.

191. Heyman, S.N., S. Rosen, and C. Rosenberger, *Animal models of renal dysfuncton: acute kidney injury.* Expert Opinion on Drug Discovery, 2009. **4**(6): p. 629-641.

192. Baud, L. and R. Ardaillou, *Reactive oxygen species: production and role in the kidney.* American Journal of Physiology Renal Physiology, 1986. **251**(5).

193. Pavlakou, P., et al., *Oxidative Stress and Acute Kidney Injury in Critical Illness: Pathophysiologic Mechanisms-Biomarkers-Interventions, and Future Perspectives.* Oxid Med Cell Longev, 2017. **2017**: p. 6193694.

194. Jeong, B.Y., et al., *Oxidative stress caused by activation of NADPH oxidase 4 promotes contrast-induced acute kidney injury.* PLoS One, 2018. **13**(1): p. e0191034.

195. Zhao, T., et al., *HIF-1-mediated metabolic reprogramming reduces ROS levels and facilitates the metastatic colonization of cancers in lungs.* Sci Rep, 2014. **4**: p. 3793.

196. Meng, X.M., et al., *NADPH oxidase 4 promotes cisplatin-induced acute kidney injury via ROS-mediated programmed cell death and inflammation.* Lab Invest, 2018. **98**(1): p. 63-78.

197. Movafagh, S., S. Crook, and K. Vo, *Regulation of hypoxia-inducible factor-1a by reactive oxygen species: new developments in an old debate.* J Cell Biochem, 2015. **116**(5): p. 696-703.

198. Chandel, N.S., et al., *Mitochondrial reactive oxygen species trigger hypoxia- induced transcription.* Proc Natl Acad Sci USA, 1998. **95**: p. 11715-11720.

199. Walton, S.L., et al., *Prenatal hypoxia leads to hypertension, renal renin-angiotensin system activation and exacerbates salt-induced pathology in a sex-specific manner.* Sci Rep, 2017. **7**(1): p. 8241.

200. Komaki, K., et al., *Lower blood pressure and risk of cisplatin nephrotoxicity: a retrospective cohort study.* BMC Cancer, 2017. **17**(1): p. 144.

201. Zhang, J., et al., *Competing Actions of Type 1 Angiotensin II Receptors Expressed on T Lymphocytes and Kidney Epithelium during Cisplatin-Induced AKI.* J Am Soc Nephrol, 2016. **27**(8): p. 2257-64.

202. Zhou, J., et al., *Gestational hypoxia induces preeclampsia-like symptoms via heightened endothelin-1 signaling in pregnant rats.* Hypertension, 2013. **62**(3).

203. Rossi, G.P., et al., *Interactions between endothelin-1 and the renin-angiotensin-aldosterone system.* Cardiovasc Res, 1999. **1**(43): p. 300-307.

204. Chen, S., et al., *Intrinsic Age-Dependent Changes and Cell-Cell Contacts Regulate Nephron Progenitor Lifespan.* Dev Cell, 2015. **35**(1): p. 49-62.

205. Tanigawa, S., et al., *Selective In Vitro Propagation of Nephron Progenitors Derived from Embryos and Pluripotent Stem Cells.* Cell Rep, 2016.

206. Boyle, S., et al., *Cited1 and Cited2 Are Differentially Expressed in the Developing Kidney but Are Not Required for Nephrogenesis.* Developmental Dynamics, 2007. **236**: p. 2321-2330.

207. Rymer, C., et al., *Renal blood flow and oxygenation drive nephron progenitor differentiation.* Am J Physiol Renal Physiol, 2014. **307**(3): p. F337-45.

208. Cargill, K. and S. Sims-Lucas, *Metabolic requirements of the nephron.* Pediatr Nephrol, 2018.

209. Rognstad, R. and J. Katz, *Gluconeogenesis in the kidney cortex.* Journal of Biological Chemistry, 1972. **247**(19): p. 6047-6054.

210. Kobayashi, A., et al., *Six2 defines and regulates a multipotent self-renewing nephron progenitor population throughout mammalian kidney development.* Cell Stem Cell, 2008. **3**(2): p. 169-81.

211. Haase, V.H., et al., *Vascular tumors in livers with targeted inactivation of the von Hippel–Lindau tumor suppressor.* PNAS, 2001. **98**(4): p. 1583-1588.

212. Sims-Lucas, S., et al., *Three-dimensional imaging reveals ureteric and mesenchymal defects in Fgfr2-mutant kidneys.* J Am Soc Nephrol, 2009. **20**(12): p. 2525-33.

213. Cullen-McEwen, L.L., et al., *Estimating Nephron Number in the Developing Kidney Using the Physical Disector/Fractionator Combination.* Methods in Molecular Biology, 2012. **886**: p. 109-119.

214. Cullen-McEwen, L.A., R.N. Douglas-Denton, and J.F. Bertram, *Estimating total nephron number in the adult kidney using the physical disector/fractionator combination.* Methods Mol Biol, 2012. **886**: p. 333-350.

215. Cerqueira, D.M., et al., *Bim gene dosage is critical in modulating nephron progenitor survival in the absence of microRNAs during kidney development.* FASEB Journal, 2017. **31**(8): p. 3540-3554.

216. Andrews, S., *FastQC A Quality Control tool for High Throughput Sequence Data.* , in *Babraham Bioinformatics.* 2010.

217. Bushnell, B. *BBMap (version 35.14) [Software]*. 2015; Available from: https://sourceforge.net/projects/bbmap/.

218. Church, D.M., et al., *Modernizing Reference Genome Assemblies.* PLoS Biology, 2011. **9**(7): p. 1-5.

219. Dobin, A., et al., *STAR: ultrafast universal RNA-seq aligner.* Bioinformatics, 2013. **29**(1): p. 15-21.

220. Team, R.C., *R: The R Project for Statistical Computing*, 2016.

221. Lawrence, M., et al., *Software for Computing and Annotating Genomic Ranges.* PloS Computational Biology, 2013. **9**(8): p. 1-10.

222. Love, M.I., W. Huber, and S. Anders, *Moderated estimation of fold change and dispersion for RNA-seq data with DESeq2.* Genome Biol, 2014. **15**(12): p. 550.

223. Huang da, W., B.T. Sherman, and R.A. Lempicki, *Bioinformatics enrichment tools: paths toward the comprehensive functional analysis of large gene lists.* Nucleic Acids Res, 2009. **37**(1): p. 1-13.

224. Huang da, W., B.T. Sherman, and R.A. Lempicki, *Systematic and integrative analysis of large gene lists using DAVID bioinformatics resources.* Nat Protoc, 2009. **4**(1): p. 44-57.

225. de Moura, M.B., et al., *Overexpression of mitochondrial sirtuins alters glycolysis and mitochondrial function in HEK293 cells.* PLoS One, 2014. **9**(8): p. e106028.

226. Collins, C.L., et al., *Multiwell 14CO2-capture assay for evaluation of substrate oxidation rates of cells in culture.* Biotechniques, 1998. **24**(5): p. 803-8.

227. Park, J.S., M.T. Valerius, and A.P. McMahon, *Wnt/beta-catenin signaling regulates nephron induction during mouse kidney development.* Development, 2007. **134**(13): p. 2533-9.

228. Brand, M.D. and D.G. Nicholls, *Assessing mitochondrial dysfunction in cells.* Biochem J, 2011. **435**(2): p. 297-312.

229. Wintour, E.M., et al., *Reduced nephron number in adult sheep, hypertensive as a result of prenatal glucocorticoid treatment.* J Physiol, 2003. **549**(Pt 3): p. 929-35.

230. O'Brien, L.L., et al., *Differential regulation of mouse and human nephron progenitors by the Six family of transcriptional regulators.* Development, 2016. **143**(4): p. 595-608.

231. Self, M., et al., *Six2 is required for suppression of nephrogenesis and progenitor renewal in the developing kidney.* The EMBO Journal, 2006. **25**(21): p. 5214-5228.

232. Chung, E., et al., *Notch signaling promotes nephrogenesis by downregulating Six2.* Development, 2016. **143**(21): p. 3907-3913.

233. Evans, A.J., et al., *VHL promotes E2 box-dependent E-cadherin transcription by HIF-mediated regulation of SIP1 and snail.* Mol Cell Biol, 2007. **27**(1): p. 157-69.

234. Gerl, K., et al., *Activation of Hypoxia Signaling in Stromal Progenitors Impairs Kidney Development.* Am J Pathol, 2017. **187**(7): p. 1496-1511.

235. Puri, T.S., et al., *Chronic kidney disease induced in mice by reversible unilateral ureteral obstruction is dependent on genetic background.* Am J Physiol Renal Physiol, 2010. **298**(4): p. F1024-32.

236. Walkin, L., et al., *The role of mouse strain differences in the susceptibility to fibrosis.* Fibrogenesis & Tissue Repair, 2013. **6**(18): p. 1-12.

237. Hartner, A., et al., *Strain differences in the development of hypertension and glomerular lesions induced by deoxycorticosterone acetate salt in mice.* Nephrol Dial Transplant, 2003. **18**(10): p. 1999-2004.

238. Hervouet, E., et al., *A new role for the von Hippel-Lindau tumor suppressor protein: stimulation of mitochondrial oxidative phosphorylation complex biogenesis.* Carcinogenesis, 2005. **26**(3): p. 531-9.

239. Chan, D.A., et al., *Targeting GLUT1 and the Warburg effect in renal cell carcinoma by chemical synthetic lethality.* Sci Transl Med, 2011. **3**(94): p. 94ra70.

240. Abdulrahman, M., et al., *Identification of novel VHL targets that are associated with the development of renal cell carcinoma.* Oncogene, 2007. **26**(11): p. 1661-72.

241. Gnarra, J.R., et al., *Mutations of the VHL tumour suppressor gene in renal carcinoma.* Nat Genet, 1994. **7**(1): p. 85-90.

242. Gossage, L., T. Eisen, and E.R. Maher, *VHL, the story of a tumour suppressor gene.* Nat Rev Cancer, 2015. **15**(1): p. 55-64.

243. Simsek, T., et al., *The distinct metabolic profile of hematopoietic stem cells reflects their location in a hypoxic niche.* Cell Stem Cell, 2010. **7**(3): p. 380-90.

244. Shiao, Y.H., et al., *The von Hippel Lindau Tumor Suppressor Targets to Mitochondria.* Journal of Cancer Research, 2000. **60**(11): p. 2816-2819.

245. Cargill, K., et al., *Von Hippel-Lindau Acts as a Metabolic Switch Controlling Nephron Progenitor Differentiation.* J Am Soc Nephrol, 2019.

246. Zhang, H., et al., *Mitochondrial autophagy is an HIF-1-dependent adaptive metabolic response to hypoxia.* J Biol Chem, 2008. **283**(16): p. 10892-903.

247. Chiche, J., et al., *Hypoxic enlarged mitochondria protect cancer cells from apoptotic stimuli.* J Cell Physiol, 2010. **222**(3): p. 648-57.

248. Hamanaka, R.B., et al., *The Mitochondrial Respiratory Chain Is Required for Organismal Adaptation to Hypoxia.* Cell Rep, 2016. **15**(3): p. 451-459.

249. Kim, J.W., et al., *HIF-1-mediated expression of pyruvate dehydrogenase kinase: a metabolic switch required for cellular adaptation to hypoxia.* Cell Metab, 2006. **3**(3): p. 177-85.

250. Stepanenko, A.A. and V.V. Dmitrenko, *HEK293 in cell biology and cancer research: phenotype, karyotype, tumorigenicity, and stress-induced genome-phenotype evolution.* Gene, 2015. **569**(2): p. 182-90.

251. Lin, Y.C., et al., *Genome dynamics of the human embryonic kidney 293 lineage in response to cell biology manipulations.* Nat Commun, 2014. **5**: p. 4767.

252. Shaw, G., et al., *Preferential transformation of human neuronal cells by human adenoviruses and the origin of HEK 293 cells.* FASEB Journal, 2002. **16**(8).

253. Baschat, A.A., *Fetal responses to placental insufficiency: an update.* BJOG, 2004. **111**(10): p. 1031-41.

254. Tapanainen, P.J., et al., *Maternal Hypoxia as a Model for Intrauterine Growth Retardation: Effects on Insulin-Like Growth Factors and Their Binding Proteins.* Pediatric Research, 1994. **36**(2): p. 152-158.

255. Fu, Q., S.P. Colgan, and C.S. Shelley, *Hypoxia: The Force that Drives Chronic Kidney Disease.* Clin Med Res, 2016. **14**(1): p. 15-39.

256. Neugarten, J., L. Golestaneh, and N.V. Kolhe, *Sex differences in acute kidney injury requiring dialysis.* BMC Nephrol, 2018. **19**(131).

257. Lopez Ruiz, A., et al., *Estrogen Receptor Contributes to Sex Differences in Acute Kidney Injury.* FASEB Journal, 2010. **24**(1).

258. Lima-Posada, I., et al., *Gender Differences in the Acute Kidney Injury to Chronic Kidney Disease Transition.* Sci Rep, 2017. **7**(1): p. 12270.

259. Perse, M. and Z. Veceric-Haler, *Cisplatin-Induced Rodent Model of Kidney Injury: Characteristics and Challenges.* Biomed Res Int, 2018. **2018**: p. 1462802.

260. Fajersztajn, L. and M. Matera Veras, *Hypoxia: From Placental Development to Fetal Programming.* Birth Defects Research, 2017. **109**.

261. Moore, L.G., S.M. Charles, and C.G. Julian, *Humans at high altitude: hypoxia and fetal growth.* Respir Physiol Neurobiol, 2011. **178**(1): p. 181-90.

262. Zhu, W., et al., *PFK15, a Small Molecule Inhibitor of PFKFB3, Induces Cell Cycle Arrest, Apoptosis and Inhibits Invasion in Gastric Cancer.* PLoS One, 2016. **11**(9): p. e0163768.

263. Seo, M., et al., *Structure-Based Development of Small Molecule PFKFB3 Inhibitors: A Framework for Potential Cancer Therapeutic Agents Targeting the Warburg Effect.* PloS One, 2011. **6**(9).

264. Schulz, K., et al., *HIF-1alpha protein is upregulated in HIF-2alpha depleted cells via enhanced translation.* FEBS Lett, 2012. **586**(11): p. 1652-7.

265. Hahne, M., et al., *Unraveling the role of hypoxia-inducible factor (HIF)-1alpha and HIF-2alpha in the adaption process of human microvascular endothelial cells (HMEC-1) to hypoxia: Redundant HIF-dependent regulation of macrophage migration inhibitory factor.* Microvasc Res, 2018. **116**: p. 34-44.

266. Hu, C.J., et al., *Differential roles of hypoxia-inducible factor 1alpha (HIF-1alpha) and HIF-2alpha in hypoxic gene regulation.* Mol Cell Biol, 2003. **23**(24): p. 9361-74.

267. Koh, M.Y. and G. Powis, *Passing the baton: the HIF switch.* Trends Biochem Sci, 2012. **37**(9): p. 364-72.

268. Wu, J., A. Ocampo, and J.C. Izpisua Belmonte, *Cellular Metabolism and Induced Pluripotency.* Cell, 2016. **166**(6): p. 1371-85.

269. Ejtehadifar, M., et al., *The Effect of Hypoxia on Mesenchymal Stem Cell Biology.* Adv Pharm Bull, 2015. **5**(2): p. 141-9.

270. Briston, T., et al., *VHL-Mediated Regulation of CHCHD4 and Mitochondrial Function.* Frontiers in Oncology, 2018. **8**.

271. Tabaro, F., et al., *VHLdb: A database of von Hippel-Lindau protein interactors and mutations.* Sci Rep, 2016. **6**: p. 31128.